U.PORTO

FEUP FACULDADE DE ENGENHARIA UNIVERSIDADE DO PORTO

DIAMETER EFFECTS OF LARGE SCALE MONOPILES

A THEORETICAL AND NUMERICAL INVESTIGATION OF THE SOIL-PILE INTERACTION RESPONSE

ANTÓNIO CABRAL VIANA DA FONSECA

Dissertação submetida para satisfação parcial dos requisitos do grau de

MESTRE EM ENGENHARIA CIVIL — ESPECIALIZAÇÃO EM GEOTECNIA

Orientador: Professor Doutor Pedro Miguel Barbosa Alves Costa

Coorientador: Doctor Ole Hededal

JULHO DE 2015

MESTRADO INTEGRADO EM ENGENHARIA CIVIL 2014/2015

DEPARTAMENTO DE ENGENHARIA CIVIL

Tel. +351-22-508 1901

Fax +351-22-508 1446

✉ miec@fe.up.pt

Editado por

FACULDADE DE ENGENHARIA DA UNIVERSIDADE DO PORTO

Rua Dr. Roberto Frias

4200-465 PORTO

Portugal

Tel. +351-22-508 1400

Fax +351-22-508 1440

✉ feup@fe.up.pt

http://www.fe.up.pt

Aos meus Pais e Irmãos

"Challenges is what makes life interesting and overcoming them is what makes life meaningful." – Joshua J. Marine

ACKOWLEDGMENTS

In this important moment of my life I would like to express my sincere gratitude to all who accompanied me during these last five years and to all who have supported and helped me during the development of this project. In particular, I would like to acknowledge:

- My supervisor in Portugal, Professor Pedro Alves Costa, for the suggestions, ideas and patience on the guidance throughout the elaboration of this project;
- To all the staff of COWI A/S that received me so well during the time that I was in the company and in Denmark, for providing me an unforgettable experience on such a recognized group and for the insights given on the offshore topics;
- To Ole Hededal, for making this experience possible, having proposed a so interesting theme and shared his experience and knowledge with me. Also, for all the interest demonstrated in the project and for all the interesting discussions we had during our meeting in the last months;
- To my mother, who always showed concern for my well-being and comforted and motivated on all times. To my father, who gave me a lot of support and help on overcoming the obstacles of this journey and, together with Ole Hededal, made this agreement with COWI A/S possible. To my brothers who, on their own way, always tried to cheer me up and motivate me;
- To all my friends and my girlfriend who, although being far away, were always present. For all the good moments, fun and joy during these years.

ABSTRACT

The aim of this thesis is the study of the effects of the diameter on large scale monopiles, characterized by its rigid behaviour, used as foundations for offshore wind turbines in clay. The study involves a numerical investigation of the soil-pile interaction followed by an interpretation and validation of the results with the existing theoretical principles of soil mechanics on this area of expertise.

After a brief overview of the current state-of-the-art of the wind energy industry and a description about the relevance of monopiles on offshore wind industry, the specificities of their geotechical design, namely the lateral-load design of these piles, is addressed. The soil-pile interaction is usually characterized by a load-displacement curve, the so called p-y curves, to which several theories were developed over the years and is the basis of current lateral-load design of offshore monopiles foundations.

In order to obtain the reaction of the soil, p, as a response to a displacement, y, the hypothesis of using a differential equation that expresses the soil reaction as a function of the fourth derivative of the displacement was explored. It was concluded that this methodology will be reliable when the deformations are not too large as to introduce plasticity to the mobilized soil – as it can be the case of flexible piles, with high slenderness – but it was concluded inefficient for rigid piles as there is no way of taking into account the plastification of the soil.

Maintaining, however, the possibility of integrating the stresses around the pile, a model in PLAXIS® 3D was built in a way to represent in the more realistic manner possible the soil-pile interaction. By analysing the results of the data exported from the finite element program, a methodology was developed for the calculation of the p-y curves taking into consideration the extensive data obtained by a significant number of complex numerical calculations, which was later programmed in MatLab®.

After exploring some other options, a hyperbolic curve was concluded to be the best fitting to characterize the shape of the obtained results for generation of the p-y curves. The obtained results were compared with the ones obtain using the suggested method of the American Petroleum Institute (API) regarding, not only the actual p-y curves, but also the results for the ultimate bearing capacity and the initial stiffness of the soil.

The formulation of the API p-y curves was concluded to not be very accurate as the shape of its curves underestimates the capacity of the soil and its evolution on depth and does not take into account the initial subgrade reaction of the soil. The diameter of the monopile was concluded to have a great influence on the initial subgrade reaction of the soil and a nonlinear one. It was concluded that there is no influence of the diameter when it comes to the resistance of the p-y curves.

Finally, the most relevant conclusions are highlighted in the end of this work and further developments are suggested on this research topic for future studies.

KEYWORDS: Offshore, monopiles, p-y curves, diameter effects, PLAXIS 3D, soil-pile interaction

RESUMO

O objetivo desta tese é o estudo dos efeitos do diâmetro em monoestacas de grande escala - caracterizada pelo seu comportamento rígido - usado como fundações em argila para turbinas eólicas offshore. O estudo envolve uma investigação numérica sobre a interacção solo-estaca seguida de uma interpretação e consequente validação dos resultados baseados nos princípios teóricos da mecânica dos solos aplicados nesta área de especialização.

Após uma breve introdução sobre a actual situação da indústria da energia eólica e uma descrição da relevância das monoestacas na indústria eólica offshore, as especificações do seu dimensionamento geotécnico, nomeadamente o dimensionamento ao carregamento lateral destas estacas, é referenciado. A interacção solo- estaca é geralmente caracterizada por uma curva de carga-deslocamento, as chamadas curvas p-y, para as quais diversas teorias foram desenvolvidas ao longo dos anos e são a base do dimensionamento do carregamento lateral das fundações de monoestacas instaladas em offshore.

De modo a obter a reacção do solo, p, em resposta a um deslocamento, Y, foi explorada a hipótese de uso de uma equação diferencial que expressa a reacção do solo em função da derivada de quarto grau do deslocamento. Foi concluído que esta metodologia será fiável caso as deformações não sejam demasiado elevadas ao ponto de introduzir plasticidade no solo mobilizado – como pode ser o caso de estacas flexíveis, com grande esbelteza - mas revelou-se ineficaz para estacas rígidas uma vez que não existe forma de ter em consideração a plasticidade do solo.

Mantendo, contudo, a possibilidade de integrar de tensões em torno da estaca, foi desenvolvido um modelo em PLAXIS® 3D de forma a representar, da forma mais realista possível, as interacções entre solo-estaca. Ao analisar os resultados dos dados exportados a partir do programa de elementos finitos, foi desenvolvida uma metodologia para o cálculo das curvas p-y, tendo em consideração a vasta informação obtida através de um significativo número de complexos cálculos numéricos, que mais tarde foi programado em MatLab®.

Depois de terem sido exploradas outras opções, a hipótese de uma curva hiperbólica foi considerada como sendo a mais apropriada para caracterizar o perfil dos resultados obtidos para as curvas p-y. Estes foram comparados com os resultados obtidos utilizando a metodologia proposta pelo American Petroleum Institute (API) tendo em conta , não só as curvas p-y reais , mas também os resultados para a capacidade de carga última e a rigidez inicial do solo.

Concluiu-se que a metodologia para a definição das curvas p-y usadas pelo API não é muito exacta já que subestima a capacidade do solo e a sua evolução em profundidade e não tem em consideração a rigidez inicial do mesmo. Concluiu-se também que o diâmetro das monoestacas tem grande influência na rigidez inicial do solo, sendo esta uma relação não-linear, ao contrário do que se verifica na resistencia das curvas em que não há dependencia nenhuma do diametro.

Finalmente, as conclusões mais relevantes são realçadas no final deste trabalho e posteriores desenvolvimentos são sugeridos neste tópico de investigação para estudos futuros.

PALAVRAS-CHAVES: Offshore, monoestacas, curvas p-y- efeitos de diâmetro, PLAXIS 3D, interação solo-estaca

TABLE OF CONTENTS

TABLE OF FIGURES

TABLE OF TABLES

SYMBOLS, ACRONYMS AND ABBREVIATIONS

A - Area (m^2)

c - Cohesion (kPa)

D – Diameter (m)

DNV – Det Norske Veritas

E - Elastic Modulus (kPa)

E_{50} – Secant Modulus (kPa)

E_{oed} - Oedometric Modulus (kPa)

G – Shear modulus (kPa)

I - Inertia (m^4)

L - Length (m)

k – Subgrade reaction modulus (kN/m^2)

k_s – Initial stiffness of the p-y curve (kN/m^3)

K – Coefficient of subgrade reaction (kN/m^3)

K_0 - At-rest earth pressure coefficient

M – Bending moment (kN.m)

N – Axial force (kN)

P – Soil pressure (kPa)

p – Soil reaction (kN/m)

p_u – Ultimate bearing capacity (kPa)

R_{inter} - Reduction of strength at the interface

S – Slope

S_u – Undrained shear strength (kPa)

V – Shear force (kN)

y – Displacement (y)

z - Depth (m)

ε_{50} – Strain at one-half of the maximum principal stress difference

σ - Total stress

ϕ - Curvature (m^{-1})

φ - Friction angle (º)

ψ - Dilation angle (º)

γ - Unit weight (kN/m^3)

γ' – Submerged unit weight (kN/m^3)

v' – Unloading-reloading *Poisson* ratio

1
INTRODUCTION

1.1. FOREWORD

Energy is the main 'fuel' for a social and economic development, and technology has become over the last two decades the main driver of this development. The rapid advancement of Information Technology (IT) all over the world has transformed not only the way we think, but also our daily behaviour, and all aspects of human life have been affected by IT and the internet, in particular.

Saying this, new ways of producing energy needed to be explored in order for its production could keep up with the development of society and the huge population growth of the last twenty five years (27% between 1993 and 2011).

Energy is the amount of force or power that when applied can move one object from one position to another or Energy defines the capacity of a system to do work and electricity way of energy. Although energy has been known since ancient times, it was never really given a second thought and the first experiments on electricity only appeared 250 years ago (1752) with Benjamin Franklin and his research. The discovery by Faraday of electromagnetic induction occurred almost 80 years later (1831) and it is still somehow used in modern power production – although on much larger scale.

Applications for electricity started to increase since then. It began with the telegraph, light bulb and telephone and continued with radio, television and many other house appliances. This situation led to the searching of new ways of producing energy explaining the increasing use of fuels like coal, gas and oil in power generation. According to the International Energy Agency (2014 Key World Energy Statistics), in 2012 the transports consumed 27.9% and the industry 28.3% of the worlds total produced energy.

The big use of non-renewable energy (energy sources that have a finite quantity and are not able to be replenished) started with the Industrial Revolution. The invention of the internal combustion engine in the 19th century transformed the Western world and led to eventual dependence on fossil fuels. Today, it is almost impossible to own an item that has been produced without the use of the energy generated by a fossil fuel, nuclear power plants or hydric sources – although nuclear energy is often though as a renewable energy, the uranium deposit on earth is finite and it produces radioactive waste.

Most of non-renewable energy resources have consequences upon the environment. The big emissions of carbon dioxide and other greenhouse gases created what we all know as the increase of the greenhouse effect that is leading to a global warming. The burning of these products also poison waterways and leach harmful toxins into the ground and water.

As these problems began to have a significant impact on the living conditions of our planet, mainly the changes on the weather of the seasons, people and the governments started to take action and try to prevent a catastrophe. The solution is renewable energies.

Figure 1.1 shows a comparison between the production of electricity using non-renewable resources and some renewable resources, through the years.

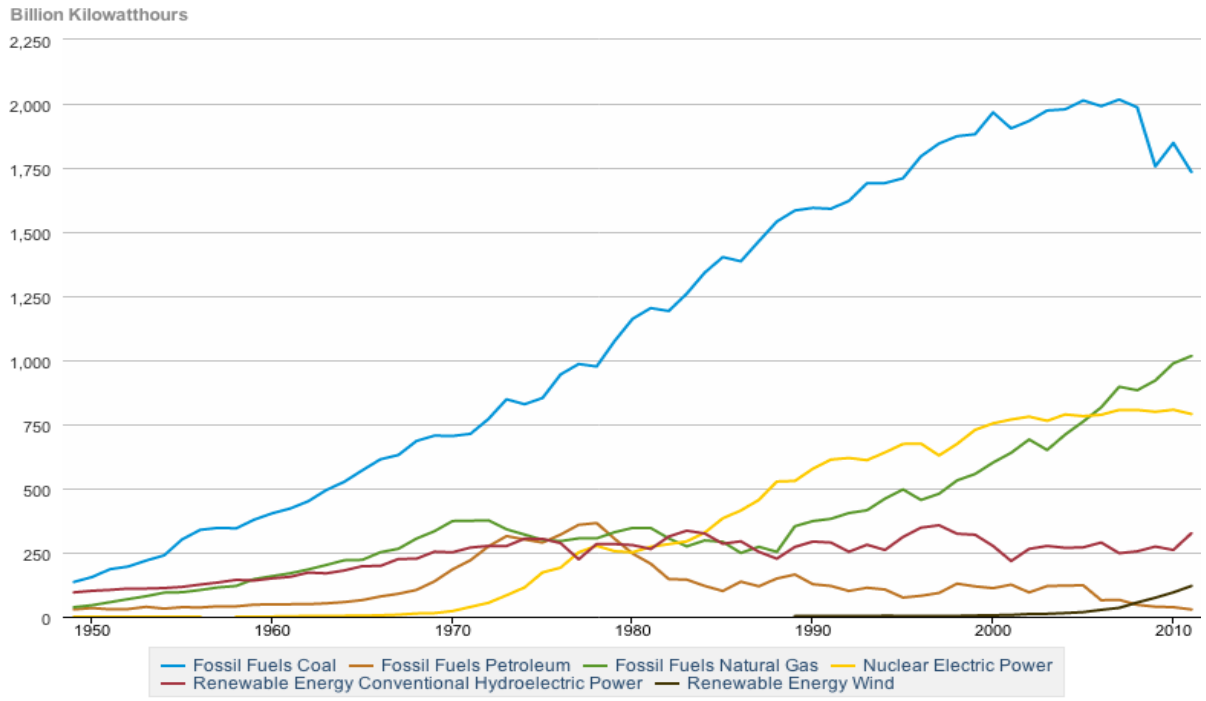

Fig. 1.1 – Comparison between the use of non-renewable and renewable resources to produce electricity, U.S. Energy Information Administration

A renewable energy is defined as an energy that comes from resources which are naturally replenished on a human timescale. Wind is one of these resources, together with sunlight, rain, tides, waves and geothermal heat. It is a source of clean, non-polluting, energy and it is becoming very popular in the last years and lots of investments are being made. The focus of this work is in the wind energy produced offshore. The offshore wind speed average is, more or less, 90% greater than on land.

As the market of offshore wind energy is increasing, many companies seek a more exact and reliable method for the design of the foundations of the wind turbines. When it comes to the lateral-load design, the current methods are based on experiments made on flexible piles while offshore foundations have a more rigid behaviour. This is leading to a lot of investigation by many experts on the field in order to find a more accurate way of describing the lateral load-response behaviour for the soil-pile interaction design. The common way of characterizing this load-response behaviour is through what is usually called as p-y curves.

In the present work, a numerical and theoretical investigation of the soil pile interaction response is made and an analytical solution for the characterization of these p-y curves is suggested as a more accurate method of design for rigid piles that takes into account the diameter of the pile.

1.2. PERSONAL MOTIVATION

Regarding the personal motivation for this work many factors had an important role on it but the one that had the biggest impact was definitely the opportunity of going through such an important stage of my academic career in a recognized and internationalized company like COWI A/S.

The work that will be here presented is the thesis developed as part of the final project of the postgraduate academic master's degree at the Faculty of Engineering of the University of Porto (FEUP) in the specialization field of Geotechnical Engineering.

An agreement between Prof. Viana da Fonseca, from FEUP, and Ole Hededal, former professor at Danmarks Tekniske Unisersitet – DTU and current Technical Director of the Marine and Foundation Engineering Department of COWI A/S in Lyngby, Denmark, allowed me to move to Denmark and develop my Master's thesis within an international business environment.

COWI A/S is an engineering, economics and environmental science consulting group with offices all over the world involved in more than 17,000 projects at any given moment anywhere in the planet. It is one of the leading companies when it concerns transportation engineering like tunnels (Abu Hamour surface & groundwater drainage tunnel and the Doha Metro Red Line North Underground, both in Qatar), bridges (Izmit Bay Bridge in Turkey and Puente Nigale in Venezuela) and ports (Al Faw Grand Port in Iraq and Värtahamnen in Sweden) but it also participates in other huge projects (Sonaref Refinery, Angola). When it comes to offshore wind farms COWI also took part of very big projects like the London Array in the UK, the Thornton Bank in Belgium, the Horns Rev in Denmark and the Wikinger in Germany.

The chance of also contributing scientifically with new progresses on the methodology of the design of offshore wind turbine foundations was also a big motivational factor. Working with people who are seen as an international reference on the field of Geotechnical Engineering and contributed for the development and understanding of many unknown soil mechanics and behaviour through published paper on international magazines and conferences was greatly satisfactory.

1.3. OBJECTIVES

The following investigation is focused on a theoretical and numerical investigation of the soil-pile interaction. The purpose is to understand whether the p-y curves used for the design of monopiles foundations should depend on the diameter of these structures or if the current linear relation assumed between the diameter and the resistance of the soil is a correct postulation.

Saying this, the following objectives were established for this work:

- Become familiar with geotechnical design approaches for monopile foundation of offshore wind turbines;
- Perform literature review of state-of-art on behaviour of monopiles;
- Establish a 3D finite element method model (in PLAXIS 3D) of a monopile in uniform soil and simulate its response when loaded;
- Use MatLab to process the data obtained from the FEM model and calculate the soil-pile interaction to and applied load or imposed displacement;
- Identify the critical parameters based on sensitivity studies;
- Propose a new methodology for the characterization of the p-y curves used for the design of monopiles foundations

1.4. STRUCTURE OF THE DOCUMENT

In order to achieve a better organization for the presentation of the previously described objectives, this work was divided into 9 chapters, being this one the first in which a general idea about the thesis scope is given.

The first half of the 2nd Chapter is dedicated to a presentation of the wind energy industry. It is a chapter explaining how this energy resource was first used, how its technology evolved over the years and its pioneers, its nowadays role on the production of energy to supply the needs of our society and who are the current world leaders on the production of wind energy. A background on how offshore wind farms evolved over the last decades is also presented and, finally, a short introduction on its types of foundations is made.

Second part of Chapter 2 is where a more detailed description of monopiles, one of the types of foundation of offshore wind turbines, is presented. It covers general features like its mechanical characteristics – mostly by comparing rigid piles with flexible piles – but also more detailed aspects like its physical structure and pile testing for lateral loads.

The theoretical background comes in the 3rd Chapter. It starts with an introduction of how the Winkler method of using springs as a representation of the soil attached to a beam was first used as a method of design for laterally loaded piles and its progress over the years in terms of numerical and analytical solutions. After this, there is an explanation of what p-y curves are followed by a presentation of the suggested methods of characterization of p-y curves developed over the years for cohesive and cohesionless soil.

The 4th Chapter is the description of the 3D FEM model, developed in PLAXIS 3D, that represents a monopile foundation. This is a very important chapter in a way that every properties of the soil and geometry of the model is presented (and its choice justified) so that, in case of a continuation of the current work by another person, it would be possible to rebuild the models and then intervene on the aspects that wish to be studied (e.g. sensitive studies that were not carried out).

The 5th Chapter is where the forth order differential equation developed by Hetenyi (1947) is explored as a hypothesis of getting to the subgrade reaction of the soil, p, from the displacement of the pile, y. This equation describes a relationship between the soil reaction and its displacement and it was applied to the results obtain from PLAXIS 3D and complemented with a structural analysis on SAP2000.

After labeling the hypothesis explored on the 5th Chapter as unsuitable for the case being here studied, the 6th Chapter describes how the results obtained from PLAXIS 3D were processed on MatLab and used to integrate the stresses around the pile in order to find the subgrade reaction of the soil in response to the applied displacement. It is also in this chapter that the resulting p-y curves from the FEM model are presented and the analytical solution for the curve that best fits the obtained outcome is shown. It is also in this chapter that the first comparison between the obtained results and the API method is made.

Chapter 7 is dedicated to sensitivity studies on the PLAXIS 3D model and a suggestion for a new method of characterization of the p-y curves. After having defined on the previous chapter that an hyperbola was the type of curve that best fits the results from PLAXIS 3D, some models were run changing some parameters in order to find which ones affect the most the results of the p-y curves. Also, different diameters were tested for the foundations of the monopiles and its effects were explored, which is in fact the main propose of this thesis. Having compared all these sensitivity studies and found consistency of the results, a comparison with the p-y curves from the API is carried out and suggestions to its method are made.

Finally, Chapter 8 summarizes the main conclusions of this thesis and some perspectives of future research are pointed out as important complements for the work that was here developed.

2
WIND ENERGY INDUSTRY

2.1. BACKGROUND AND EVOLUTION

Wind power has been used for human benefits since man started to explore the sea using sailboats. Although sailors didn't have the physics to help them understanding the mechanics of wind, their empirical achievements were very important for the later development of windmills.

Windmills were the first big progress regarding wind-powered machines and they were used to grind the grains and to pump water. There is few information about this subject from the ancient years so the first known windmills go back to the time of the Persians (500-900 B.C.) and they were used for water pumping. The design was of the vertical axis system – vertical sails attached to a central vertical shaft by horizontal struts (Figure 2.1). These systems were also used in China. They claim that China was the birthplace of windmills and that they were first used more than 2000 years ago but there is no documentation to prove that.

In Europe the first illustrations date back to 1270 A.C. and the design is based in a horizontal axis system with four blades mounted on a central post, much more efficient than the vertical ones. 120 years later the Dutch attached these 'postmills' to a tower (towermill) that used the different floors to different tasks (grinding grain, removing chaff, storing grain, etc). In Greece, in the island of Crete, windmills are still used to pump water for crops and livestock (Figure 2.2).

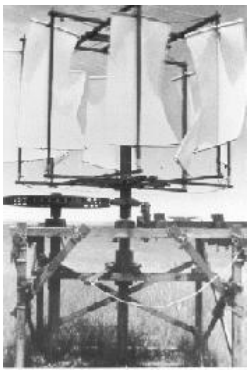

Fig. 2.1 – Windmills with vertical axis system

Fig. 2.2 – Windmills in Crete, Greece

Over the years the windmill sail was improved in many ways and modern designers recognize that after 500 years this process was already completed and all the major features crucial to the performance of modern wind turbine blades were present on these structures. Windmills were very important on the pre-industrial Europe as they were used to several applications like waterwell, irrigation and drainage pumping, grain pumping, saw-milling of timber, and processing of many spices as cocoa, paints and

dyes, and tobacco. During the 19th century, due to the appearance of the steam engines, the use of tower mills declined.

It was only in 1888 that Charles F. Brush first used wind power to produce electrical energy. He incorporated a step-up gearbox in order to turn a direct current generator at its required operational speed but it was still very limited in terms of low-speed and high-solidity rotor for electricity production applications. In 1891, an electrical output wind machine was developed with aerodynamic design principles (resulting in low-solidity rotors) but cheaper and larger fossil-fuel steam plants soon put these machines out of business. In Denmark there were about 2500 windmills by the end of the century and by 1908 there were more than 70 wind-driven electric generators from 5kW to 25kW.

By 1920, the two dominant rotor configurations were labelled as inadequate for generating enough amount of electricity. Yet, small electrical-output wind generators (1 to 3 kilowatts) found a lot of use in the rural areas of the US in some small applications like lighting farms and charge batteries used to power crystal radio sets and later they were extended to refrigerators, freezers, washing machines and power tools. However, due to the increase of the demand of farms for even larger amounts of power and also because the government extended the electrical grid to those areas (because of the New Deal), these systems felt into disuse again. In Australia small hundreds of small wind generators were also produced to provide power at isolated postal service stations and farms.

The world's first megawatt-size wind turbine (1.25MW) was connected to the local electrical distribution system in 1941 (Vermont, USA) and it was only on 1978 that a multi-megawatt wind turbine was created (2MW).

During the Second World War, small wind generators were used to recharge submarine batteries as a fuel-conserving measure. In Europe, after the World War II, the developments on wind energy continue when temporary shortage of fossil fuels led to higher energy costs particularly the post war activity in Denmark and Germany, which was largely important for the future of horizontal axis design of wind turbine.

During the 70s, many people begun to search and rebuilt farm wind generators from the 1930s, as they desired a self-sufficient life-style and solar cells were too expensive for small-scale electrical generation. From 1974 through the mid-1980s the US government worked with industry to advance the technology and enable large commercial wind turbines. Research and developments programs pioneered many of the multi-megawatt turbine technologies in use today. When oil prices declined by a factor of three from 1980 through the early 1990s many turbine manufactures, both large and small, left the business.

Energy security, global warming and possible fossil fuel exhaustion led to an expansion of interest in renewable energy at the beginning of the 21st century. Each year more and more investments are made on the wind energy and it is nowadays the fastest developing renewable energy in the world, with the US leading the way. This energy source is considered by many experts as the only renewable energy source which can compete in price with coal and other fossil fuels, and the price of wind power technologies is expected to continue to decline in years to come.

During the year of 2014, 11.791 MW of wind power was installed across the European Union from which 10.308 MW were onshore and 1.483 MW were offshore. The biggest investor country of 2014 was Germany (with more than 5.000 MW), followed by UK (with more than 1.700 MW of which almost 50% were offshore) and then Poland and Sweden both with a little bit more than 1.000 MW.

Overall, during 2014, 26,9 GW of new power generating capacity was installed - 21,3 GW of renewable energy - in EU in which 43,7% were from wind power and 29,7% from Solar Photovoltaic System (8

GW). Since 2000, 412,7 GW of new power capacity has been installed in the EU and of this, 29,4% is from wind power and 56,2% is renewable energy.

Figure 2.3 shows the evolution over the 21th century of the investment of the United States of America on wind energy and Figure 2.4 compares, also in the US, the investment made between the onshore and the offshore wind energy.

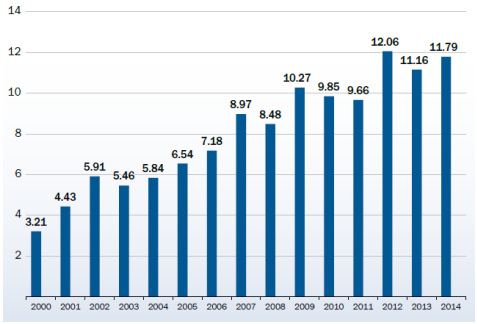

Fig. 2.3 – Annual wind power installations in the EU

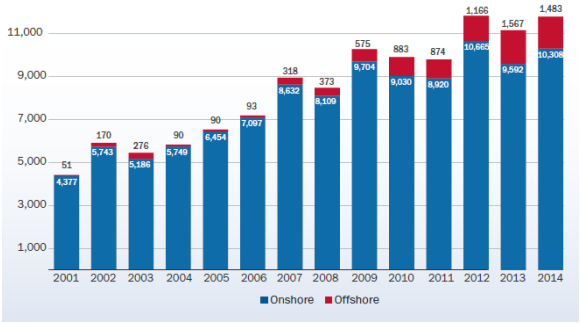

Fig. 2.4 – Annual wind power installations onshore vs offshore

On a global level, 51.477 MW of wind power capacity were installed in 2014. China leads the top 3 with 23.351 MW installed wind power capacity, followed by Germany in second and the USA comes in third place with 4.854 MW. The world total installed wind power capacity is 369,6 GW with China again leading the top 3 with 114,8 GW, followed by the USA with 65,9 GW and then Germany with 39,2 GW.

Denmark, who was once a pioneer in the field of wind energy, is not a world leader anymore. However, its wind turbines delivered in 2014 an equivalent to 39,1% of Danish energy consumption which is a 'world record'.

In Portugal (Madeira and Azores included), in 2013, the wind power capacity was of 4,731 MW a total share of electricity consumption of 23%, saving nearly 8,182,900 tons of carbon dioxide emissions.

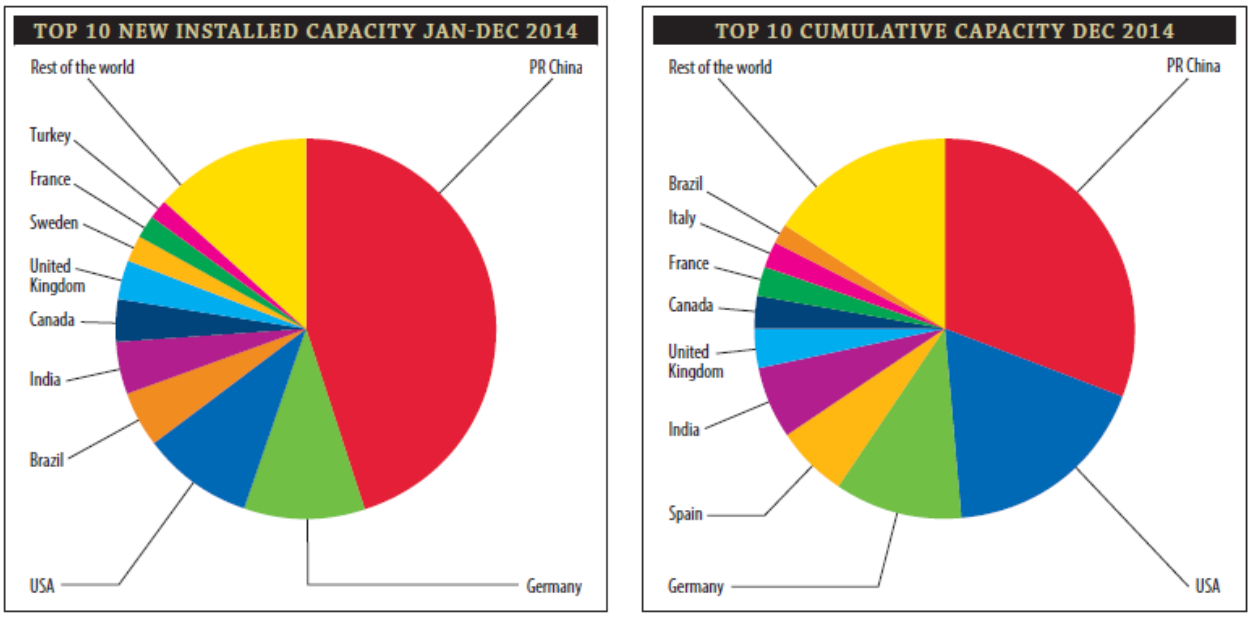

Fig. 2.5 – Global Wind Energy Statistics

2.2. OFFSHORE WIND ENERGY FARMS

The first wind farm – group of wind turbine at one only location which are interconnected and are used for production of energy – was built in 1980 in New Hampshire. It consisted on 20 wind turbines with a capacity of 30kW each (600kW total) but it is not working anymore. Today, the biggest wind farm in the world is the Gansu Wind Farm in the Gobi desert, China, with a capacity of over 6000 MW of power in 2012 and a goal of 20000 MW by 2020. The largest offshore wind farm in the world is the London Array wind farm in England with a capacity of 630 MW.

In Portugal, the first offshore wind farm near Póvoa de Varzim (the Windfloat farm) is planned to be finished by 2018 and should be able to produce enough energy to provide energy to the whole city of Castelo Branco (40 thousand families).

Wind farms are not an economically viable renewable solution in all parts of the world as they depend a lot on the frequency and speed of the wind. This is the main reason why experts believe that the future of the wind energy lies offshore where winds blow 40 percent more often than on land. Yet, due to extreme weather conditions, offshore wind turbines have much higher construction costs than onshore.

Offshore wind farms have significantly smaller negative impact on aesthetics of the landscape compared to wind farms onshore because most offshore wind farms are not visible from shore. When constructing an offshore wind farm it is important to consider whether the nearby ecosystems will be disturbed or not. The interference with shipping lanes or fishing areas must also be taken into account.

Europe has already started huge offshore wind power expansion with the United Kingdom leading the way followed by Germany and Denmark. China is also starting some big investments and the US is seriously considering this clean energy as an option.

Siemens (German multinational conglomerate company and the biggest engineering company in Europe) and Vestas (Danish company and the largest in the world manufacturer, seller, installer and servicer of wind turbines) are the leading turbine suppliers for offshore wind power and DONG Energy (Denmark largest energy company), Vattenfall (a Swedish government's company) and E.ON (European holding company) are the leading operators.

Figure 2.6 shows the biggest producers (countries) of offshore wind energy worldwide and its evolution between the years of 2013 and 2014.

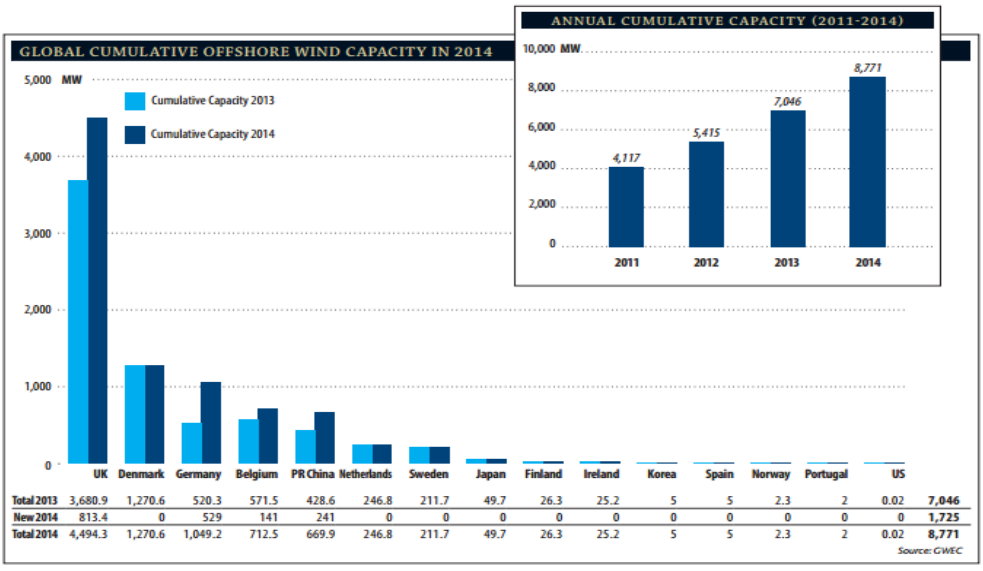

Fig. 2.6 – Global Offshore Wind Energy Statistics

2.3. OFFSHORE WIND TURBINES FOUNDATIONS

Offshore wind turbines need to be fixed to the seabed with a permanent or semi-permanent support structure. For deep waters a floating structure is used but the most common ones are the fixed foundations used to shallow depths (up to 50 meters). The foundation at the bottom of the turbine transfers loads into the soil so its design is of extreme importance for the good performance of the structure. There are five types of foundations: Jackets; Gravity foundations; Tripods; Tripiles; and Monopiles. Figure 2.7 shows different types of foundations for wind turbines depending on the depth of the water.

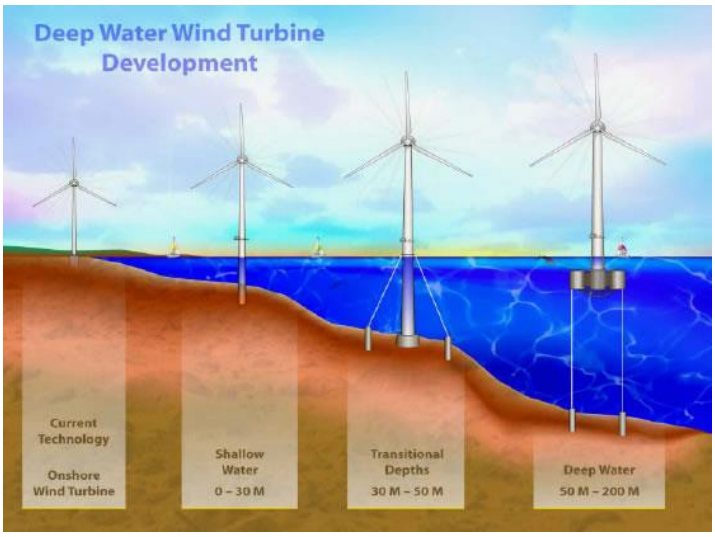

Fig. 2.7 – Different types of foundations for offshore wind turbines according to the depth of the water

2.3.1. MONOPILES

Monopiles are large diameter (4 to 6 meters), thick walled, steel tubular structures. They are currently the most common foundation in shallow water (< 30 meter) and will be the scope of this thesis.

2.3.2. JACKETS

A jacket (Figure 2.8 (a)) is a three or four-legged steel structure with corner piles interconnected with bracing with diameters up to 2 meters to provide the required stiffness. These structures can be used for deep water (100 meters) but, according to the DNV, they should be used between depths of 20 to 50 meters.

2.3.3. GRAVITY FOUNDATIONS

Gravity foundations (Figure 2.8 (b)) are concrete structures that use their weight to resist wind and wave loading. They require a ballast to anchor the foundation and are typically used at sites where installation of piles in the seabed is difficult, such as hard rock or competent soils in shallow depths. Concrete is much cheaper and is more durable in the marine environment than steel so these structures are cost-effective when the environmental loads are low or when additional ballast can be provided at a reasonable cost.

2.3.4. TRIPODS

A tripod (Figure 2.8 (c)) is a relatively lightweight three-legged steel jacket connected to a central pipe foundation that absorbs the wind energy turbine. These structures have good stability and overall stiffness and are suitable for 20 to 80 meters

2.3.5. TRIPILE

The tripile structure (Figure 2.8 (d)) is a three-legged jacked structure in the lower section, connected to a monopile in the upper part of the water column, all made of steel tubes.

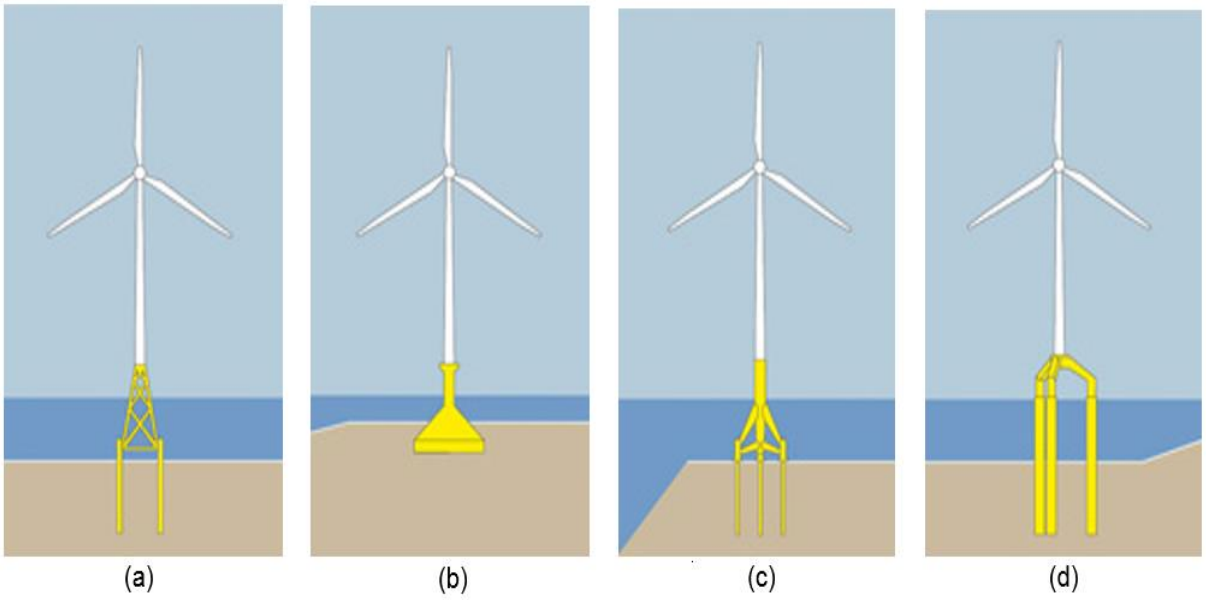

Fig. 2.8 – Different types of foundations for offshore wind turbines: jacket (a), gravity base (b), tripod (c) and tripile (d)

2.4. MONOPILES

In up to 30 meters of water with a firm seabed, monopiles are the most commonly form of foundation used nowadays for offshore wind turbines. These giant steel hollow cylindrical tubes range usually from 2,5 to 6 meters in diameter, are 50-60 meters long and weight around 500t (although on deeper sites they can weight more than 800t). It is filled with soil or concrete if a greater resistance is required.

Its shape lends itself to simple calculations, straightforward fabrication and tight packing on transport vessels. It is also easier to install at shallow to medium water depths and relatively cheap compared to the other types of foundations.

Figure 2.9 (a) shows an installed monopile foundation (dark part under water), with the transition piece already slided in on the top (yellow part), to which the turbine's tower and the rest of the required equipment (access ladders, J-tubes, crane) can be bolted – the description of each of these components will be further given. Figure 2.9 (b) illustrates the transportation of a monopile using trucks and gives an idea of the size of these structures.

Fig. 2.9 – Monopile installed (a) and its transportation (b)

This single pile is driven into the seabed by impact driving (using a hammer blowing system – hydraulic or pneumatic – striking on the protected head of the pile) or by vibratory driving (vibrating pile drivers are fixed at the head of the tube). These equipment operate from a platform that has to be able to keep its correct vertical position. A wind turbine must be designed to resist to its self-weight load – essentially associated to its vertical capacity – and the environmental loads like wind and waves – mostly transversal, therefore conditioning the lateral capacity. The focus of this thesis is directly related to the design of this lateral capacity.

Because of their large diameters, the length/diameter ratio of these monopiles is usually very small. Therefore, these structures tend to behave like short and rigid piles instead of long and flexible ones. There some significant differences of behaviour between these two types of piles: 1) the failure mechanism (Figure 2.10) for the rigid piles is due to the yielding ("fatigue") of the soil while for the flexible the ultimate load capacity is conditioned by the structural failure of the cross section; 2) while on the toe of the rigid pile there is a "kick" (a small reverse movement), on the flexible pile usually there is no movement on the lower part; 3) the rigid pile has a rotation point, mobilizing active and passive soil pressures over the total length of the pile, whereas the slender pile will deflect around several points (depending mostly on the geomechanical characteristics of the soil layering) leading to soil pressures mostly concentrated in the upper layers, as systematically depicted in Figure 2.11.

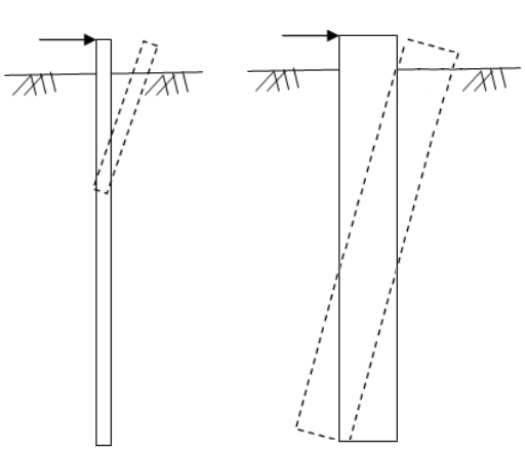

Fig. 2.10 – Failure Mechanisms and 'toe kick'

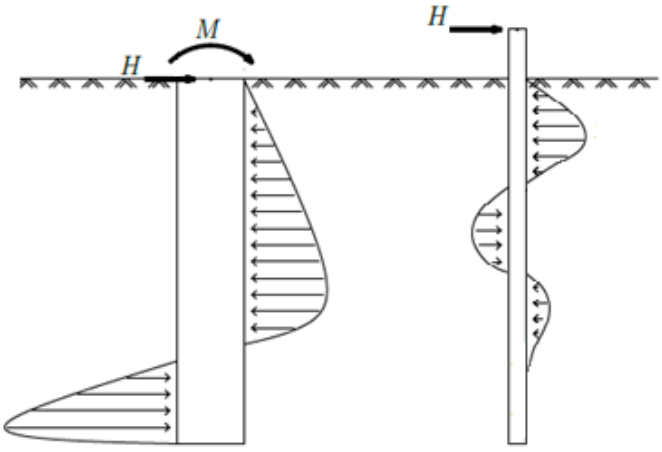

Fig. 2.11 – Soil pressures

The design of rigid piles has been largely discussed over the last years. According to most of the researchers, for the design of flexible piles the best approach is the use of p-y curves. Notwithstanding, for the monopiles of offshore wind turbines – rigid piles systems – although this methodology is not adequate, being less accurate, it has been used frequently with unreliable results. This p-y- method is actually the Winkler model applied on a beam with non-linear springs that represent the soil behaviour for discrete intervals, that is, corresponding to distinct soil layers in depth (which does not mean different types of soils, but different soil behaviour layers, as conditioned by the evolution of the stress state in depth). Finite element method became recently more popular, as it tends to be more representative of the involved factors. Moreover, the codes are becoming more friendly, slowly resolving the trend to use the Winkler method, popular for its simplicity, its ease application and the small required time for the calculation (finite element models are still not very popular for engineering design due to their time-demanding calculations).

2.5. COMPONENTS OF A MONOPILE

2.5.1. TRANSITION PIECE

The transition piece has three different functions: to add a perfect flange on top, to level the transition tower and to provide the whole structure with a boat landing, stairs and a working platform. The process of pile driving (usually hammering) always leads to some tilt of the monopile so the transition piece keeps it perfectly vertical.

It consists of a sleeve, usually with a larger diameter than the monopile (the opposite is possible but impractical for mounting external equipment), placed around it. The overlap length is of 1.5 times the diameter with a gap between the tubes that allows the transition piece to be vertical. The lower and bigger part of it is grouted up to the monopile. This steel cylinder extends between 4 up to 12 meters above sea level.

2.5.2. GROUTED CONNECTION

To fix the transition piece in place, grout (high-strength, fast-curing cement) is injected into the annular gap between the transition piece and the monopile.

The grouted joint (see Figure 2.12) between the transition piece and the monopile must be capable of supporting the weight above it (the transition piece itself, the turbine's tower and other components) and to resist the compression induced by the bending moments and shear induce by torsion in order for them to be transmitted to the monopile.

The union between the grout and the steel cannot exclusively depend on grout's adherence to steel. Connectors must be used to assure that the steel and grout work together and they transmit each other the longitudinal shear forces. The quantity and distribution of connectors depend on the resistance capacity of them so a structural analysis must be conducted.

These connectors can be either key connectors or shear connectors, although the first ones lead to stress concentrations around the welded zones and consequently critical areas when considering lifetime estimation of the structure.

2.5.3. EMBEDMENT

The soil in which the monopile is embedded has to be treated as a flexible medium that allows lateral movement and flexure of the pile below seabed. This consideration, which is very realistic, may have big impact on the natural frequency of the structure because its effective fixed level is lower the seabed level.

Monopiles do not need any preparation of the seabed for their installation but are not suited for locations with many boulders in the soil. Still, in the case of encountering a boulder while piling, it is possible to drill it out and blast it with explosives.

The interaction between the pile and the soil is usually modelled using nonlinear lateral springs, known as the p-y curves.

2.5.4. SCOUR

Scour occurs when floodwater passes around an obstruction in the water flow. As the water flows around the object, it must change direction and accelerate. Soil can be loosened and suspended by this process and be carried away.

In the case of monopiles, currents and water motion due to waves will cause significant seabed erosion around it if the seabed is formed of sand or another granular material. This phenomenon would certainly have implications for the stability of the foundations and natural frequency of the support structure. Yet, some projects have been design to accommodate scouring with appropriate allowance in the design for the resulting reductions in the overturning resistance and support structure natural frequency. The occurrence of scour might lead to two problems: damages on the transition piece coating, secondary structures or subsea cables; and the need for occasional replenishment and possible increased environmental impact due to increased volumes of material imported to site.

A design aid for scour whole depth prediction and scour protection design, known as Opti-Pile Design Tool, has been developed and calibrated using model test results and data from existing wind farms. This calculates the size of rock that is stable under maximum current conditions and the required radial extent of the protection.

2.5.5. CORROSION PROTECTION

The approach for corrosion protection is different for the three different zones in which the structure is divided: atmospheric zone, splash zone and submerged zone, which includes the embedded portion.

DNV-OS-J101 (design of submarine pipeline systems) requires the steel monopile to be protected by a high quality multi-layered surface coating in the atmospheric zone. In the splash zone, in addition to the surface coating, it requires an extra plate thickness to be provided as a corrosion allowance. Cathodic protection must be provided to the submerged zone together with a 2 mm corrosion allowance in the scour.

2.5.6. CABLE DUCTS

The wind turbine power cables are routed through steel protective tubes known as J tubes, which may be located either inside or outside the transition piece/monopile. The J tubes are so called because they incorporate a 90º bend ate seabed level to enable the cable to exit horizontally.

2.6. MONOPILE DESIGN

The sizing of the monopile is governed by three key factors: resistance to extreme loads, resistance to fatigue loads and tuning of support structure natural frequency to avoid excitation by cyclic loading.

Wave and wind fatigue loads depend on the support structure mode shape which in turn depends on the stiffness distribution so the design of monopile against fatigue loads is inevitably an iterative process. It is simpler to develop an initial design based on resistance to extreme wave and wind loads which can then be used to obtain an initial mode shape and set of fatigue loads.

The other key design factor is the restriction on support structure natural frequency and it is often best to take it into account early on in the process of design iteration.

2.7. LATERALLY LOADED PILE TESTING

A horizontal load test on slender piles is carried out to determine the lateral bearing capacity of the soil and the best way to evaluate it is by measuring the bending moment of the pile and then obtain the soil reaction using the second derivative of the bending moment.

For a short and rigid pile the horizontal load test is carried out to determine bearing capacity of the soil, as the failure occurs due to ultimate capacity of the soil. So, if the pile shaft is properly instrumented, it allows the determination of the transfer curves of the side pressure (the so called p-y curves), which best represent the behaviour and failure of the soil.

The most common test procedure is the incremental load test in which the load is applied by steps and in each step the load is kept constant for a certain time, enough to stabilize the associated displacement and measure a reliable value.

The application of the load is made by means of a hydraulic jack and a support to hold the jack horizontally is to be arranged (something heavy enough to stand still). The reaction of the jack is usually provided by another pile or by another set of piles (more commonly two piles connected by a beam).

The usual way to measure the displacement along the pile shaft is to install an inclinometer tube along the axis of the pile or to fit strain gauges on various depths of the pile on two opposite peripheral fibres to measure the strains. In both cases the curvature of the pile is obtained, allowing the determination of the bending moments, shear forces and soil pressure by derivation. It is also imperious to measure the absolute value of the displacement of the pile-head, which can be done by topographic means.

The degree of constraint at the pile head must be taken into proper account. During the test, the head of the pile is free to rotate while in real cases the pile cap or a load applied at a higher level (not the ground level) introduces moments at the head.

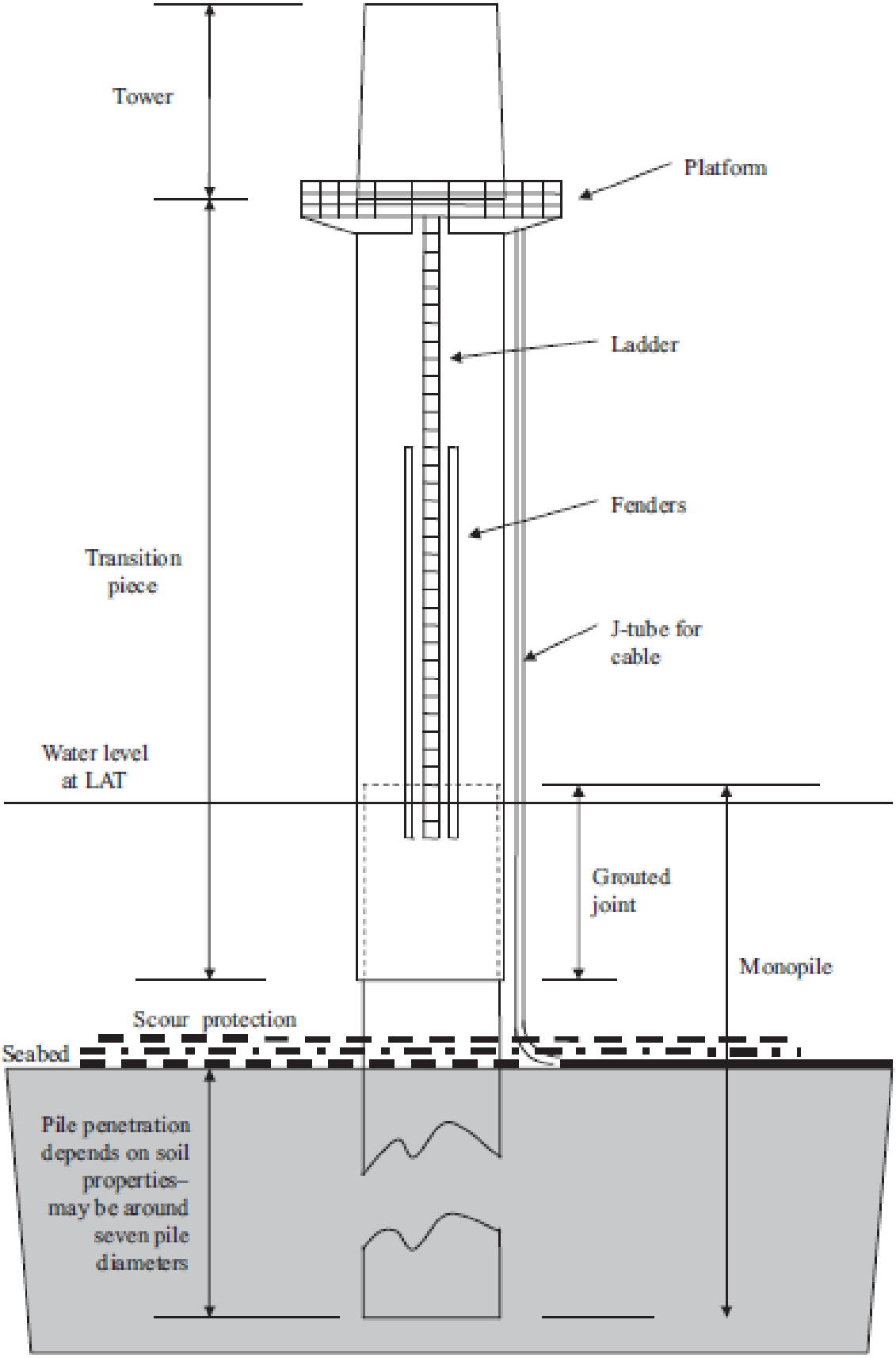

Fig. 2.12 – Typical arrangement of Monopile and Transition Piece

2.8. FINAL COMMENTS

The relevance of monopiles in nowadays offshore wind structures is, as stated before, very large and it is critical that its design is not oversized as it might lead to extremely high costs. For this reason, many researchers focus on the investigation of the interaction between these pile with large diameters and the surrounding soil in order to better understand this relation and improve its methods of design and achieve better performances.

Big investments are predicted in the industry of offshore wind energy, as this is one of the most clean and cheap renewable energy, so it is essential that this field of engineering is deep explored so that the companies and the governments feel confident to participate in these big projects.

3

THE WINKLER METHOD AND THE P-Y CURVES

3.1. OVERVIEW

Offshore wind turbines are always subjected to very significant lateral load induced by the waves and by the wind. Therefore, the foundations of these structures are likely to suffer horizontal displacements. A precise prediction of these displacements on these rigid foundations is being investigated by many researchers from all over the world since the second half of the 20th century. For this, two types of models were developed over the years - discrete models and continuum models – and both have their advantages and disadvantages.

In a discrete model the pile is divided into layers, corresponding to soil layers with prospectively distinct soil-structure interaction response, and in each layer there is a spring (primarily elastic or, more correctly, inelastic) representing the soil interacting with the pile and independent from all the others. This means that the displacement of one point of the pile is not affected by the displacements of the other points. The most famous discrete model is the Winkler model and, nowadays, this methodology has been used by most engineers in design of monopiles foundations, although quite demanding in calculation.

A continuum model takes into account the continuity of the soil so the displacement at any point is influenced by and influences all the other points. The two more common applications of this model is the finite element approach and the elastic continuum approach. Therefore, this type of model is much more realistic, when compared to the Winkler method.

3.2. WINKLER MODEL

Winkler (1867) suggested that the resistance that the ground offers against an external force is proportional to its deflection. He formulated his hypotheses as a beam interacting with a linear elastic support which was later adapted to a pile foundation with a lateral load as these two cases can be perfectly compared (Figure 3.1).

While there are no loads acting on the pile, the surrounding soil remains in at rest stresses state. The idea is that, as the load starts to increase, the structure tends to deviate more and more from its initial position and that introduces additional stresses on the soil. The higher the load, the higher reaction offered by the soil.

This theory was first calibrated for slender (long) piles, although nowadays it has been indiscriminately used for the design of rigid (short) piles with diameters of more than 4 meters, in which their soli-structure interaction differs due to the high rigidity condition.

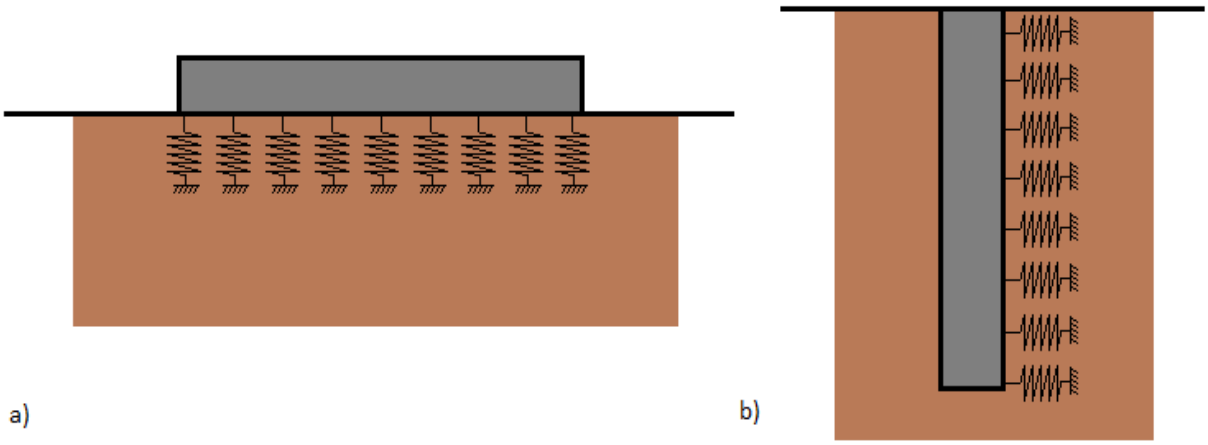

Fig. 3.1 – a) beam on an elastic support; b) pile foundation with subjected to lateral load

The springs represent the soil, so its deformation and consequently its force should be proportional. This method is also called subgrade reaction method because the constant of the spring can be assumed as the subgrade reaction modulus of the soil [FL^{-2}] (usually denoted by 'k'). This subgrade reaction modulus is described as the soil reaction (the force acting in each support point, distanced by one meter), p [FL^{-1}], per unit of displacement, y, (3.1). One other way of representing is by using the coefficient of subgrade reaction, K [FL^{-3}], which relates the pressure induced by the pile, P[FL^{-2}], with the displacement (3.2). The diameter of the pile, D, allows an interaction between these two formulations (3.3). The negative sign on the equation indicates that the soil reaction as an opposite direction to the displacement of the pile.

$$p = -k.y \tag{3.1}$$

$$P = -K.y \tag{3.2}$$

$$k = K.D \tag{3.3}$$

Because of its simplicity the Winkler method does not represent accurately the behaviour of the soil for this kind of problems. The lack of connection and dependency between the springs creates displacement discontinuities between the loaded and the unloaded part of the structure which does not represent the reality (Figure 3.2). This difficulty was later overcome by introducing some interaction between the springs and making the displacements of one spring dependent on the others surrounding it. The problem can be solved analytically or numerically. Yet the analytical solution has much more limitations than the numerical one, although it is easier to apply.

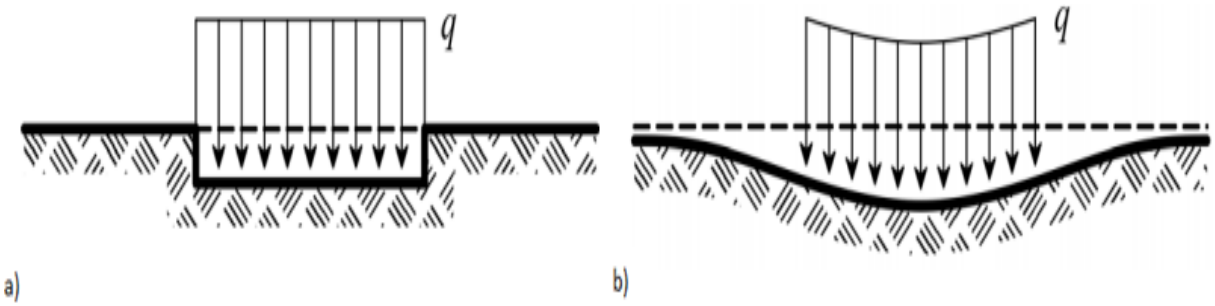

Fig. 3.2 – a) lack of connection between springs; b) interaction between springs – reality

3.2.1. Analytical Solution

Hetenyi (1946) developed a wave equation (3.4a) – affected by attenuation using the sine and cosine function – that represents the beam-on-foundation concept for the most generic case, which is an infinite beam.

The constants of the equation (C1, C2, C3 and C4) are dependent of the boundary conditions imposed to the problem. Therefore, in order to adapt it to the current problem, it is necessary to consider specific boundary conditions like 'y=0 for x=∞' (for this condition C_1=C_2=0). λ is given by the equation (3.4b) and it is equal to the inverse of the elastic length, L_e and k is the subgrade reaction modulus of the soil.

$$y = e^{\lambda z}(C_1 \cos \lambda z + C_2 \sin \lambda z) + e^{-\lambda z}(C_3 \cos \lambda z + C_4 \sin \lambda z) \tag{3.4a}$$

$$\lambda = \sqrt[4]{\frac{k}{4EI}} = \frac{1}{L_e} \tag{3.4b}$$

According to Broms (1964), for a pile with a free head, if the length of the pile, L, divided by β (equation (3.5)) is higher than 3.5 the pile is considered long or slender, if it is lower than 2 the pile is short or rigid.

$$\beta = \left(\frac{EI}{k}\right)^{1/4} \tag{3.5}$$

Equation (3.6) is the solution for a semi-infinite beam and Figure 3.3 shows the curves which strictly represent a slender pile. It is possible to obtain the shear force and the bending moment along the beam by triple and double derivation, respectively, of the deflection y (w in the figure). In equation (3.6), P is the applied force, E is the Young's modulus of the beam and I is the rotational inertia of the beam.

$$y = \frac{P}{2\lambda^3 EI} e^{-\lambda z} \cos \lambda z \tag{3.6}$$

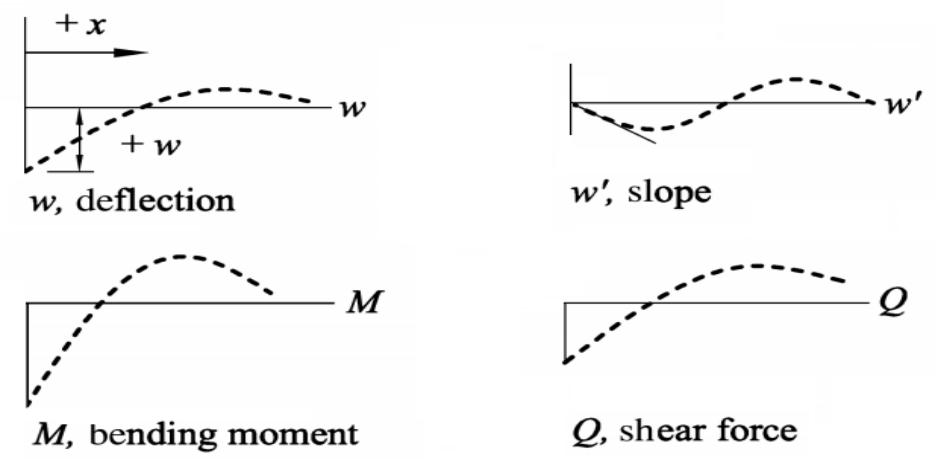

Fig. 3.3 – deflection, slope, bending moment and shear force curves for a semi-infinite beam using equation (3.6)

For slender and long piles, this type of solution is reasonable and very useful, since it gives the exact curves of deflection, bending moment and shear force. For a rigid and short pile this analytical solution is far from being accurate so other options must be found. This method is very limited because it does not allow, for example, the variation of the subgrade reaction modulus with depth, neither the consideration of non-linear behaviour of the soil.

3.2.2. Numerical Solution

The governing equation for the beam-on-foundation Winkler method is a forth order differential equation (3.7) that was developed by Hetenyi (1946). Knowing that the vertical load (N) is very small when compared to its critical buckling load this part of the equation is always despised so it's possible to get a more simplified equation that is actually used for the calculations. Equation (3.8) is obtained from equation (3.7) and equation (3.1).

$$E.I.\frac{d^4y}{dz^4} + N.\frac{d^2y}{dz^2} = p(z,y) \tag{3.7}$$

$$E.I.\frac{d^4y}{dz^4} + k.y = 0 \tag{3.8}$$

By using this forth order differential equation it is possible to obtain significant information about the problem. By solving of this equation, the curve of the soil pressure surrounding the pile can be obtained by integration, being also possible to get the curves of the shear forces, bending moments and the deflection along the pile. The critical design issue for pile foundations is generally the maximum bending moment installed on the pile, rather than its deflection, so this integration is really important. The relation between these curves is explained in Figure 3.4 and the following equations.

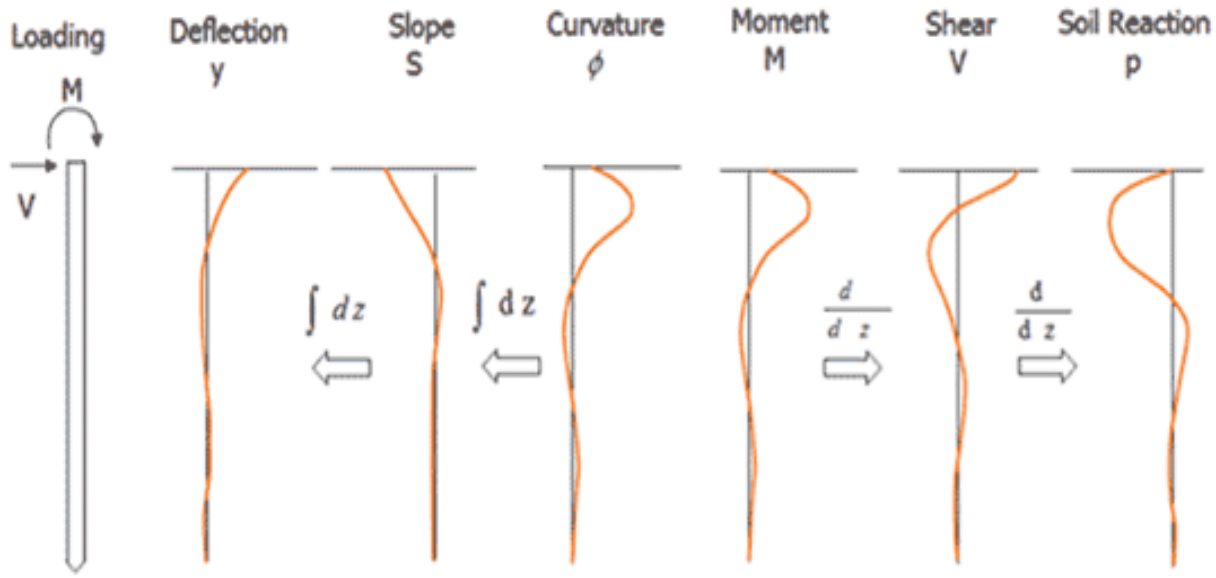

Fig. 3.4 – Relation between curves of deflection, slope, curvature, bending moment, shear force and soil reaction

Equation (3.9) represents the soil reaction, equation (3.10) the shear force installed one the pile, equation (3.11) the bending moment installed on the pile and equation (3.12) the slope of the pile.

$$p = E.I.\frac{d^4y}{dz^4} \tag{3.9}$$

$$V = E.I.\frac{d^3y}{dz^3} \tag{3.10}$$

$$M = E.I.\frac{d^2y}{dz^2} \tag{3.11}$$

$$\Phi = \frac{d^2y}{dz^2} = \frac{M}{E.I} \tag{3.12}$$

The best way to solve the differential equation (3.8) presented before is by using a method based on finite differences. By dividing the pile into several points (Figure 3.5) and discretizing the differential equation, it is possible to apply compatibility equations to almost all the points (points *0* to *n* in Figure 3.5) and boundary conditions to the others (points *-2*, *-1*, *n+1* and *n+2*). Equations (3.13) to (3.16) represent the discretization of the differential equation and equation (3.17) gives the compatibility condition between displacements.

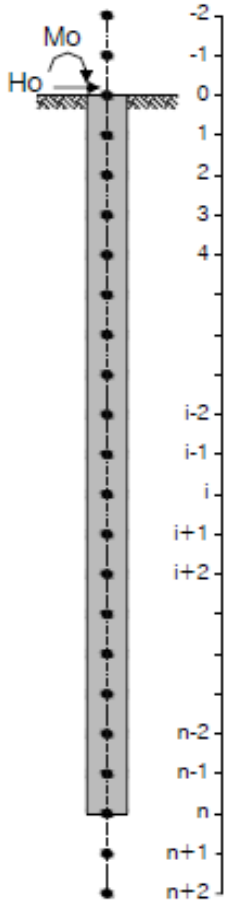

Fig. 3.5 – Discretized pile

$$\left(\frac{dy}{dz}\right)_i = \frac{y_{i-1}-y_{i+1}}{2h} \tag{3.13}$$

$$\left(\frac{d^2y}{dz^2}\right)_i = \frac{y_{i-1}-2y_i+y_{i+1}}{(2h)^2} \tag{3.14}$$

$$\left(\frac{d^3y}{dz^3}\right)_i = \frac{-y_{i-2}+2y_{i-1}-2y_{i+1}+y_{i+2}}{(4h)^3} \tag{3.15}$$

$$\left(\frac{d^4y}{dz^4}\right)_i = \frac{y_{i-2}-4y_{i-1}+6y_i-4y_{i+1}+y_{i+2}}{(4h)^4} \tag{3.16}$$

$$E_iI_i\left[\frac{y_{i-2}-4y_{i-1}+6y_i-4y_{i+1}+y_{i+2}}{(4h)^4}\right] + k_iy_i = 0 \tag{3.17}$$

The distance between each node is represented by *h* and there are *n+5* nodes, and consequently unknown variables, in which *n* is equal to L/h (being L the length of the pile). There are n*+1* real nodes, for which the compatibility equation is applicable (from *0* to *n* in Figure 3.5), and *4* fictional nodes. These *4* nodes demand the introduction of 4 more equations into the system which will correspond to the boundary conditions regarding the shear forces and the bending moment for both the top and the toe of the pile. Therefore, the number of equations is the same as the number of unknown variables, which are the displacements of each node y_i.

One other way of solving this type of problems is to apply the compatibility equation on the top and toe nodes of the pile and, instead, to add two equilibrium equations, one for the shear force and another for the bending moment.

This numerical method is much better than the analytical one since it allows for changes on the boundary conditions in almost every situations and it is also possible to change the stiffness of the soil with its depth and also the cross section of the pile. Because of this, the finite differences method is frequently used nowadays by engineers and it is very easily programmed on software codes like MatLab®.

3.3. P-Y CURVES

On the beginning of the second half of the 20th century several researchers decided to reformulate the Winkler method in order to take into account the nonlinear behaviour of the soil (McClelland and Focht (1956) were the pioneers). The previous linear springs were replaced by nonlinear ones and so the solution became much more realistic. The idea is that the value of the spring constant – the subgrade reaction modulus of the soil – changes with the deflection of the pile.

This was how the first p-y curves appeared in order to represent the nonlinear relation between the soil reaction, *p*, and the pile deflection, *y*. Figure 3.6 shows a typical shape of one of these curves. The ratio p/y represents the secant soil stiffness (secant modulus) and the slope of the curve represents the tangent soil stiffness (tangent modulus). These two parameters of the curves are usually used to define the nonlinear behaviour of the springs that represent the soil – e.g. in a finite differences program – by using progressive fitting/adjusting techniques in increment stress-strain variation, based on equilibrium (secant) and iteration (tangent). The curve always tends to an ultimate value of soil resistance, p_u, in which the soil will not bear additional load (ultimate or limit).

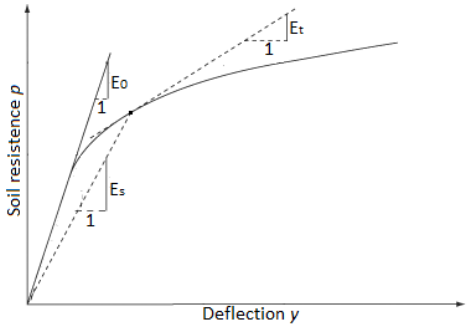

Fig. 3.6 – p-y curve

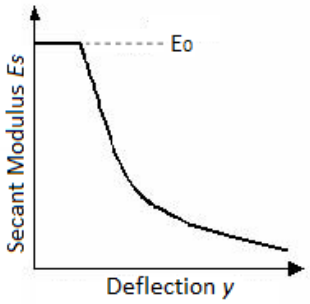

Fig. 3.7 – Variation of the stiffness of the soil

As the stiffness of the soil varies in depth (usually increasing) the p-y curves will be different along the pile length. This is represented as shown in Figure 3.8, with different p-y curves for different depths. The ultimate soil resistance is higher for deeper levels and, for the same deflection, both the secant and the tangent modulus are also higher in depth. Notice that, the bearing capacity of the soil increases with the depth due to the confining weight of the overlying material.

The problem with this method, and with any method that aims to reproduce an interaction along interfaces between distinct materials and largely dependent of several factors (installation processes and geometry, etc), is the determination of the curves that can represent the real behaviour. Because the soil stress-strain processes surrounding the pile evolve in a very complex and nonlinear way – taking into account the evolution of stiffness, the active lateral soil resistance by one side and the passive lateral soil resistance, by other, both related to friction and cohesive components (Figure 3.9), - many empirical solutions have arisen. Each of these solutions was developed by different researchers basing their work on very few full-scale lateral load on slender piles of diameters ranging from 0.30 to 0.40 meters: Matlock (1970) for soft clay, Reese et al. (1974) for sand, Reese and Welch (1975) for stiff clay above and below water table. The API (American Petroleum Institute) developed a design method for stiff clay, soft clay and sand based on some of these previous works and that is now the most popular method by geotechnical engineer.

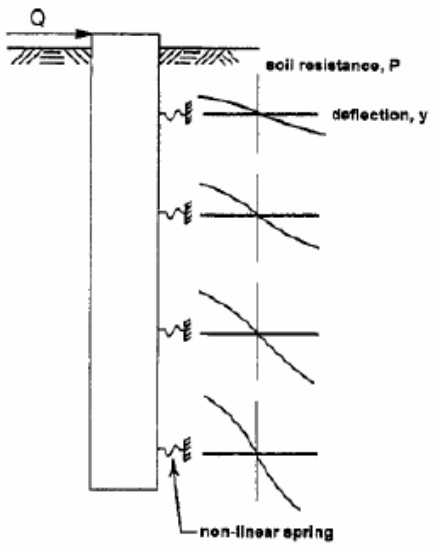

Fig. 3.8 – p-y curves along the length of the pile

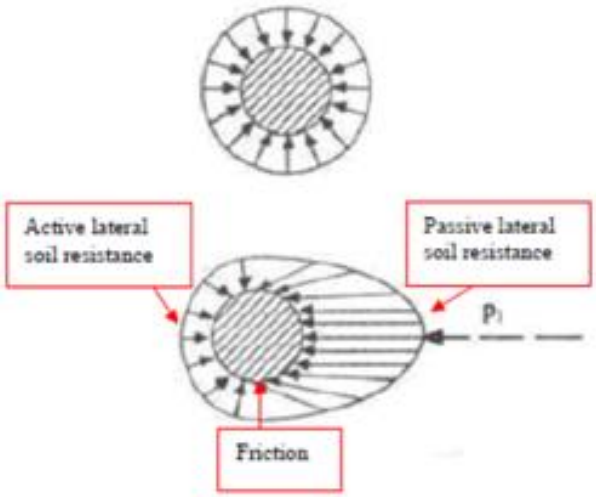

Fig. 3.9 – Development of stresses around the pile

3.4. RECOMMENDATIONS FOR P-Y CURVES IN COHESIVE SOILS

3.4.1. RESPONSE OF SOFT CLAY BELOW WATER TABLE

This method was developed by Matlock (1970). This author performed a few lateral load-tests with a slender steel-pipe pile (324 mm of diameter and 12.8 m long) in a lake in Texas, US. He used an extremely precise device to take the readings of the strain gauges so the soil resistance was found, through bending moment readings, by numerical differentiation. He also performed cyclic loading with a number of cycles at which there was no changing at all, or only a very small amount, in the deflection of the pile so he assumed that an equilibrium system was reached.

Steps a), b) and c) describe the procedure to obtain the p-y curves for short-term static loading and d) and e) for cyclic loading.

a) Obtain the best estimation of the variation of undrained shear strength, *Su*, of the submerged unit weight, γ', and of the strain at one-half of the maximum principal stress difference (maximum deviator stress) in an undrained triaxial test, ε_{50}.

b) Compute the ultimate soil resistance per unit of length of pile, using the smaller of the values given by the equations (3.18) and (3.19). *J* is an empirical constant determined to be 0.5 for soft clays and 0.25 for medium clays. *D* is the diameter of the pile.

$$p_u = \left[3 + \frac{\gamma'}{S_u} + \frac{J}{D} z\right] S_u * D \tag{3.18}$$

$$p_u = 9 * S_u * D \tag{3.19}$$

c) From equation (3.20) it is possible to calculate the deflection at one-half of the ultimate soil resistance. Equation (3.21) defines the relationship necessary to compute the p-y curves. The value *p* remains constant when *y* is larger than $8*y_{50}$.

$$y_{50} = 2.5 * \varepsilon_{50} * D \tag{3.20}$$

$$\frac{p}{p_u} = 0.5\left(\frac{y}{y_{50}}\right)^{\frac{1}{3}} \tag{3.21}$$

d) For the cyclic p-y curve the value of *p* is the same as for the static loading for values of p/p_u up to $0.72p_u$. Solve equations (3.18) and (3.19) simultaneously, taking into account the variation of S_u and γ' to find the depth z_r where the transition occurs.

e) If the depth to the p-y curve is greater than or equal to z_r. Select *p* as $0.72p_u$ for all values of *y* greater than $3y_{50}$. If the depth of the p-y curve is less than z_r, note that the value of *p* decreases to $0.72p_u$ at $y=3y_{50}$ and to the value given by equation (3.22) at $y=15y_{50}$ and remains constant beyond that.

$$p = 0.72p_u\left(\frac{z}{z_r}\right) \tag{3.22}$$

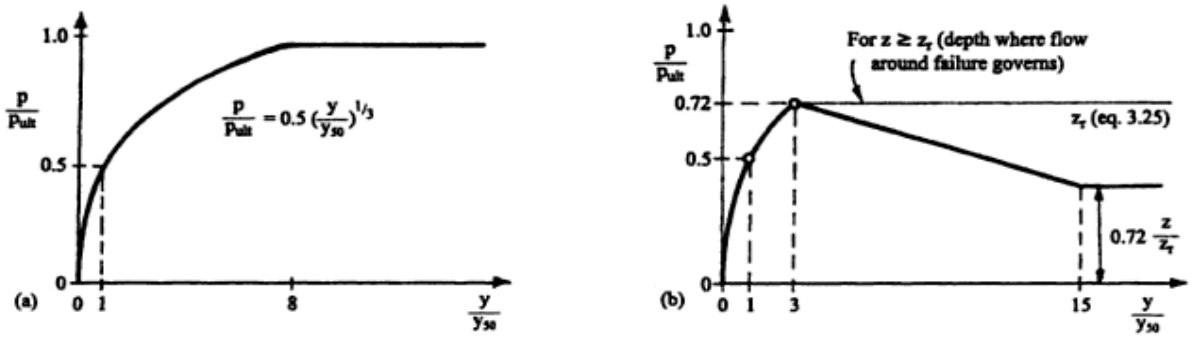

Fig. 3.10 – p-y curve for soft clay in the presence of free water: (a) static loading; (b) cyclic loading

3.4.2. Response of Stiff Clay Below Water Table

Reese and Welch (1975) performed lateral-load with steel-pipe piles that were 641 mm in diameter and 15.2 m long. The loading of the pile was carried out in a similar manner as described for Matlock's tests.

a) Obtain the best estimation of the variation of undrained shear strength, *Su*, the submerged unit weight, γ', and pile diameter D.

b) Compute the ultimate soil resistance per unit length of the pile using the smaller of the values given by equations (3.23) and (3.24).

$$p_{ct} = 2S_uD + \gamma'Dz + 2.83S_uz \tag{3.23}$$

$$p_{cd} = 11S_u D \tag{3.24}$$

c) Choose the appropriate value of *As* from Figure 3.11 for shaping the p-y curve.

d) Compute equation (3.25). Use an appropriate value of ε_{50} from results of laboratory tests or, in the absence of laboratory tests, from Table 3.1.

e) Establish the initial straight-line portion of the p-y curve using equation (3.25). Use an appropriate value of K_{py} from Table 3.1.

f) Establish the first parabolic portion of the p-y curve, using equation (3.27) in which p_c is the lowest value of equations (3.23) and (3.24). Equation (3.27) should define the portion of the p-y curve from the point of the intersection with equation (3.26) to a point where *y* is equal to $A_s y_{50}$.

g) Establish the second parabolic portion of the p-y curve. Equation (3.28) should define the portion of the p-y curve from the point where *y* is equal to $A_s y_{50}$ to a point where *y* is equal to $6A_s y_{50}$.

h) Establish the next straight-line portion of the p-y curve. Equation (3.29) should define the portion of the p-y curve from the point where *y* is equal to $6A_s y_{50}$ to a point where *y* is equal to $18A_s y_{50}$.

i) Establish the final straight-line portion of the p-y curve. Equation (3.30) should define the portion of the p-y curve from the point where *y* is equal to $18A_s y_{50}$ and it remains constant beyond that.

Note: Figure 3.13 (a) is drawn as if there is an intersection between equations (3.26) and (3.27). However, there may be no intersection of equation (3.26) with any of the other equations defining the p-y curve. Equation (3.26) defines the p-y curve until it intersects with one of the other equations and if no intersection occurs it defines the complete p-y curve.

$$y_{50} = \varepsilon_{50} D \tag{3.25}$$

$$p = (K_{py} z) y \tag{3.26}$$

$$p = 0.5 p_c \left(\frac{y}{y_{50}}\right)^{0.5} \tag{3.27}$$

$$p = 0.5 p_c \left(\frac{y}{y_{50}}\right)^{0.5} - 0.055 p_c \left(\frac{y - A_s y_{50}}{A_s y_{50}}\right)^{1.25} \tag{3.28}$$

$$p = 0.5 p_c (6A_s)^{0.5} - 0.411 p_c - \frac{0.0625}{y_{50}} p_c (y - 6A_s y_{50}) \tag{3.29}$$

$$p = p_c (1.225 (A_S)^{0.5} - 0.75 A_s - 0.411) \tag{3.30}$$

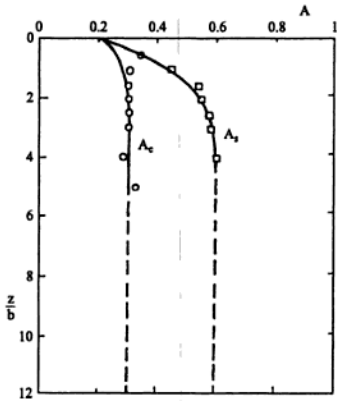

Fig. 3.11 – *As* and *Ac*; b is diameter

Table 3.1 – ε_{50} and K_{py}

	Average undrained shear strength kPa		
	50-100	100-200	300-400
$k_{py,s}$(static) MN/m^3	135	270	540
$k_{py,c}$ (cyclic) MN/m^3	55	110	540
ε_{50}	0.007	0.005	0.004

*The average shear strength should be computed from the shear strength of the soil to a depth of 5 pile diameters. It should be defined as half the total maximum principal stress difference in an unconsolidated undrained triaxial test.

A similar method is used for cyclic loading. Figure 3.12 shows a typical p-y curve under this type of loading and the following equations show how to draw it.

$$y_p = 4.1 A_c y_{50} \tag{3.31}$$

$$p = A_c p_c \left(1 - \left|\frac{y - 0.45 y_p}{0.45 y_p}\right|^{2.5}\right) \tag{3.32}$$

$$p = 0.936 A_c p_c - \frac{0.085}{y_{50}} p_c (y - 0.6 y_p) \tag{3.33}$$

$$p = 0.936 A_c p_c - \frac{0.102}{y_{50}} p_c y_p \tag{3.34}$$

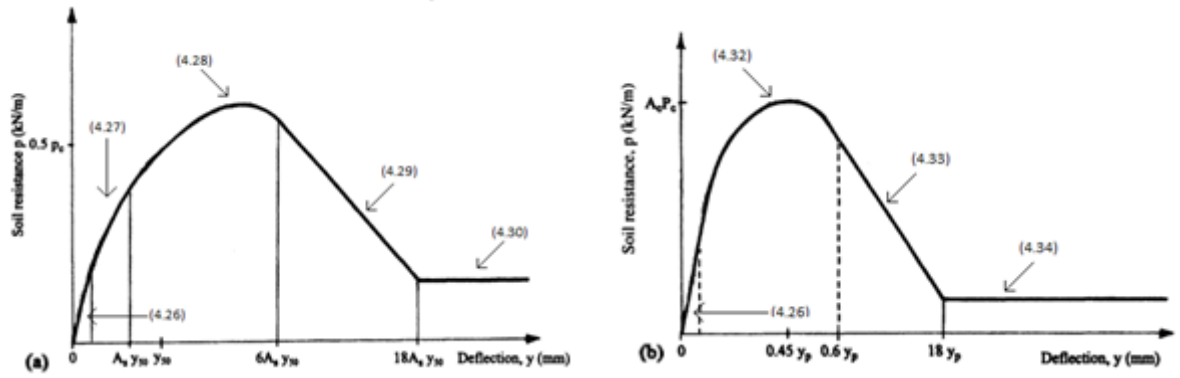

Fig. 3.12 – p-y curve for stiff clay in the presence of free water: (a) static loading; (b) cyclic loading

3.4.3. Response of Stiff Clay Above Water Table

The case here described is not related to the one explored in this work as the water level is below the area of study. Yet, it was chosen to include it here in order to have a more complete work about this topic.

Also in 1975, Reese and Welch performed a lateral-load test at a site in Houston with a bored pile 915 mm in diameter and an embedded length of 12.8 m. A pipe with a diameter of 254 mm, instrumented along its length with electrical-resistance-strain gauges, was positioned along the axis of the pile before concrete was placed.

The same experiment was used to develop both static and cyclic p-y curves and the load was applied in only one direction. The load was applied and maintained until the strain gauges were read with a high-speed data acquisition system. The same load was then cycled several times and held constant while the strain gauges were read at specific number of cycles. The load was then increased and the procedure repeated.

a) Obtain the best estimation of the variation of undrained shear strength, *Su*, the submerged unit weight, γ', and pile diameter D. Also obtain the values of ε_{50} from stress-strain curves and if no stress-strain curves are available use a value from the table of Figure 3.13.

b) Compute the ultimate soil resistance per unit length of the pile using the smaller of the values given by equations (3.18) and (3.19). From equation (3.20) is possible to calculate the deflection at one-half of the ultimate soil resistance.

c) Compute points describing the p-y curve from equation (3.35).

d) Beyond $y=18y_{50}$, p is equal to p_u for all values of y.

$$\frac{p}{p_u} = 0.5\left(\frac{y}{y_{50}}\right)^{0.25} \tag{3.35}$$

e) Determine the p-y curve for the short-term static loading by the procedure previously given.

f) Determine the number of times the lateral load will be applied to the pile.

g) Obtain the value of *C* for several values of p/p_u, where *C* is the parameter describing the effect of repeated loading on deformation. The value of C is found from a relationship develop by laboratory tests or, in absence of tests, from equation (3.36).

h) Equation (3.36) gives the values of *y* for cyclic loading.

$$C = 9.6\left(\frac{p}{p_u}\right)^4 \tag{3.35}$$

$$y_c = y_s + y_{50}C * logN \tag{3.36}$$

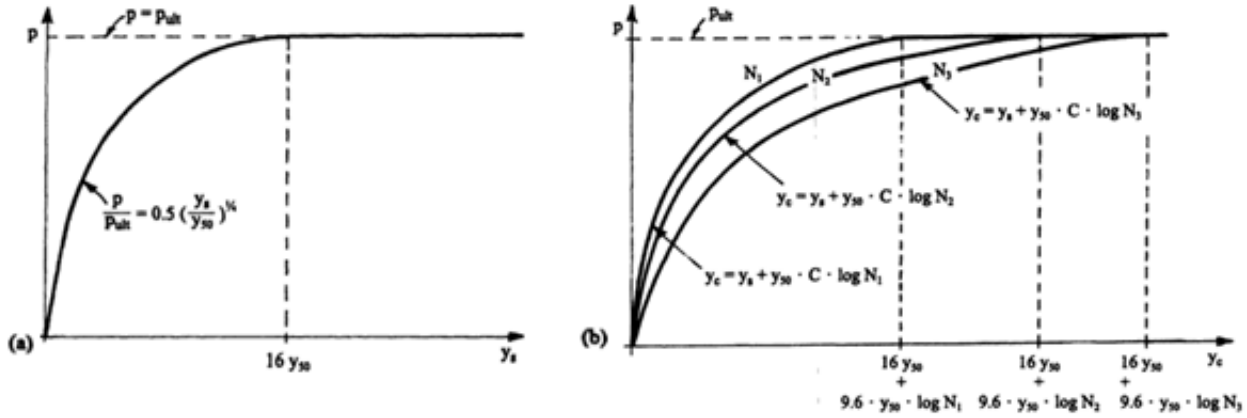

Fig. 3.13 – p-y curve for stiff clay in the presence of free water: (a) static loading; (b) cyclic loading

3.4.4. API CLAY MODEL

For static lateral loads the ultimate bearing capacity p_u of stiff clay (S_u > 1 Tsf or 96 KPa) as for soft clay would vary between $8S_u$ and $12S_u$ except at shallow depths where failure occurs in a different mode due to minimum overburden pressure. Due to rapid deterioration under cyclic loadings the ultimate resistance will be reduced to something considerably less and should be so considered in cyclic design.

The ultimate soil resistance is the smaller of the values given by equations (3.37) and (3.38). These equations differentiate a wedge failure mechanism at shallow depths – with the ultimate bearing capacity increasing with depth and defined by equation (3.37) – and a flow mechanism of the soil around the pile in the horizontal plane for deep depths – constant over depth and defined by equation (3.38). z_{cr} is the depth at which the two equations intersect and there is a change of failure mechanisms.

The p-y curves for the short-term static load case may be generated from equation (3.39). For the cyclic loading the equation (3.39) stops at the value of $p/p_u=0.72$. Beyond that, it remains constant for $z \geq z_{cr}$ or, for $z \leq z_{cr}$, decreases to a value of $0.72*z/z_{cr}$ (between the values of ratio deflection y/y_{50} of *3* and *8*) and remains constant. y_{50} is also usually denoted as y_c.

$$p_u^{shallow} = 3S_u + \gamma' z + J\frac{S_u z}{D} \tag{3.37}$$

$$p_u^{deep} = 9S_u \tag{3.38}$$

$$\frac{p}{p_u} = 0.5\left(\frac{y}{y_{50}}\right)^{\frac{1}{3}} \tag{3.39}$$

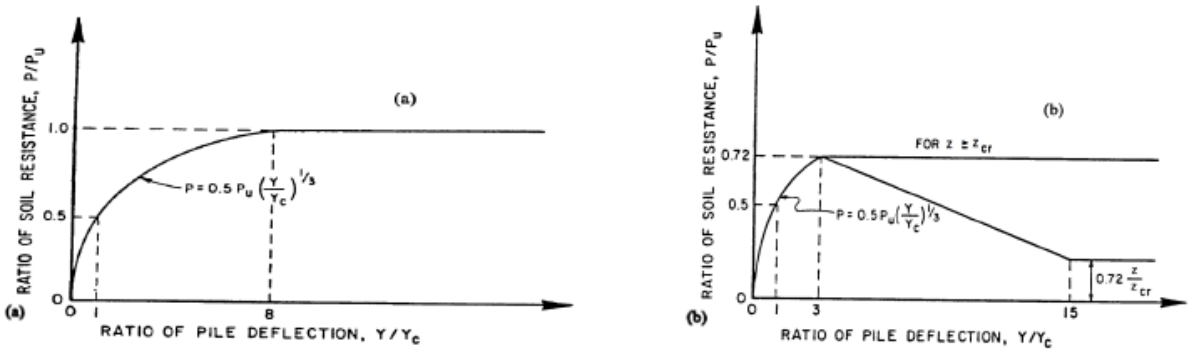

Fig. 3.14 – p-y curve for soft and stiff clay given by API code for (a) static loading (b) cyclic loading

3.5. RECOMMENDATION FOR P-Y CURVES IN COHESIONLESS SOILS

3.5.1. RESPONSE OF SAND ABOVE AND BELOW THE WATER TABLE

Reese et al. (1974) developed a characteristic shape for p-y curves for static and for cyclic loading in sand based on two different experiments - steel-pipe piles with 610 mm of diameter and an embedded length of 21 m -, one for short-term loading and another for repeated loading.

The assessment of the p-y curves can be summarized as follows.

a) Obtain values for the friction angle Φ, the soil unit weight γ, and the pile diameter D (note: use buoyant unit weight for sand below the water table and total unit weight for sand above the water table).

b) Compute the soil resistance per unit length of pile using the smaller of the values given by equations (3.37) and (3.38). $\alpha=\Phi/2$, $\beta=45^o+\alpha$ and $K_A=tan^2(45^o-\alpha)$.

$$p_{st} = \gamma z\left[\frac{K_0 \tan\Phi \tan\beta}{\tan(\beta-\Phi)\cos\alpha} + \frac{\tan\beta}{\tan(\beta-\Phi)}(D + z\tan\beta\tan\alpha) + K_0 z\tan\beta\,(\tan\Phi\tan\beta - \tan\alpha) - K_A D\right] \tag{3.37}$$

$$p_{st} = K_A D\gamma z(\tan^8\beta - 1) + K_0 D\gamma z\tan\Phi\tan^4\beta \tag{3.38}$$

c) Select a depth at which a p-y curve is desired

d) Establish y_u as *3D/80* and compute p_u by equation (3.39). Use the appropriate value of $\overline{A_s}$ and $\overline{A_c}$ from Figure 3.15 for the particular nondimensional depth and for either the static or cyclic case. In this figure *x* is the coordinate axis along the pile measured from the pile head and *b* the diameter of the pile.

e) Establish y_m as *D/60* and compute equation (3.40). Use the appropriate value of B_s and B_c from figure 3.16 for the particular nondimensional depth and for either the static or cyclic case.

f) These last two points define the two final straight-line portions of the p-y curve. Use the appropriate value of K_{py} from the Table 3.2 to establish the initial straight-line portion of the p-y curve through equation (3.41).

$$p_u = \overline{A_s} p_s \quad \text{or} \quad p_u = \overline{A_c} p_s \tag{3.39}$$

$$p_m = B_s p_s \quad \text{or} \quad p_u = B_c p_s \tag{3.40}$$

$$p = (K_{py} z) y \tag{3.41}$$

g) Use equations (3.42), (3.43), (3.44) and (3.45) to establish the parabolic section through equation (3.46) between points *k* $(y_k ; p_k)$ and *m* $(y_u ; p_u)$.

$$m = \frac{p_u - p_m}{y_u - y_m} \tag{3.42}$$

$$n = \frac{p_m}{m\, y_m} \tag{3.43}$$

$$\bar{C} = \frac{p_m}{y_m^{1/n}} \; \frac{x}{b} \tag{3.44}$$

$$y_k = \left(\frac{\bar{C}}{K_{py} z} \right) \tag{3.45}$$

$$p = \bar{C} y^{1/n} \tag{3.46}$$

Note: Figure 3.16 is draw as if there is an intersection between the initial straight-line portion of the p-y curve and the parabolic portion of the curve at point *k*. Equation (3.41) defines the p-y curve until there is an intersection with another branch of the p-y curve and, if there is no intersection, it defines the complete p-y curve.

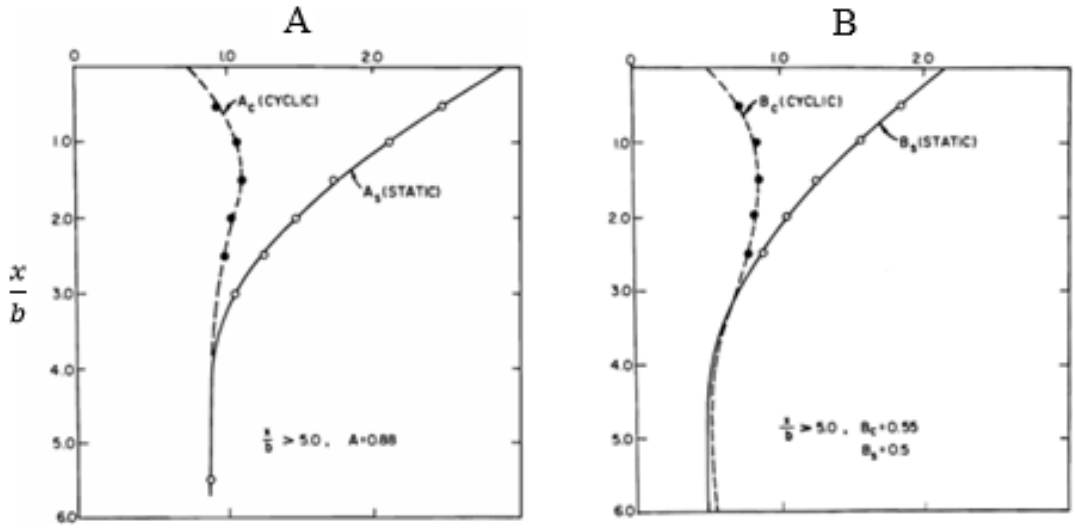

Fig. 3.15 – (a) value of $\overline{A_s}$ and $\overline{A_c}$; (b) value of B_s and B_c

Table 3.2 – Value of K_{py}

Representative values of k_{py} for submerged sand			
Relative density	Loose	Medium	Dense
Recommended k_{py} (MN/m^3)	5.4	16.3	34
Representative values of k_{py} for sand above the water table (Static and Cyclic Loading).			
Relative density	Loose	Medium	Dense
Recommended k_{py} (MN/m^3)	6.8	24.4	61

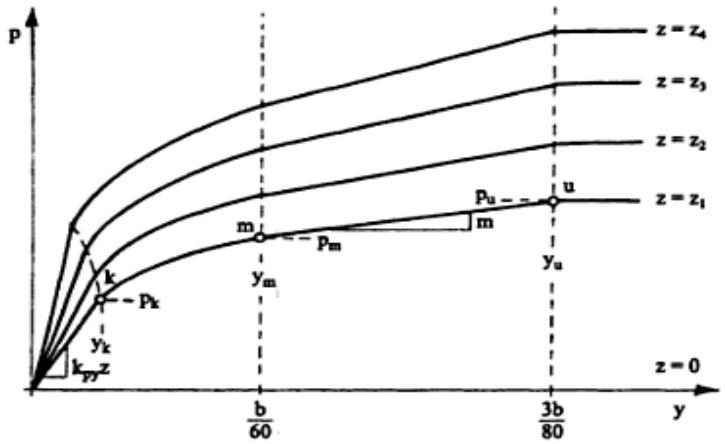

Fig. 3.16 – p-y curve for static and cyclic loading in sand

3.5.2. API SAND MODEL

The API p-y curves for sand are characterized only by a hyperbolic equation (defined by equation (3.47)). The ultimate bearing capacity for sand has been found to vary from a value at shallow depths determined by equation (3.48) to a value at deep depths determined by equation (3.49). At a given depth the equation giving the smallest value of p_u should be used as the ultimate soil resistance.

The coefficients C_1, C_2 and C_3 can be determined from Figure 3.18 or through equations (3.50). k is the initial modulus of subgrade reaction that can be determined from Figure 3.19 or through equations (3.51) and (3.52). γ is the total unit weight of the soil and A has a constant value of *0,9* for cyclic loading and can be determined by equation (3.53) for static loading.

As the units of Figure 3.18 and equations (3.50) are not the same, equations (3.54) and (3.55) are here presented.

$$p = A\, p_u\, \tanh\left[\frac{k\, z}{A\, p_u} y\right] \tag{3.47}$$

$$p_{us} = (C_1\, z + C_2\, D)\, \gamma\, z \tag{3.48}$$

$$p_{ud} = C_3\, D\, \gamma\, z \tag{3.49}$$

$$C_1 = 0.115 * 10^{0.0405\Phi}\,, \quad C_2 = 0.571 * 10^{0.022\Phi}\,, \quad C_3 = 0.646 * 10^{0.0555\Phi} \tag{3.50}$$

$$k_{sand} = (0.008085\Phi^{2.45} - 26.09) * 10^3 \qquad \text{[kPa/m]} \tag{3.51}$$

$$k_{sand} * z = 50000 \left(\frac{z}{z_{ref}}\right)^{0.6} \left(\frac{D}{D_{ref}}\right)^{0.5} \Phi^{3.6} \tag{3.52}$$

$$A = (3.0 - 0.8\ z/D) \geq 0.9 \tag{3.53}$$

$$1\ lb/in^3 = 27680\ Kg/m^3 \tag{3.54}$$

$$1\ Kg/m^3 = 9.80665 * 10^{-3}\ kPa/m \tag{3.55}$$

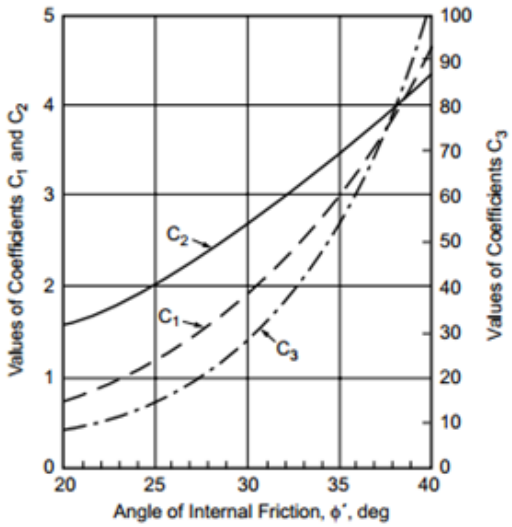

Fig. 3.18 – coefficients as function of Φ

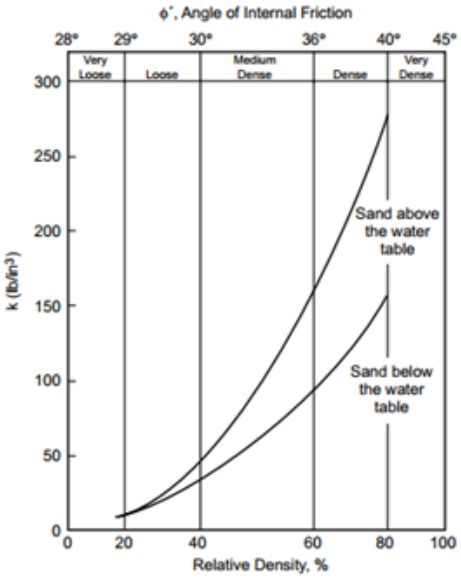

Fig. 3.19 – k as function of Φ

3.6. FINAL COMMENTS

The exclusive use of finite element analyses to solve an engineering problem is not feasible on the present days. It takes too much time because of the complexity of these interface systems and the number of degrees of freedom of the models due to its tridimensionality. The precision of the model and its representativeness requires a big amount of data and it is very time consuming, therefore expensive. However, FEM has become very popular on the research groups working in foundation engineering in order to validate the p-y curves used on the Winkler spring models employed in practice.

Using the relations between the deflection and the soil resistance (deriving them by back-analyses of well monitored pile load tests) it is possible to obtain p-y curves with high accuracy, as long as the constitutive models are realistic enough and the model is well built.

4

DEFINITION OF A NUMERICAL MODEL FOR THE MONOPILE

4.1. OVERVIEW

The main propose of this thesis is to compare the p-y curves obtained from the results of a finite element program with the ones used for current engineering design. Therefore, the definition of all the characteristics of the model is a key step of this.

The number of variables that contribute for the definition of the model is very vast. It is important to define all the variables in the most precise way but it is also important to take into account that the high rigor of some variables might increase too much the time of the calculations.

This chapter consists on a detailed description of the model regarding its variables. Every parameter of the materials, the different geometries, dimensions of the model and all the other aspects will be presented, being its choice justified.

The information presented in this chapter is believed to be essential to understand the results of the calculations. An engineer must be able to tell if the response presented by the model to a certain imposed displacement or load is realistic or not. That is only possible if all the information about that model is available to check and it makes it conceivable to reproduce the models here built and work on the parameters for, e.g., sensitivity studies.

4.2. GEOMETRY

4.2.1. SYMMETRY AND BOUNDARY CONDITIONS

For this problem, a symmetry behaviour is assumed for the model, allowing it to have its size reduced to half and so the calculation timing is much lower due to a lower number of degrees of freedom of the system.

In order for this to be true, there must be symmetry along an axis regarding geometry, loading, material properties and boundary conditions.

For this model, as there is a cylindrical steel structure surrounded by a homogenous soil, it is possible to say that, concerning the geometry and the material properties, there is symmetry of the model along any vertical plane.

Considering a horizontal load applied on the pile with a radial direction, along the vertical plane that contains the vector of that load there will only exist displacements on the direction of the plane (no movement of the points on the perpendicular direction to the plane).

To sum up, the model can be reduced to half its size by considering symmetry along a vertical plane with a tangential direction equal to the direction of the horizontal load or imposed displacement. Fixed displacements on a perpendicular direction to this plane is the boundary condition imposed to the model, which is automatically defined in PLAXIS 3D.

4.2.2. SIZE OF THE MODEL

In order to get to the final size of the model, several tests had to be run. The procedure consisted on trying different lengths on the three directions and analyse whether the displacements and stresses of the model were affected by its limits and, even if they were, decide whether it would be indispensable to increase it or not.

The aim was to get a model with the smallest size possible in order have less elements and, consequently, less computational effort. On the other hand, it could not be too small to a point of it interfering with the deformations and stresses of the soil and structures.

To facilitate a standard construction of a model for different piles, all the lengths in the different direction are expressed in terms of number of diameters of the pile for the corresponding model. This way all the models were built in the same proportion of size and they were affected by the same effects, mainly when it comes to deformations and stresses. Figure 4.1 show the dimensions used for the model, normalized by the diameter of the pile. Notice that, these dimensions are applied to a case here being studied which is a length of the pile 5 times bigger its diameter.

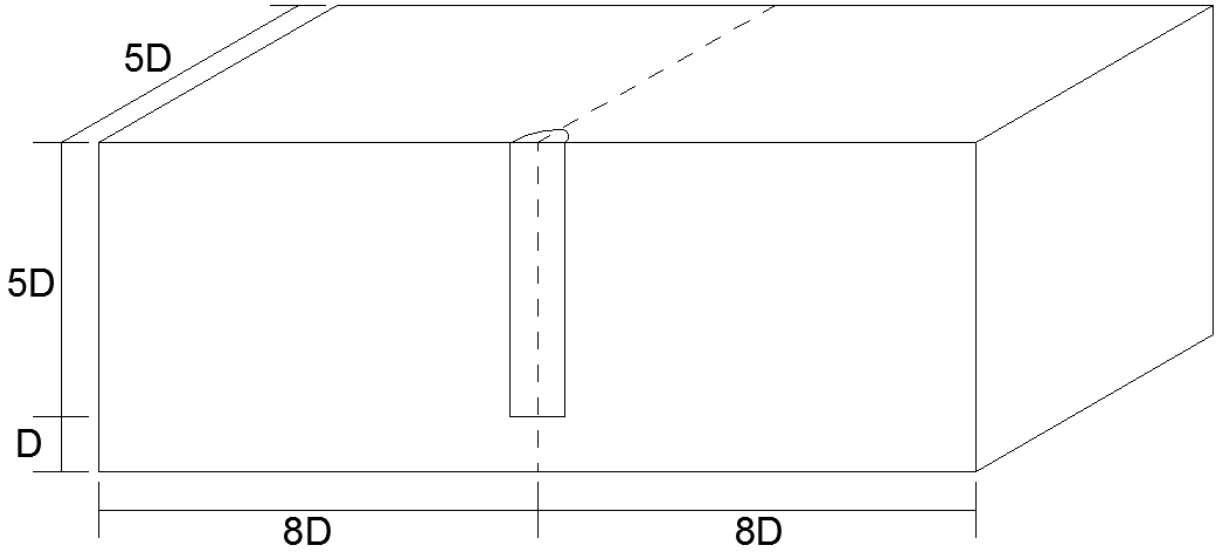

Fig. 4.1 – Dimensions of the model

On the direction perpendicular to the movement of the pile (chosen as the Y direction in PLAXIS 3D) the critical displacements of the soil to take into account were the horizontal ones but these didn't spread far beyond the pile. Therefore, 5 diameters of the pile was considered a sufficient length of the model

in this direction. The stresses on the soil near this boundary after the movement of the pile were the same as the resting stresses.

On the direction of the movement of the pile (chosen as the X direction in PLAXIS 3D) the critical displacements of the soil to take into account were the vertical. This occurs because at relatively shallow depths the failure of the soil involves an uplift of a wedge of soil in front of the pile and a gap forming behind the pile that leads to settlement of the soil and the results of the calculations showed that these effects are felt at very far distances. Yet, the interference of these vertical movements of the soil close to the borders of the model is irrelevant for what is being studied in this work. Also, the distance of the boundary is considered to be enough if a plane strain state is verified. In this case, the horizontal extension (ε_{xx}) was checked and its highest value was less than 0.2% which proves that a distance 8 diameters for the pile to each side of the X direction is sufficient.

On the vertical direction, one diameter was added to the 5 diameters length of the pile in order to represent the soil below the pile that introduces a couple system in the toe of the pile that produces moment. This leads to a total of 6 diameters in the vertical direction (chosen as the Z direction in PLAXIS 3D).

4.3. CONSTITUTIVE MODELLING - HARDENING SOIL MODEL

4.3.1 INTRODUCTION

The Hardening soil model is an advanced model for simulating the behaviour of different types of soil, both soft and stiff soils. When subjected to primary deviatoric loading ($\sigma_1 - \sigma_3$), soil shows a decreasing stiffness and simultaneously irreversible plastic strains develop. This is usually represented as in the case of a drained triaxial test in a normally consolidated soil where the observed relationship between the axial strain (ε_1) and the deviatoric stress can be well approximated by a hyperbola (Figure 4.2 (b)).

Such relationship is very well-known by the hyperbolic model formulated by Duncan and Chang (1970). Instead of using a combination of a linear elastic behaviour (Hooke's single stiffness) with perfect plasticity (Figure 4.2 (a)), the hyperbolic model uses a double-stiffness model for elasticity with combination with isotropic strain hardening.

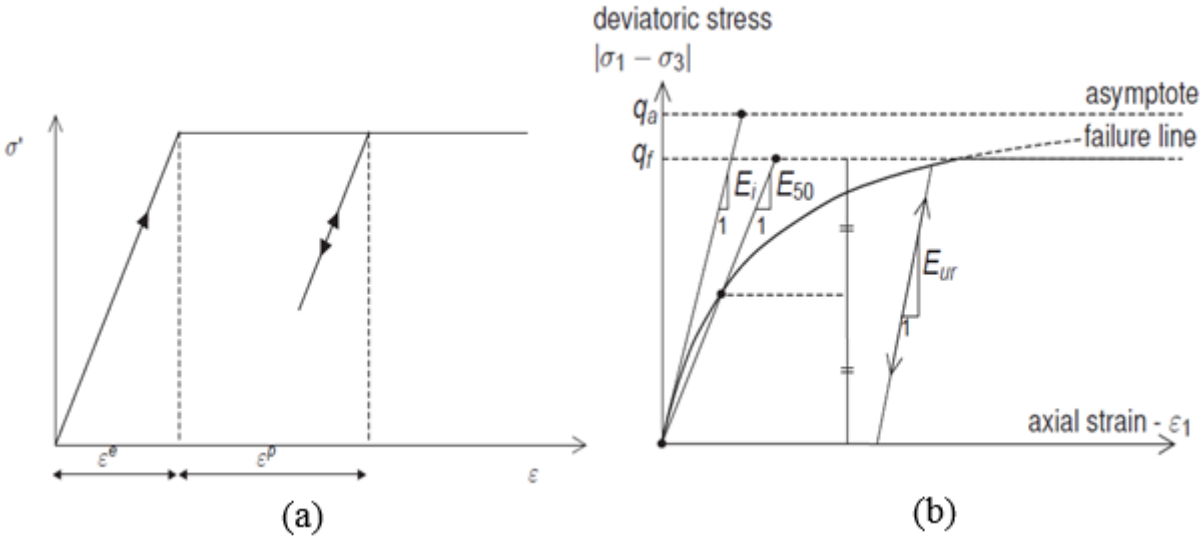

Fig. 4.2 – linear elastic perfectly plastic model (a) versus Hardening Soil model (b)

The major inconsistency of this model developed by Duncan and Chang is that a hypo-elastic model (almost hyper-elastic/almost fully recovers its deformations when unloaded/pseudo-elastic) cannot consistently distinguish between loading and unloading. The hardening soil model, however, supersedes the hyperbolic model by far: firstly by using the theory of plasticity rather than the theory of elasticity; secondly by including soil dilatancy; and thirdly by introducing a yield cap.

4.3.2 DILATANCY

After extensive shearing, dilating materials arrive in a state of critical density where dilatancy has come to an end as shown in Figure 4.3. This phenomenon of soil behaviour can be included in the Hardening Soil model by means of a *dilatancy cut-off*.

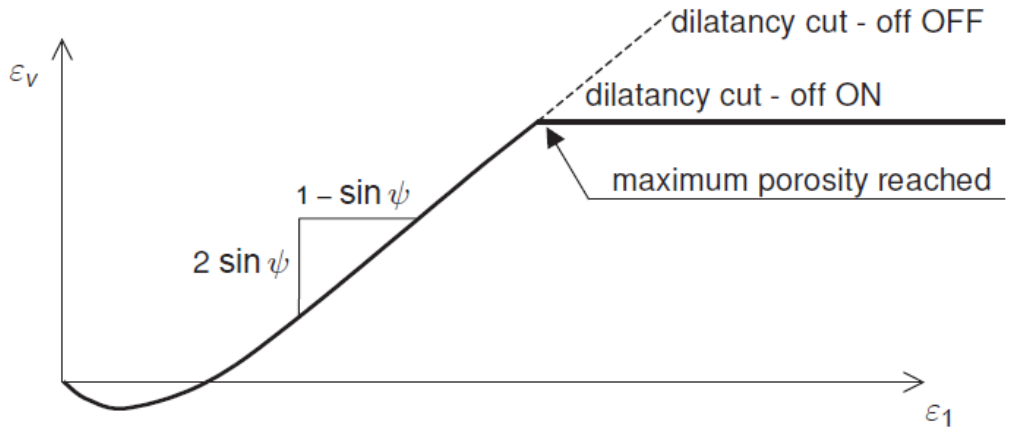

Fig. 4.3 – Dilatancy cut-off

4.3.3 YIELD CAP

In contrast to an elastic perfectly plastic model, the yield surface of a hardening plasticity model is not fixed in principal stress space, but it can expand due to plastic hardening. Distinction can be made between two main types of hardening, namely shear hardening and compression hardening and both of them are contained in the present model.

The Hardening Soil model in PLAXIS 3D defines the shape of the yield surface (Figure 4.4 on the left) depending on an exponent parameter *m* that ranges between 0.5 for sands and 1.0 for clays. For m=1.0, straight lines are obtained but slightly curved yield surface correspond to lower values of the exponent. This exponent is used to calculate the stiffness modulus and the unloading-reloading modulus.

Shear hardening yield surfaces as indicated on the left of Figure 4.4 do not fully explain the plastic strain that is measured in isotropic compression so a second type of yield surface (Figure 4.4 on the right) must be introduced to close the elastic region for compressive (compaction hardening) stress paths.

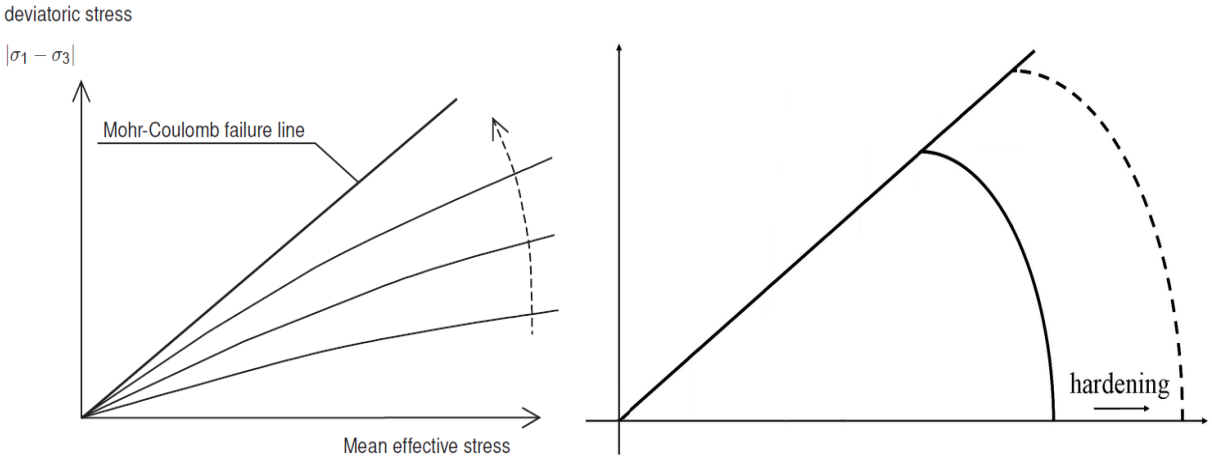

Fig. 4.4 – Yield surface of a hardening plasticity model

4.3.4 SOIL TESTS

The *SoilTest* tool available in PLAXIS (both 2D and 3D) offers a quick and convenient way of simulating soil lab tests on the basis of a single point algorithm. It uses the same soil models and calculation methods as the PLAXIS finite element calculation Kernel (computer program responsible for the interaction of hardware and software and translates input and output into data processing instructions).

SoilTest offers the possibility of performing five kinds of tests: Triaxial test, Oedometer test, CRS test, DSS test and a general test where stress and strain condition can be defined at will. This allows to quickly test whether the behaviour of soil materials in PLAXIS matches existing measurements and expectations.

Figure 4.5 shows a graphic of differential stress (difference between the greatest and the least compressive stress, $|\sigma_1 - \sigma_3|$) in function of the strain in the principal direction (ε_1). It compares the two cases of using different Secant Modulus, E_{50}^{ref}, (and consequently Unloading-Reloading Modulus, E_{ur}^{ref}, and Oedometer (or constrained) Modulus, E_{oed}^{ref}), one of 10MPa and the other of 50MPa.

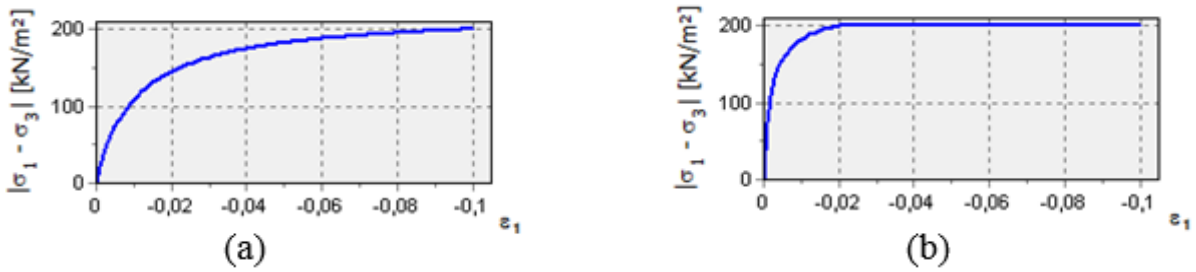

Fig. 4.5 – Stress-Strain relationship for a Secant Modulus of 10 MPa (a) and 50 MPa (b)

From looking at the previous figure it is possible to see what to expect from the p-y curves with respect to the different cases. The ultimate bearing capacity should be the same whereas the initial stiffness is much higher for the higher Secant Modulus.

4.4. MATERIALS

4.4.1 SOIL

The type of soil adopted for this work was clay. This option was for two main reasons: first, there is much less information and studied cases regarding cohesive soils than granular soils; and secondly, both the North Sea and the Baltic Sea, located mainly close to the UK, Scandinavia and Germany, have a seabed composed of cohesive soils. For this reason, it is of big interest for COWI to study this particular condtions as they have there a very strong market in this areas.

A Zomergem Clay was considered to best suit the purpose of this work. It is classified as high plasticity clay according to BSCS (Biological Sciences Curriculum Study) and its characteristic stiffness parameters are presented in Table 4.1.

Table 4.1 – Characteristic stiffness parameters for a Zomergem Clay according to the BSCS

Geotechnical Identification	Geotechnical Unit	$E_{oed,ref}$ [MPa]	$E_{50,ref}$ [MPa]	ε_{50} [%]	$G_{0,ref}$ [MPa]	m [-]
CLAY	Zomergem	4	10	1	35	0.8

In order to not complicate the achievement of the objective of this thesis a homogeneous soil for the whole seabed was implemented at a depth of 30 meters below the water level. Some of the assumed parameters used in PLAXIS 3D for the soil are presented the in Table 4.2

Undrained model of type B is an undrained or short-term material behaviour option in PLAXIS 3D in which stiffness is defined in terms of effective properties and strength is defined as undrained shear strength. A large bulk stiffness for water is automatically applied to make the soil as a completely incompressible and (excess) pore pressures are calculated, even above the phreatic surface.

Using an Undrained model of type B provides the option of increasing the undrained shear strength with depth, which is of great interest for comparison of results with and without this variation of S_u. It is very common to see clays or tills in the North and Baltic Seas with an undrained strength of around 100-200 kPa.

Table 4.2 – Input parameters in PLAXIS 3D for the soil material

Parameters	**Value**	**Unit**
Unit weight (γ_{sat})	19	kN/m^3
Secant Modulus (E_{50}^{ref})	10.00E3	kN/m^2
Oedometer (or constrained) Modulus (E_{oed}^{ref})	4.00E3	kN/m^2
Unloading-Reloading Modulus (E_{ur}^{ref})	30.00E3	kN/m^2
Undrained Shear Strength ($S_{u,ref}$)	100	kN/m^2
Unloading-Reloading Poisson Coefficient (ν'_{ur})	0.200	-

The definition of the soil is made through the creation of one single borehole. This layer goes from 0 to 6 diameters depth (negative distance) and a head water at 30 meters height.

The volume of the soil will be divided into vertical layers parallel to the pile (Figure 4.6). The purpose of this is to allow the user to assign different coarseness factors to the different volumes to ensure more accuracy in the calculation of the stresses in the areas closer to the pile. The mesh should be finer in the volumes closer to the foundation and less finer as it moves away from the foundation.

In order to do it, semi-circular polycurves were drawn and, with the "*extrude"* option, a new layer was created (Figure 4.7). The diameters of these polycurves were normalized for the following dimensions: 1D (for the polycurve of the plate of the pile), 2D, 4D and 8D (these last 3 are the polycurves to divide the different areas).

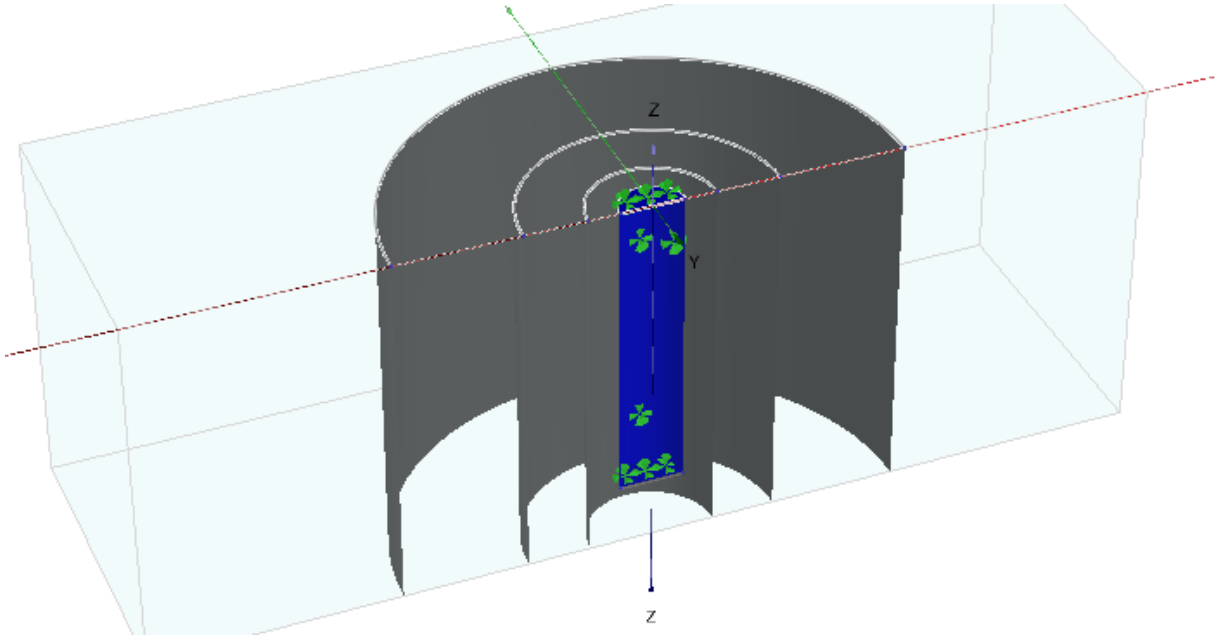

Fig. 4.6 – Representation of the surfaces defining the different volumes of soil

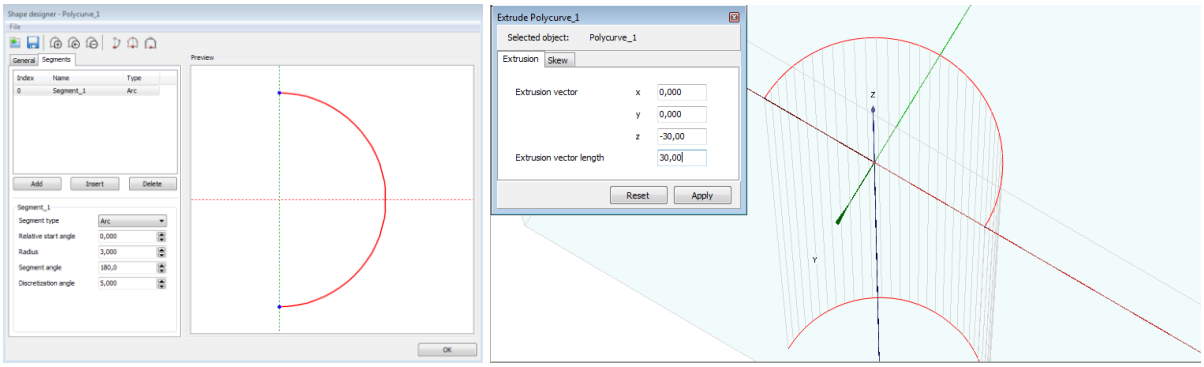

Fig. 4.7 – Creation of a Polycurve (on the left) and "*extrude*" (on the right) to define a layer

4.4.2. MONOPILE

As the monopile is a steel hollow cylindrical tube, the best way to model it in PLAXIS 3D is by using a plate. This plate is composed by steel with properties as indicated in Table 4.3. The length of the pile was normalized by its diameter, as it happened with the size of the model, so it should always be 5 times the diameter. The same occurs to the thickness of the wall of the pile, which is 90 times smaller than the diameter of the pile and constant over depth.

Another plate is closing the top of the plate whereas the bottom remains opened in order to allow the interaction between soil on the inside and the outside of the monopile. The same material was used for the soil surrounding the pile and the soil inside the pile.

Lastly, a beam with 60 meters of length was added at the top of the pile, attached to the plate closing it (Figure 4.8). The function of this beam is to allow the user to apply the load at different heights and study the effect of a bending moment on the deflection of the pile. The properties of this beam are not important, as the transmission of the moment and load do not depend on these. However, if a bending moment is being applied, the plate closing the top should be very rigid so that the pile receives all the moment. If a different scenario is being tested (e.g. horizontal translation of the whole pile), the same properties as the pile can be attributed to this plate and the beam should be deleted.

Table 4.3 – Input parameters in PLAXIS 3D for the plate material

Parameters	**Value**	**Unit**
Unit weight (γ)	78.50	kN/m^3
Young's Modulus (E)	210.00	GPa
Poisson Coefficient (ν)	0.30	-
Shear Modulus (G)	80.77	GPa

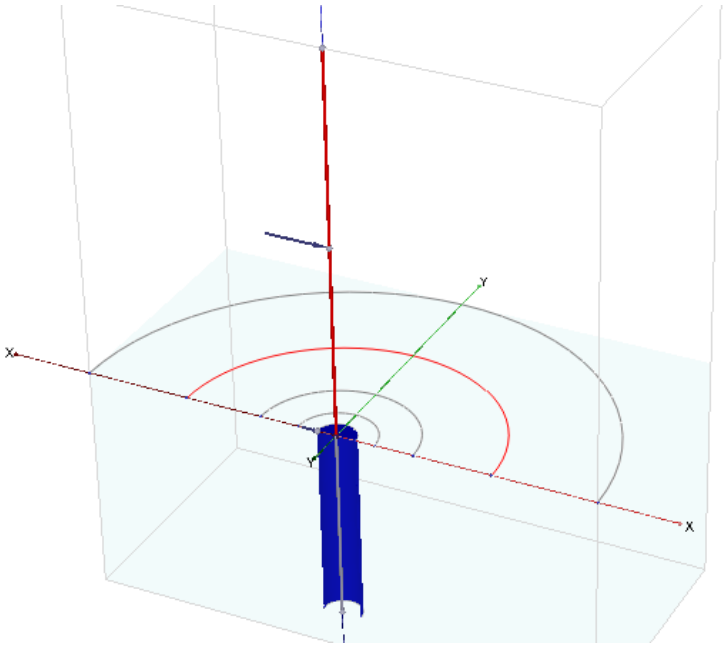

Fig. 4.8 – Representation of the plates and beams

4.4.3. INTERFACES

An interface simulates the interaction between a structure and soil. This permits relative displacements between soil and structure not allowing them to stay tied together – no slipping and no gapping is possible.

When an interface is used two nodes are created at the interface, one belonging to the soil and the other to the structure (Figure 4.9 – the spacing between the nodes doesn't really exist, the nodes have the same coordinates). The interaction between these nodes consists of two elastic-perfectly plastic springs: one on the normal direction to model the gap and the other on the tangential direction to model the slip displacement.

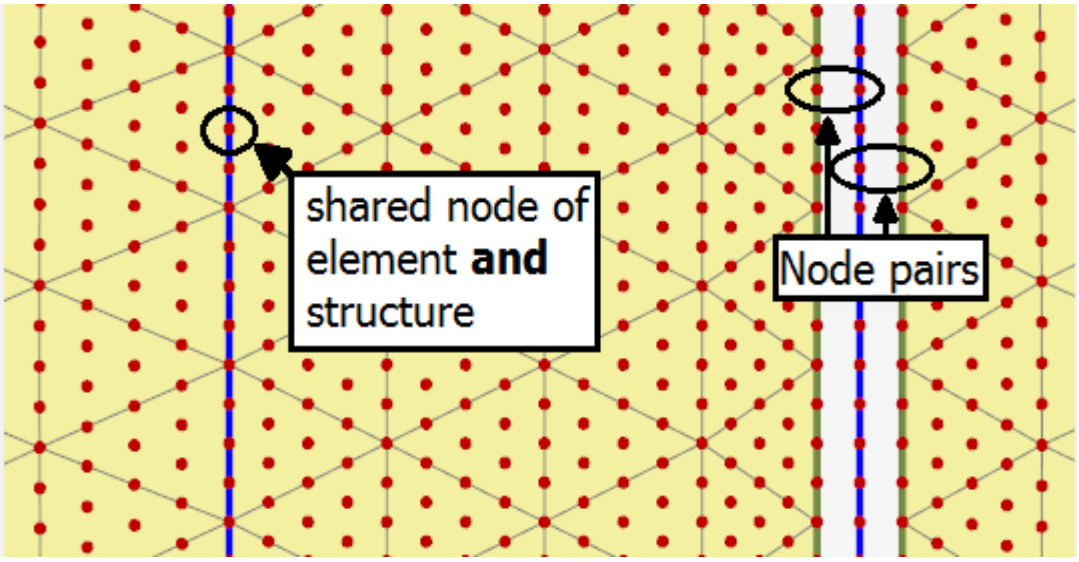

Fig. 4.9 – Plate without interface (left) and with interface (right) (PLAXIS, 2015)

When creating a soil material, in the "*interfaces*" label, there is a parameter R_{inter}. This parameter relates the strength of the interface to the strength of the soil: it gives a reduced interface friction and interface cohesion (adhesion) compared to the friction angle and the cohesion in the adjacent soil. Table 4.4 shows the usual used values for this parameter and for this work a R_{inter} of 0.5 was considered.

Table 4.4 – Values of R_{inter} for different types of interactions of soil-structure

Interaction sand/steel	$R_{inter} \approx 0.6 – 0.7$
Interaction clay/steel	$R_{inter} \approx 0.5$
Interaction sand/concrete	$R_{inter} \approx 1.0 – 0.8$
Interaction clay/concrete	$R_{inter} \approx 1.0 – 0.7$
Interaction soil/geogrid (interface may not be required)	$R_{inter} \approx 1.0$
Interaction soil/geotextil (foil, textile)	$R_{inter} \approx 0.9 – 0.5$

4.4.4. AT REST STRESS RATIO

The initial stress state of a soil is still very difficult to predict nowadays and it is usually represented by the lateral stress coefficient (or at rest earth pressure coefficient), $K_0=\sigma'_h/\sigma'_v$.

For the Mohr-Coulomb failure criterion the default value used by PLAXIS for K_0 is based on equation (4.1) (Jaky's formula). For more complex models like the Hardening soil the default value is based on the K_0^{nc} parameter and is also influenced by the overconsolidation ratio (OCR) or the pre-overburden pressure (POP), as shown in equation (4.2). These formulas were developed based on instrumented Oedometer tests, triaxial stress-path tests and other laboratory devices.

For this work, equation (4.2) was used to calculate the K_0 and K_0^{nc} was estimated using Figure 4.10 with an *OCR=1* and *POP=0* (data compiled by Lunne et al. 1990). A value of 0.67 was used for $K_{0,x}$ and $K_{0,y}$.

$$K_0 = 1 - \sin\varphi \tag{4.1}$$

$$K_{0,x} = K_{0,y} = K_0^{nc}.OCR - \frac{\nu_{ur}}{1-\nu_{ur}}(OCR-1) + \frac{K_0^{nc}.POP - \frac{\nu_{ur}}{1-\nu_{ur}}POP}{|\sigma_{zz}^0|} \tag{4.2}$$

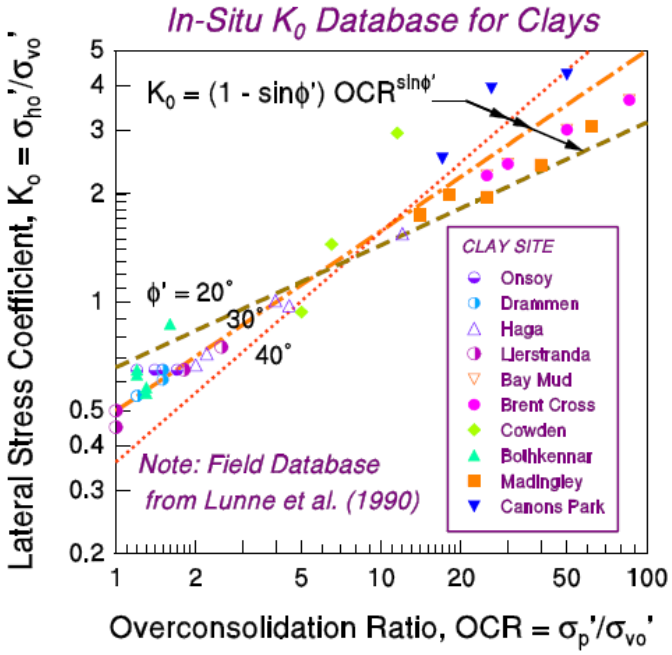

Fig. 4.10 – Field data from K_0 measurements in clays (Mayne, P. W., 2001)

4.5. MESH

The next phase after the definition of all materials and structures of the model is the definition of a mesh, essential to perform finite element calculations. This consists on dividing each geometry into elements in order to compose a finite element mesh.

The mesh should be sufficiently fine to obtain accurate numerical results but, on the other hand, a too fine mesh should be avoided since this will lead to excessive calculation time. In the case of this work,

as MatLab will be used to process all the exported data from PLAXIS 3D, it is also important to take into account the capacity of MatLab and its own calculation time.

A medium mesh with a moderate number of elements was used during the exploration of the results and a definition of a procedure to obtain the p-y curves as this leads to obtain good results in relatively short times and lots of calculations need to be run. However, to obtain the final results, a much more refined mesh was used in order to get more accurate results.

Figure 4.11 shows a typical mesh of a model of this thesis, where it is clear the previous discussed option to use a more refined mesh in a volume close to the pile. In Figure 4.12 it is possible to see the soil with different colors each one representing a different coarseness factor - small coarseness factors for the volumes closer to the pile and higher coarseness factors for the volumes furthest away from the pile.

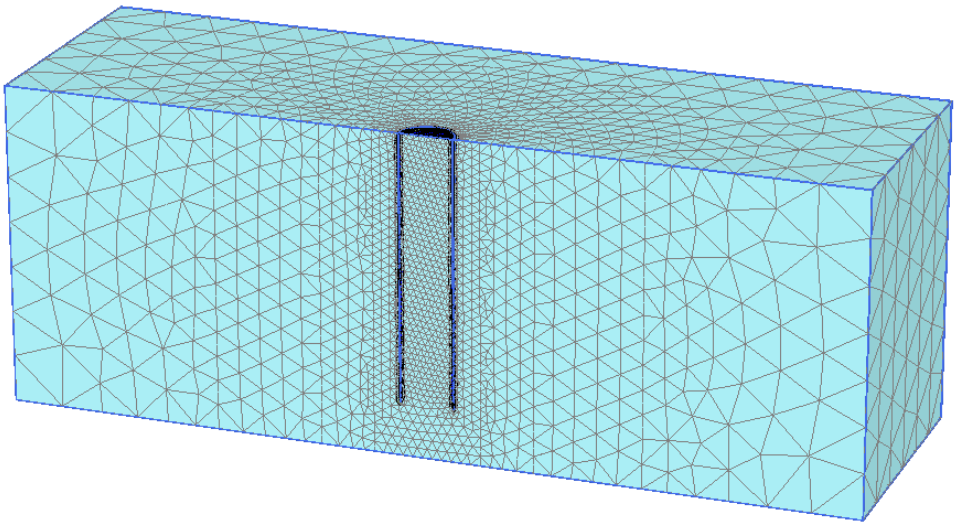

Fig. 4.11 – Example of the mesh of the PLAXIS 3D model

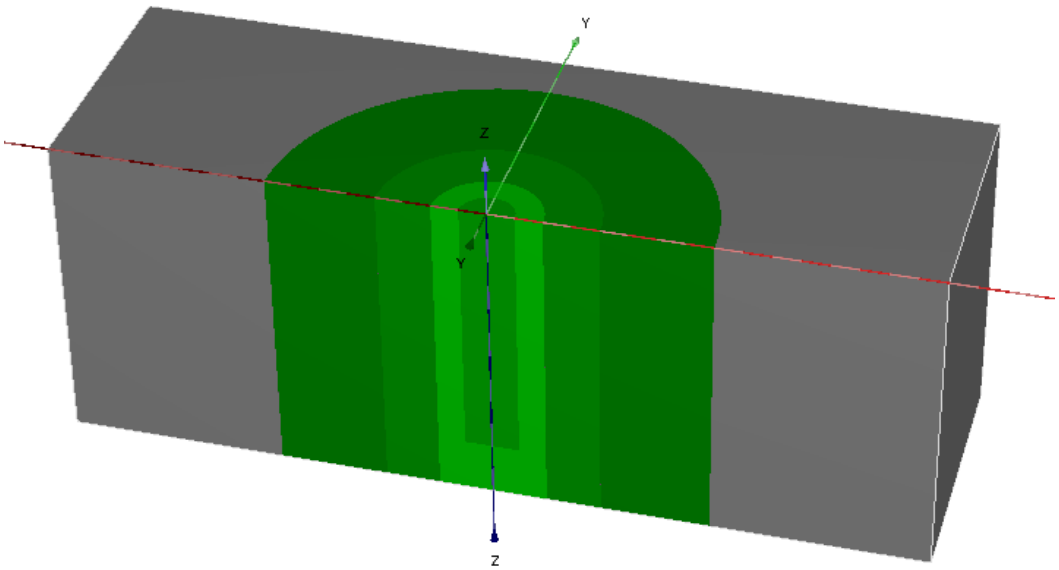

Fig. 4.12 – Colors for the different soil volumes representing different coarseness factors

4.6. STAGED CONSTRUCTION

Before proceeding to the imposition of displacements it is necessary to establish the at rest state. Three stages are needed in order to do this: firstly, a stage in which only the soil is present; secondly, a stage in which the structures are installed; finally, as the second stage introduces changes in the state of the stresses and the structures are affected by gravity, a third stage, in which the previous displacements are reset, is introduced. This allows the next stages to take into account only the imposed horizontal displacements.

4.7. FINAL COMMENTS

Having defined a model in PLAXIS 3D, it is now time to proceed to the calculations and two different type of analysis will be run.

The first analysis consist on a reproduction of a real case scenario with a point load applied at the top of the monopile simulating the loads of the wind and the waves. In this case, there will be a deflection of the pile and, using the data of the deflection over the depth, a procedure to obtain the soil reaction and the p-y curves will be explored and studied.

The second case, which was chosen to be analyzed due to the problems associated with the first one, consists on the application of a horizontal translation of the whole structure through the application of a displacement along the whole length of the pile. Although this is an unrealistic scenario, it gives a response of the soil throughout the whole depth of the pile whereas in the first case, a great part of the pile does not have significant displacements.

While in the first analysis the soil reaction is achieved using the differential equation developed by Hetenyi (1946), the second analysis involves much more numerical calculations and data processing as the exported information from PLAXIS 3D is much larger than in the first case. The use of MatLab is essential to process the numerical data and to define an analytical procedure for the optimization of these results.

5

DIFFERENTIAL EQUATION APPROACH TO OBTAIN THE SUBGRADE REACTION OF THE SOIL

5.1. OVERVIEW

In this chapter all the different analyses regarding an attempt to obtain the subgrade reaction of the soil through the derivation of the deflection is presented. The idea is to find the deflection of the pile along all its length and use the previously presented equation (3.7) developed by Hetenyi to calculate the respective reaction of the soil.

The analysis requires the use of several computer programs. The main one was PLAXIS 3D from which all the information of the deflection of the pile when subjected to a horizontal lateral load was extracted. Excel, MatLab and even the structural program SAP2000 were then used in order to perform different analysis and compare results.

5.2. PROCEDURE

According to the previously presented equation (3.7) developed by Hetenyi (1946) the subgrade reaction modulus is obtain from the 4th derivative of the pile deflection, being, therefore, the first step of this procedure.

The workshop provided by PLAXIS bv (Hamburg, Germany, 28-29 September 2014) on "Introduction to PLAXIS 3D & Offshore Applications" suggests the use of a very slender beam element with low stiffness in the centre of the pile (e.g. $E_{beam}=E_{pile}/1000$) that will move together with the soil inside the pile (Figure 5.1 (a)). As a result of this, the slender beam will have the same deflection as the pile which allows the extraction of the horizontal displacement along the pile. The reason for this beam to be so slender is that will have no interference on any deformations of either the soil or the pile.

The problem with this slender beam is that the movement between the soil inside the pile and the soil surrounding influences its behaviour giving it a different deflection from the pile at the bottom of it (Figure 5.1 (b)). It's the existence of a relative movement between the soil inside the pile and the pile itself that causes this problem so in order to overcome this obstacle it would be necessary to introduce a plate at the bottom of the pile to prevent this interaction between the inside and the outside of the pile.

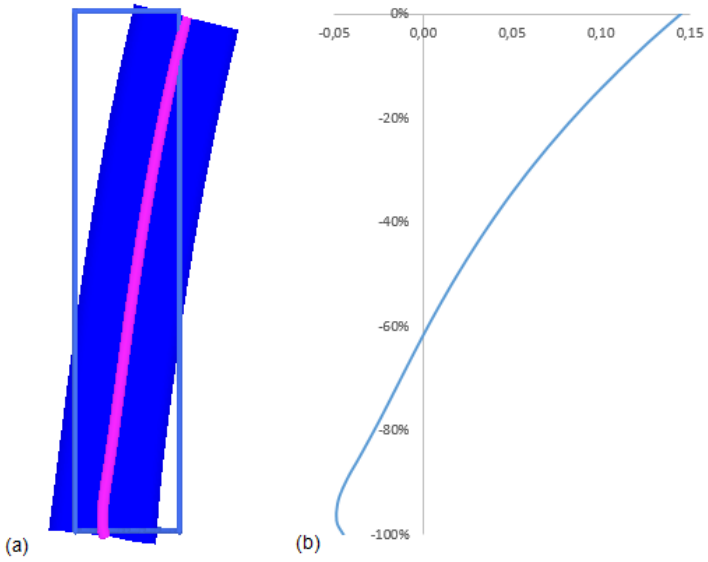

Fig. 5.1 – (a) Deflection of the pile and the slender beam; (b) Graph of the deflection of the slender beam

The other option was to intercept a vertical plane with the central fibre of the monopile and assume the movement of the fibre as representative of the movement of the monopile (Figure 5.2). This way, no extra elements needed to be added to the model and the deflection of the pile could be easily obtained.

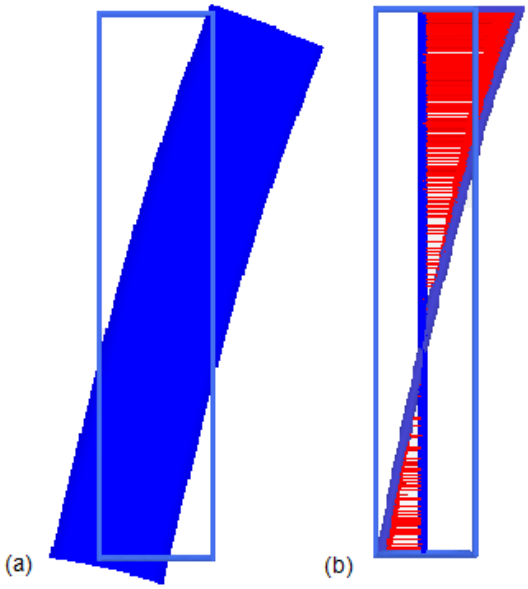

Fig. 5.2 – (a) Resulted deflection of the pile; (b) Diagram of horizontal displacements on the central fiber

Having exported from PLAXIS 3D the data of the horizontal movement of the points along the pile two options remain to obtain the 4th derivative: a numerical derivative (Figure 5.3 and equation (5.1)) applied successively directly to the exported data from PLAXIS; or, an analytical derivative deduced from an approximated curve exported from PLAXIS.

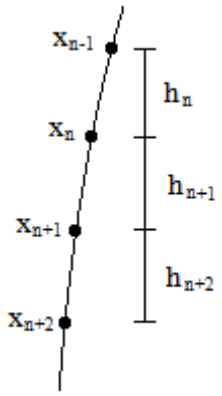

Fig. 5.3 – Numerical derivative

$$f'(x_n) = \frac{x_{n-1} - x_{n+1}}{h_n + h_{n+1}} \tag{5.1}$$

Both options were deeply explored and more than one approach carried out. The results will be presented in what follows and compared to each other.

5.3. Analytical Derivative

The first and simplest approach was the approximation of the data exported from PLAXIS 3D to a polynomial curve using Microsoft Excel. The data was plotted in a graph and a trendline was calculated as a 6th degree polynomial (this is the highest degree possible to calculate using Microsoft Excel) in a coefficient of determination (or, Goodness of fit), R^2, of 1.0.

The outcome of the soil reaction would be a 2nd degree polynomial curve, as a consequence of the 4th derivative of a 6th degree polynomial. It might be a very low degree for the accuracy expected but it should provide a first impression of what to expect using this methodology. Figure 5.4 shows the result of this analysis. The bending moment was also added to the figure for later comparison.

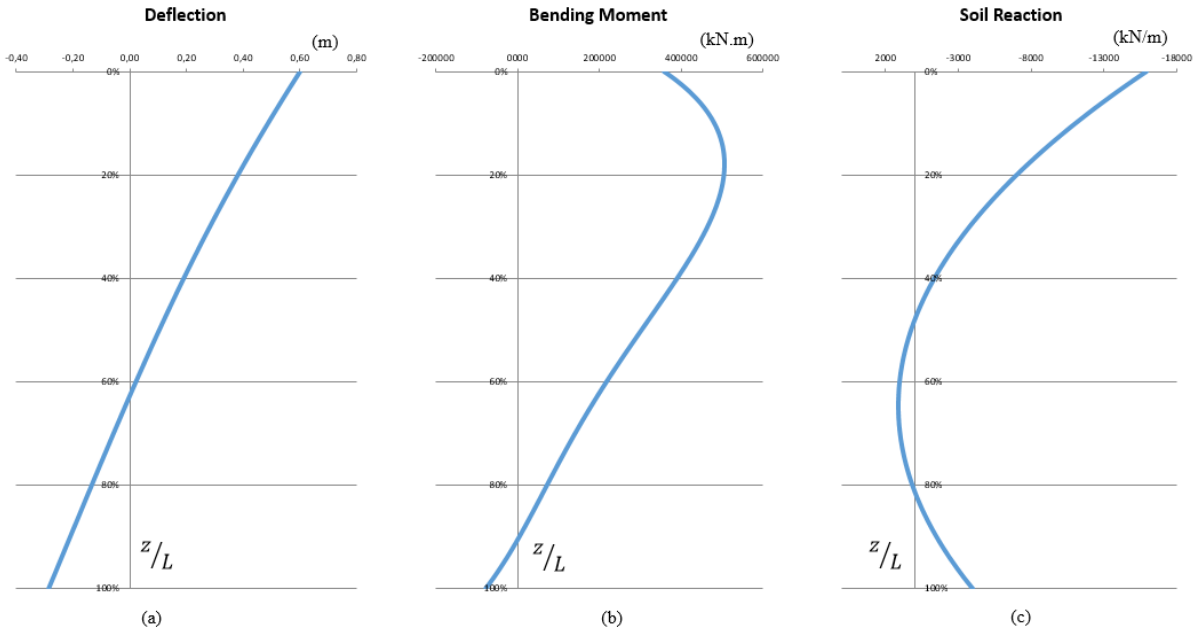

Fig. 5.4 – Curve fitting using *Microsoft Excel* for the Deflection of the pile (a), Bending Moment (b) and Soil Reaction (c)

By observing the previous figure, it is possible to conclude that this first approach is incorrect. The soil reaction should occur on 'the same side' of the graph as the deflection. That is, if the pile deforms in one direction the reaction of the soil is expected to be opposite, while from this process the derived reaction has, in some depths, the same direction of the pile, which is paradox.

Considering the possibility of the 2nd order polynomial curve for the soil reaction might be the problem due to the very small degree, a second analysis was made using MatLab. The *polyfit* function was used as *polyfit(x,y,n)* and the coefficients of a polynomial *p(x)* of a degree *n* were calculated to fit the *y* data by minimizing the sum of the squares of the deviations of the data from the model (least-squares fit).

After defining the best deflection fitting curve with a degree of 10, a 6th order polynomial curve was calculated for the soil reaction, from the 4th derivative of the first. Figure 5.5 shows the result of this analysis performed using MatLab.

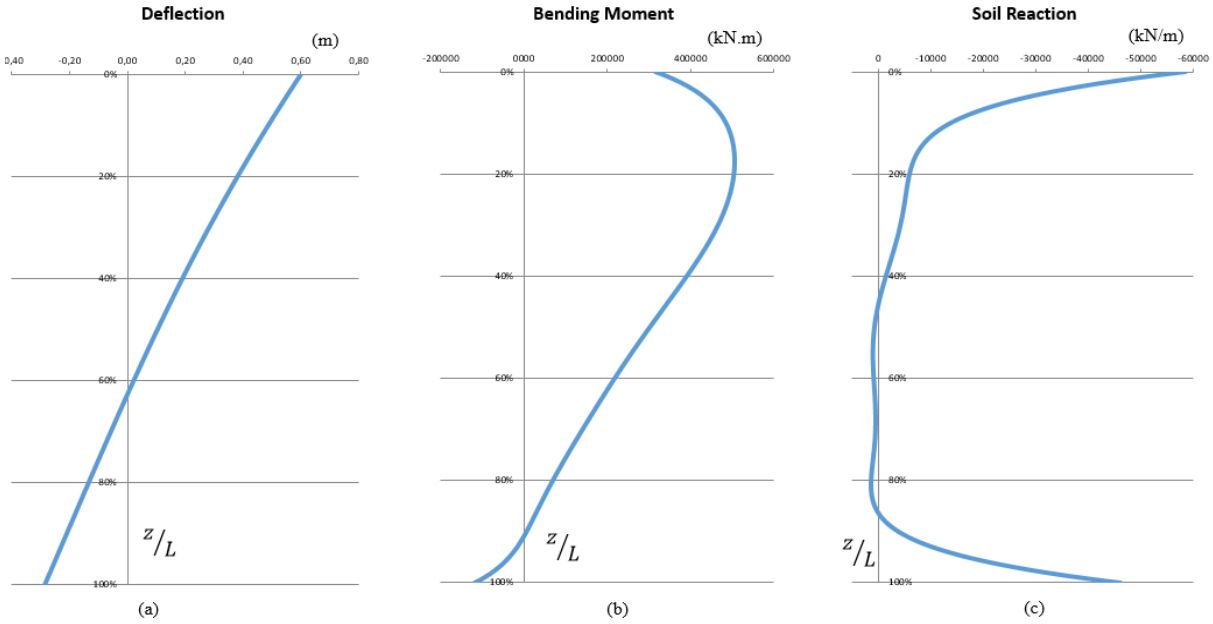

Fig. 5.5 – Curve fitting using *MatLab* for the Deflection of the pile (a), Bending Moment (b) and Soil Reaction (c)

There are almost no differences between the obtained curves for the deflection and the bending moment using Microsoft Excel or MatLab. Still, the results for the soil reaction, although looking very different in the two cases, have a fitting curve that has essentially the same trend.

The analytical derivative of the deflection of the pile was concluded to be inefficient for the deduction of the soil reaction.

5.4. NUMERICAL DERIVATIVE

Believing that a polynomial curve might not be the ideal fitting process for this case or that this analytical approached is essentially wrong, a second type of analysis was explored, using a numerical process to calculate the derivative.

The idea is to apply equation (5.1) to the points exported from PLAXIS 3D to calculate the first derivative. The second derivative is then obtained by applying the same equation to the results obtained one the first derivative. Then the process proceeds repeating itself, until the forth derivative, which corresponds to the soil reaction, is reached. Figure 5.6 shows the first results of this method.

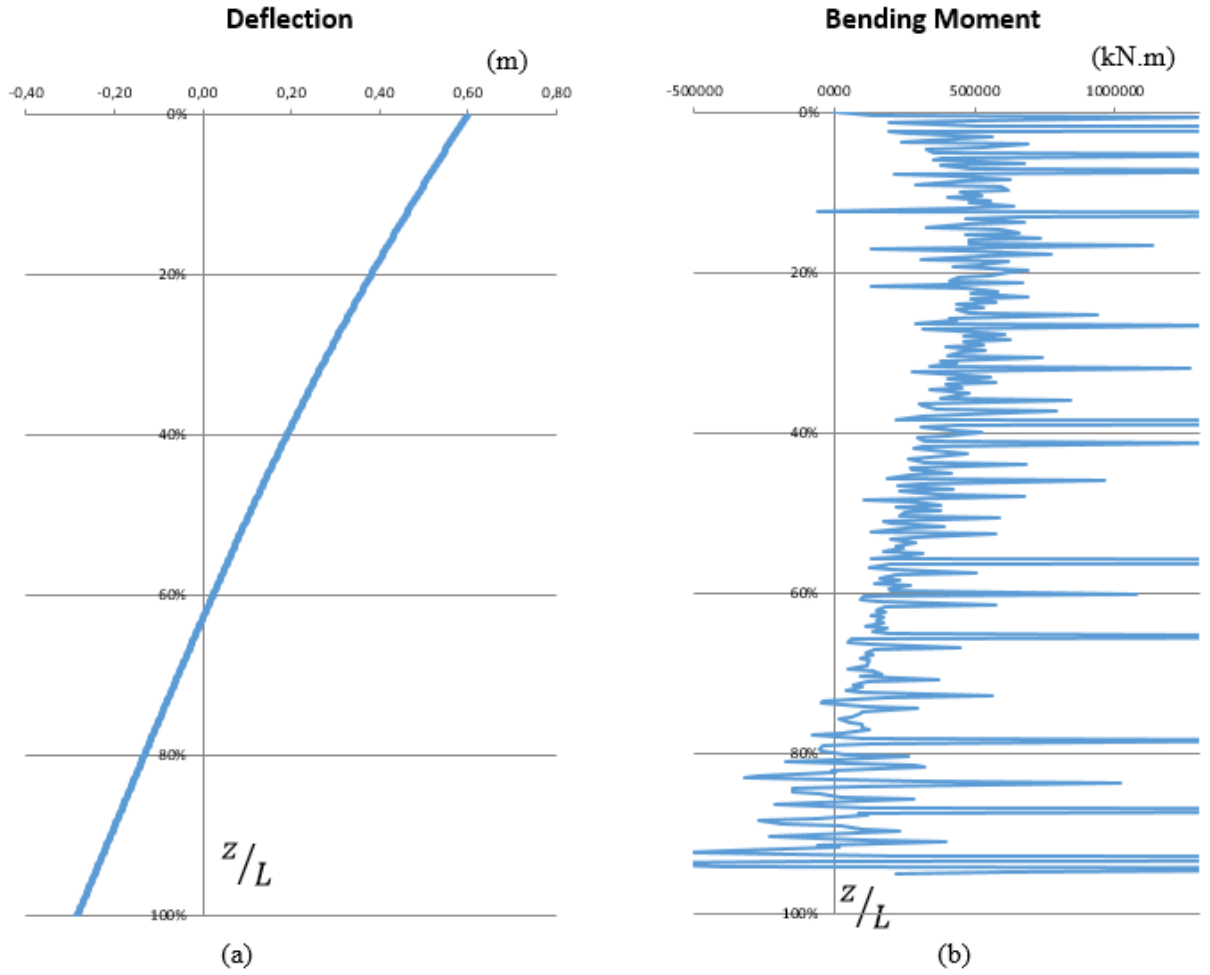

Fig. 5.6 – Numerical derivative for the bending moment (b) using the data of the deflection (a)

As it is possible to see from the previous figure, the results are very inaccurate and unreliable and this is only for the 2nd derivative (bending moment) which leads to the conclusion that the results for the soil reaction will be of even lower quality.

This happens because the points associated to the deflection are too distanced and also because they already have some very small numerical errors (which is acceptable for such a complex program as PLAXIS 3D) that will increase and have a larger impact in each derivative.

A simple procedure was developed in order to solve this problem. A polynomial curve was approximated to the deflection of the pile and, using the equation of that fitting curve, very small spaced points were calculated for the deflection of the pile. Figure 5.7 shows the result of the "transformation" of the data exported from PLAXIS 3D into a more reliable data obtained using the fitting curve.

As these points were obtained using the polynomial curve, they barely have any error. Therefore, the first numerical derivative (the slope of the pile) was calculated with sufficiently high precision. The second, the third and the forth numerical derivatives were then obtained using the data of, respectively, the first, the second and the third numerical derivative and are equally precise as the first numerical derivative because the initially calculated points are already very accurate.

Depth	Deflection
0,000	0,599479751
-0,176	0,592722550
-0,222	0,590927915
-0,246	0,590010834
-0,440	0,582593775
-0,643	0,574808326
-0,645	0,574753675
-0,647	0,574674592
-0,852	0,566851653
-1,002	0,561181947
-1,069	0,558622556
-1,222	0,552852947
-1,285	0,550452454
-1,325	0,548956793
-1,484	0,542972786
-1,664	0,536198710
-1,682	0,535534207
-1,695	0,535039216
-1,902	0,527295382

Depth	Deflection
0,000	0,599484400
-0,100	0,595632549
-0,200	0,591786546
-0,300	0,587946488
-0,400	0,584112467
-0,500	0,580284577
-0,600	0,576462906
-0,700	0,572647541
-0,800	0,568838565
-0,900	0,565036062
-1,000	0,561240110
-1,100	0,557450787
-1,200	0,553668168
-1,300	0,549892325
-1,400	0,546123330
-1,500	0,542361250
-1,600	0,538606151
-1,700	0,534858099
-1,800	0,531117154

Depth	Slope
-0,050	0,03851851
-0,150	0,03846003
-0,250	0,03840059
-0,350	0,03834020
-0,450	0,03827890
-0,550	0,03821671
-0,650	0,03815365
-0,750	0,03808975
-0,850	0,03802503
-0,950	0,03795952
-1,050	0,03789323
-1,150	0,03782619
-1,250	0,03775843
-1,350	0,03768995
-1,450	0,03762080
-1,550	0,03755098
-1,650	0,03748053
-1,750	0,03740945

Fig. 5.7 – Processing of the data exported from PLAXIS 3D

Figure 5.8 shows the results of the previously described analysis. A comparison between the deflection, the bending moment (2nd derivative) and the soil reaction (4th derivative) was chosen in order to shown the presence (or not) of errors as the degree of derivation increases.

As stated before, the soil reaction must be in accordance with the deflection of the pile meaning that if the pile deflects in one direction the soil reaction should have an opposite direction as if the pile deflects in the other direction. By observing figure 5.8 it is possible to see that this doesn't occur.

The conclusion for the numerical derivative approach was the same as the previous ones: inefficient for the extraction of the reaction of the soil in response to its respective displacement.

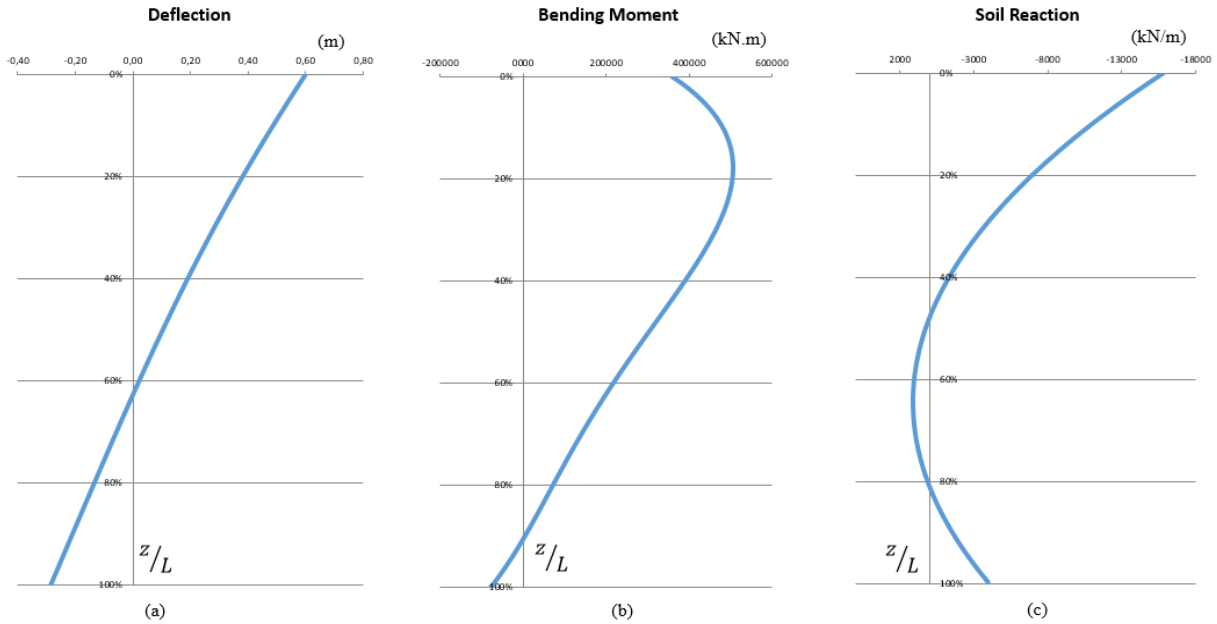

Fig. 5.8 – Numerical derivative for the bending moment (b) and soil reaction (c) using the data of the deflection (a)

5.5. Structural Analysis of the Monopile

A structural analysis of the pile was carried out in order to compare its results with the ones obtained from the previous analyses. This comparison is important to understand whether the derivative of the deflection of the pile is providing realistic results or not, assuming that the structural analysis is correct. The program used was SAP2000.

As SAP2000 is a structural program, the only useful information provided, for the work here by developed, is the bending moment and the shear force along pile. These results will be then compared with, respectively the third and the second derivative.

The first step of this analysis consisted on the structuring of the monopile as a beam and applying a support restrained only on the direction perpendicular to the direction of the development of the beam. Figure 5.9 shows a portion of the beam and the supports represented in SAP2000.

Fig. 5.9 – Pile represented in SAP2000

The supports were equally spaced at intervals of 20 centimeters with a total of 151. The idea was to apply displacements to the supports with the value of the deflection of the pile corresponding to its position. The displacements of the supports were calculated using a polynomial curve fitting the deflection of the pile, as performed before, and then importing to SAP2000 using Microsoft Excel. Figure 5.10 shows the deflection of the beam after applying the displacements to the supports and Figure 5.11 shows the result of the bending moment along the length of the beam/pile.

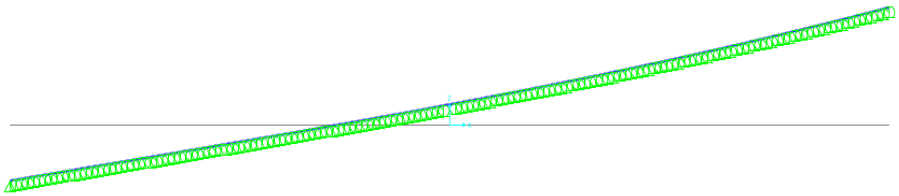

Fig. 5.10 – Deflection of the beam

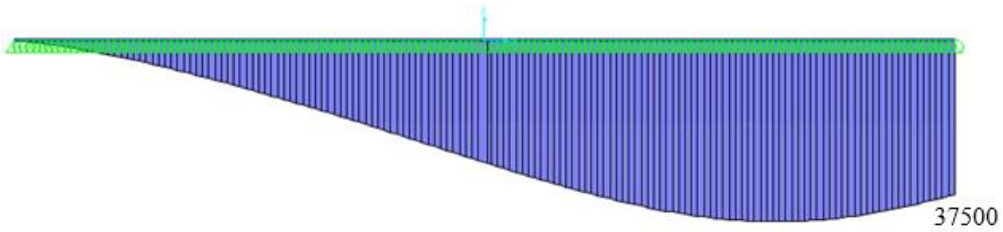

Fig. 5.11– Bending moment along the length of the beam/pile

Using SAP2000 the results of the bending moment along the pile should be the most precise way. By observing Figure 5.11 it is possible to conclude that the results obtained from the previous analyses are not very different from these most realistic values. Yet, a comparison between all the analyses will be shown in Figure 5.12 with respect to the bending moment and the shear force. It is clear from the observation of the following figure that all the analyses made so far lead more or less to the same results.

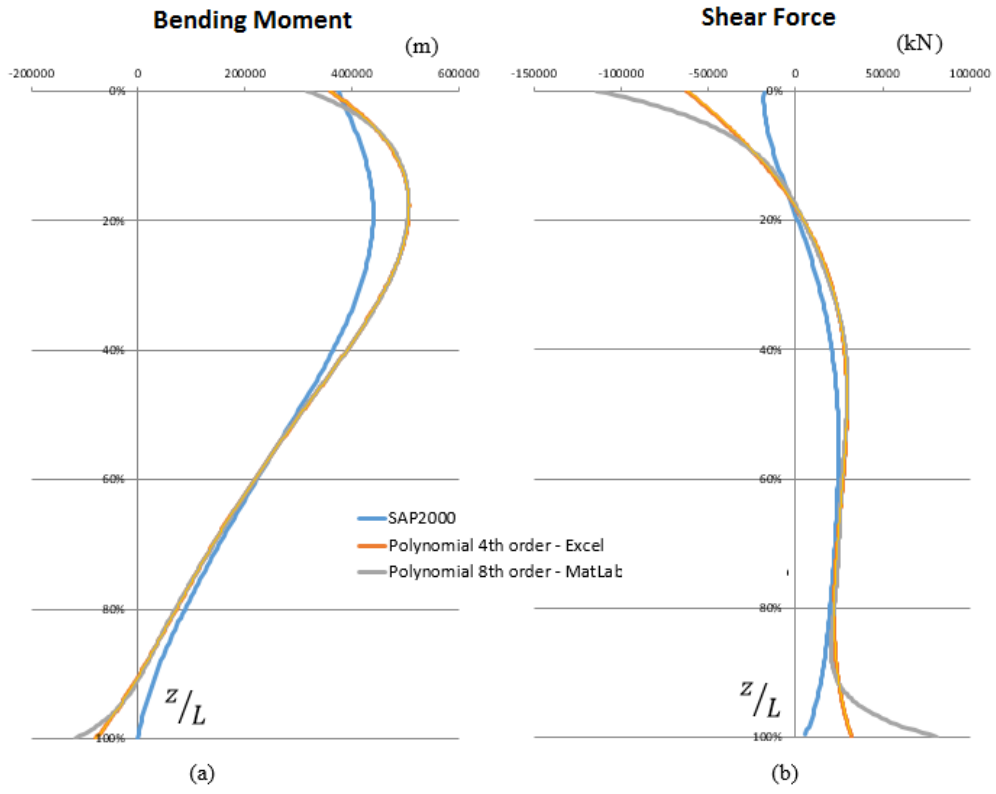

Fig. 5.12– Different results for bending moment (a) and shear force (b)

5.6. CONCLUSIONS

After all the different approaches for obtaining the soil reaction from the deflection of the pile have been explored it is concluded that this method is not suitable for the purpose of the work being developed in this thesis.

To strengthen this statement one final analysis will be made in this chapter. Figure 5.13 illustrates the outcome of some p-y curves achieved using one of the previous methods, revealing a quasi-elastic-linear behaviour of the material.

On the other hand, a qualitative analysis of the kind of response that would be expected for the reaction of the soil under this loading is presented in Figure 5.14. This was obtained by plotting the stress on an element of the soil on the direction parallel to the loading direction and repeating this to different depths.

Figure 5.13 illustrates p-y curves with no plastification of the soil (linear-elastic behaviour) while, in contrast, Figure 5.14 demonstrates that there is an increasing plastification of soil, whit more emphasis to the zone nearby the pile. It should be highlighted each curve of Figure 5.14 represents only the stress of one single point at a certain depth, so its shape is necessarily the p-y curve for that depth.

This leads to one conclusion: the application of the differential equation developed by Hetenyi can only be used for the first, second and third derivative (respectively, slope, curvature/bending moment and shear force), as these are characteristics of the pile, and not to the forth derivative since it refers to the reaction of the soil.

By analyzing equation (3.7), it is possible to perceive that the input parameters concern only the properties of the pile (Young's modulus, E) and the size of it (Inertia, I), do not take into account any properties of the soil. It is therefore understandable why the given relationship between the deflection of the pile and its forth derivative (previously believed to be the reaction of the soil) was inexplicably perfectly linear-elastic.

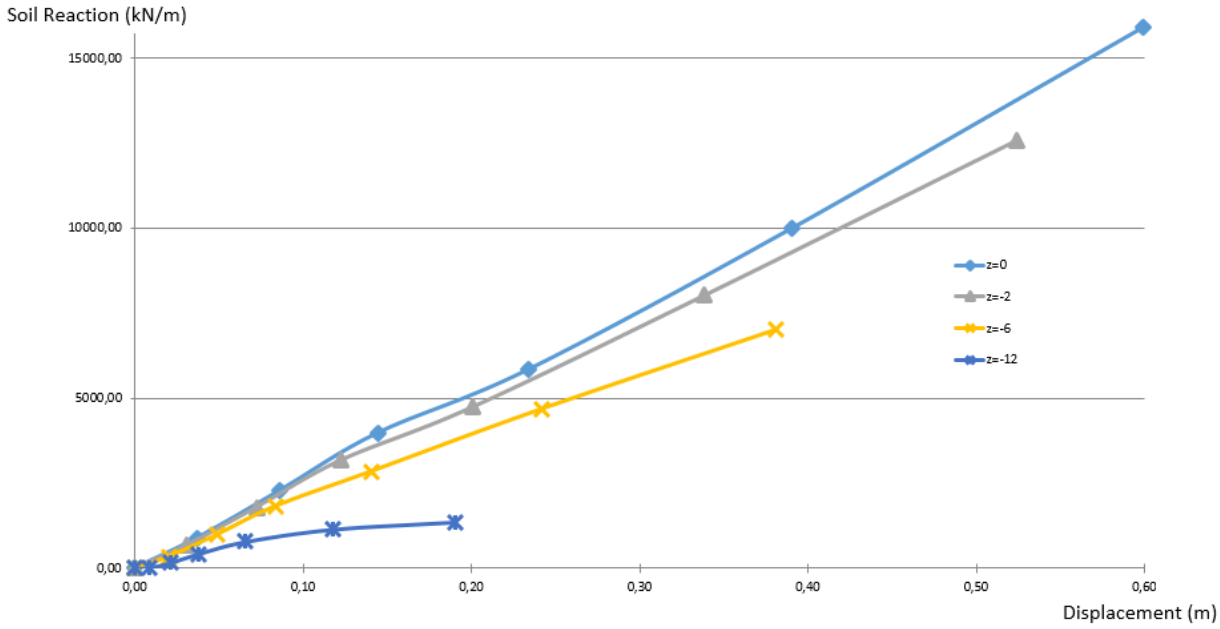

Fig. 5.13– p-y curves using the differential equation approach

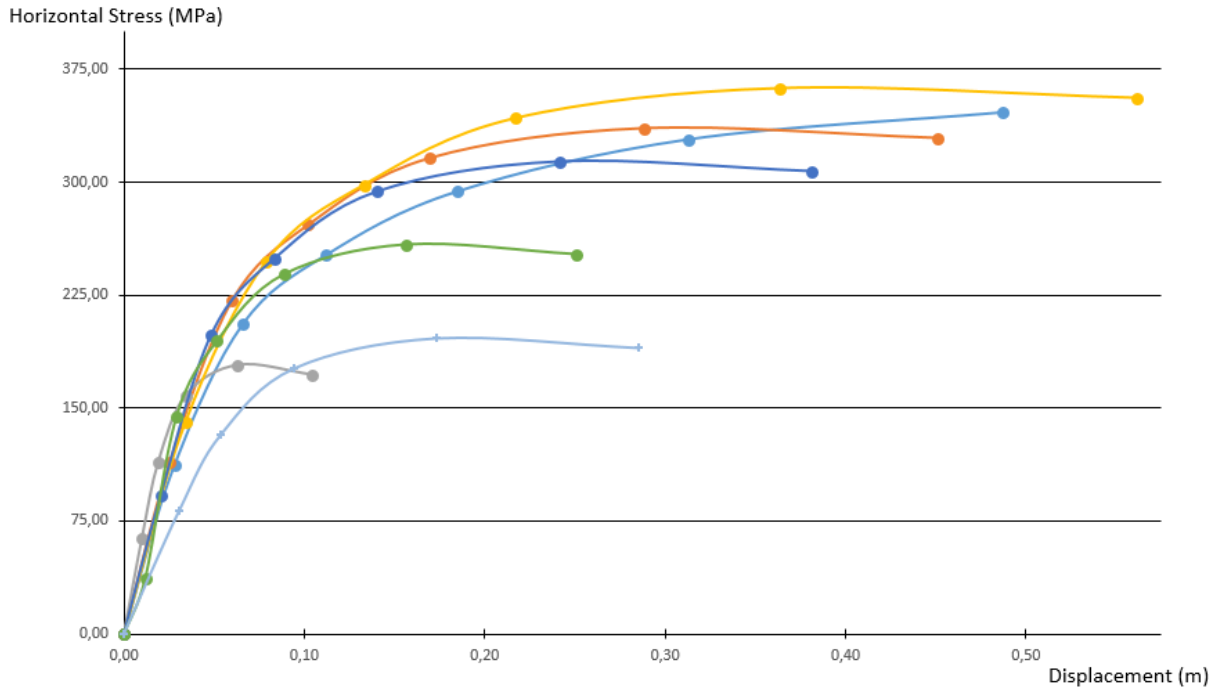

Fig. 5.14– Stress on the soil on the direction parallel to the loading direction

6

ANALYTICAL PROCEDURE FOR OPTIMIZATION OF THE NUMERICAL RESULTS

6.1. OVERVIEW

Having put away the hypotheses of using the differential equation (3.7) developed by Hetenyi to obtain the soil reaction, the only remaining option to calculate it is to integrate the generated stresses around the pile.

After building and perfecting a robust and realistic model, several calculations were carried out in order to find the best estimation for the distribution of the stresses around the pile. This estimation will be an analytical law that best suits the verified distributions using the data exported from PLAXIS 3D.

Finally, a methodology will be developed with the purpose of calculating hyperbolic p-y curves, using MatLab to find the best fitting curve for the determined points of the p-y curves.

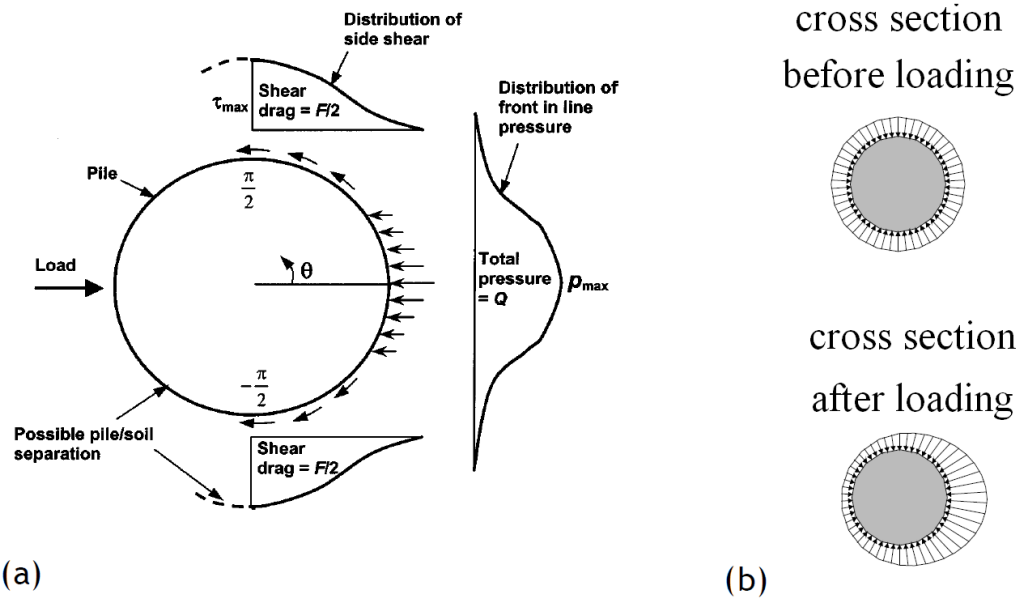

Fig. 6.1 – (a) Distribution of front earth pressure and side shear around the pile subjected to lateral load (Zhang et al., 2005); (b) Distribution of stresses around the pile before and after loading (Tuna, 2006)

6.2. EXTRACTION OF DATA FROM PLAXIS 3D

In order to obtain a good load-response development (or, in this case, displacement-response development) different levels of load have to be applied and this will lead to different levels of responses. In PLAXIS this is controlled by means of phases. By increasing the load/displacement amplitude in each phase, different responses will be generated by the model.

Once the calculation in PLAXIS has finished it is necessary to proceed with the extraction of results and each phase has its own results. For the work being here developed the extracted data was the resulting stresses corresponding to each applied displacement.

All the data would be lately processed using MatLab so the extraction from PLAXIS 3D needed to be done in a way that could be afterwards imported and used in MatLab. There were two options: Microsoft Excel or a Text Document. Microsoft Excel would have the advantage of a better consulting and manipulation of the data but the files were extremely heavy which would lead to very time-consuming calculations in MatLab. On the other hand, exporting the data into a Text Document saves a lot time on the calculations and the data import is very simple. The use of a *script* in MatLab to import the data in the Text Document is the best option (and probably the only one) and, if the user is experienced enough and able of understanding the used commands, it is possible to manipulate it and change it in a way to save even more time. Notice that, even though these implemented measures lead to a lot of time saving, these calculations might still last a few hours due to the amount of extracted data from each phase.

6.3. METHOD FOR INTEGRATION OF THE STRESSES AROUND THE PILE

After taking in possession the response, in terms of stresses, to the applied displacement, it is time to integrate these stresses around the pile in order to obtain the subgrade reaction modulus of the soil. There are two ways of doing so: using the stresses on interface or using the stresses on the soil surrounding the pile.

Whatever the case may be used, there are always numerical errors in these type of calculations so, instead of finding for each phase the stresses around the pile and then integrate it, a few tests will be run and analysed and, using those results, an analytical curve for the shape of these stresses may be empirically determined. By assuming this analytical curve as the shape of the stresses around the pile for all the calculations, it is possible to avoid errors and each calculation uses the same 'assumption' as the others.

The stresses on both the interface and the soil surrounding the pile will the analysed and a comparison between the two will be made with the aim of finding the best solution possible.

6.3.1. STRESSES ON THE INTERFACE

Using the interface to integrate the stresses around the pile would be the ideal solution but these elements sometimes are not very reliable. If the interface is very fine the calculation will take too long but if it is not fine enough there will be huge concentrations of stresses on the elements of the interface and the model will fail due to the interface (not realistic). However, even if the model doesn't fail due to the interface, there might still be high concentration of stresses on some of the elements of the interface that will lead to errors on the calculations. Having said that, the assumed value of the stress on a specific point will not be the value of the closest point to it but an average of all the points in its surrounding area.

First of all, it is important to highlight that only the stresses in the direction of the displacement will be accounted (in this case, the xx direction). This is a very fair assumption as the stresses on the perpendicular direction to the one of the displacement (yy direction) on one side of the pile cancel the ones of the other side of it proving that only the direction of the displacement is relevant.

The output of PLAXIS 3D provides, for interfaces, the normal and the shear stresses on it (among others). By knowing the coordinates of the element of the interface it is possible to find the xx component of the normal and shear stresses acting on it (for this work, only the shear stress in the horizontal direction is needed). Figure 6.2 (a) shows the normal and shear stresses acting on the interface and Figure 6.2 (b) shows the expected shape of the integrated stresses around the pile.

Figure 6.3 shows the distribution of the shear stress, the pore pressure and the total normal stress around the pile. As expected, there is a bigger concentration of shear stress in the center (from the perspective of this image) of the pile while on the two zones closer to the boundary and specially on the bottom, the concentration of pore pressure and total normal stresses are much bigger. It is also possible to notice in Figure 6.3 (c) that the distribution on for the high values is not very uniform. This is due to what was referred previously as the errors associated to the high concentration of stresses on some of the elements of the interface.

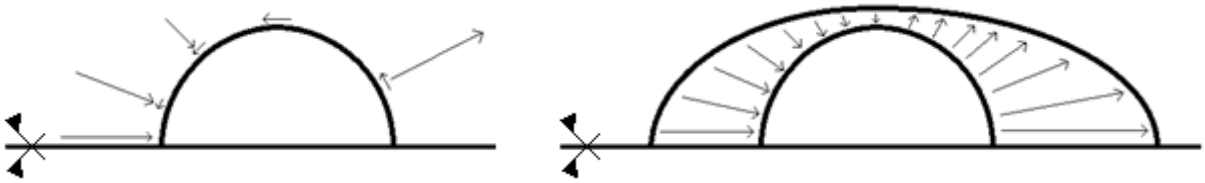

Fig. 6.2 – (a) normal and shear stresses; (b) resulting stresses around the pile

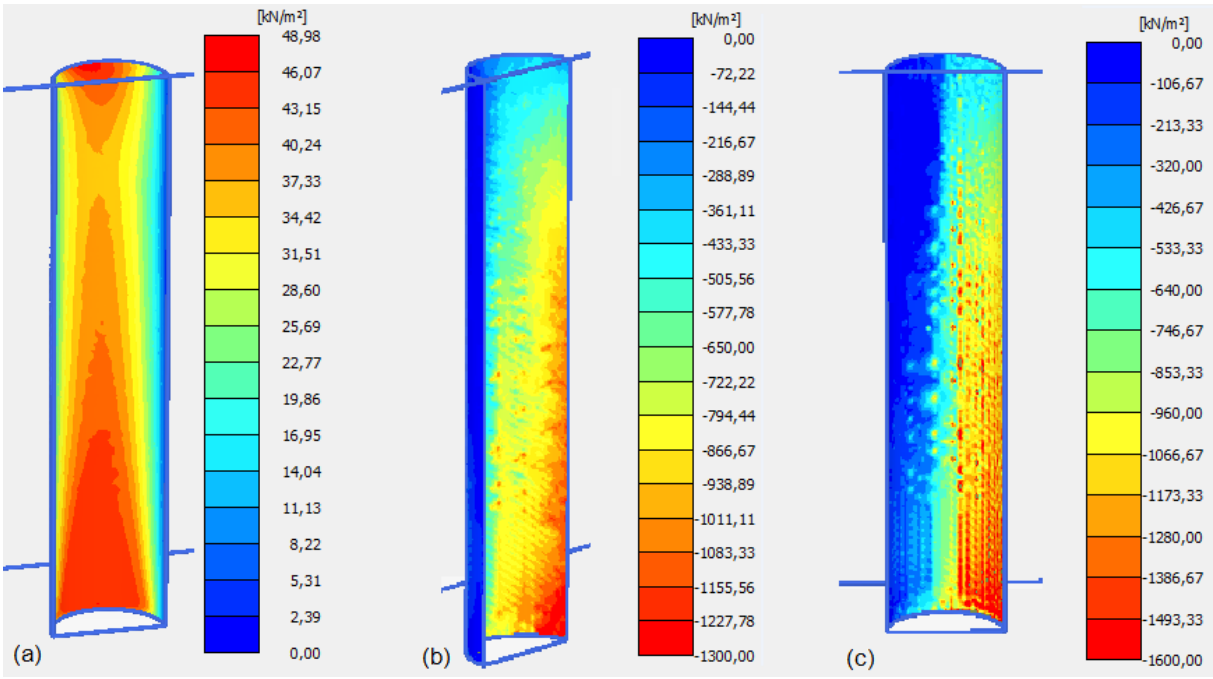

Fig. 6.3 – Interface shear stresses (a), pore pressures (b) and total normal stresses (c)

By using MatLab to interpolate the value for the total stresses acting on the interface on the xx direction, it was possible to obtain the results shown in Figure 6.4. This figure shows the results like in Figure 6.2 (b) but only in the xx direction. The different curves of each graph represent the different responses obtained from the different levels of applied displacements. It is now possible to see, on the less stressed part of the pile (top of the graphs), that these calculations are vulnerable to errors - there were even some cases in which the curves were much more irregular (although this figure is very representative of the common results obtained).

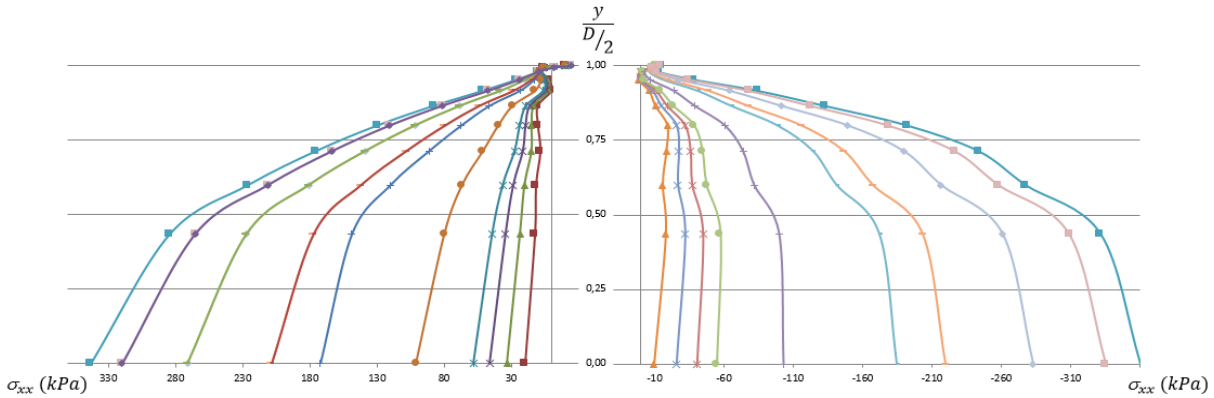

Fig. 6.4 – Obtained results for xx stresses around the pile using the Interface

6.3.2. Stresses on the Soil

Using the soil to integrate the stresses around the pile has one big disadvantage compared to the interface: the amount of exported data from PLAXIS is much bigger (Text Document files almost 50 times heavier) as the soil represents the all volume of the model and the interface is just a surface. The results are more precise than the ones from the interface (much smaller elements) but also not entirely reliable due to numerical errors in the area close to the interface. In addition, when asked the stresses at a specific point, PLAXIS does a very simple interpolation between other known points that might lead to very significant errors.

Figure 6.5 shows the variation of the total stresses in the soil at rest on the xx direction where it is possible to see that the soil inside the pile and the soil on the zone surrounding it has an overall increase of horizontal stress due to the driving of the monopile (confinement of the soil on that area).

Figure 6.6 shows the variation of the total stresses in the soil but now it is due to an applied displacement to the pile. There is clearly an increase of stresses on the loaded side of the pile (right) and a decrease of stresses on the unloaded side of the pile (left). It is also possible to see that, by allowing an interaction between the inside and the outside soil of the pile, there is a change on the stress state at the toe of the monopile that will lead to high concentration of stresses and will make it more difficult to find a good law for the p-y curve at these high depths.

Finally, by comparing Figures 6.6, 6.7 and 6.8, it is clear that there is a big volume of liquefied soil on the unloaded side of the model. Two types of liquefaction happen in this model: on the volume closer to the surface of the pile not only the effective stresses are zero but the total stresses and the pore pressures are also zero; on the same side of the model but further from the pile the effective stresses are still zero (liquefaction) whether the total stresses and the pore pressures are not zero and have the same value, as it should.

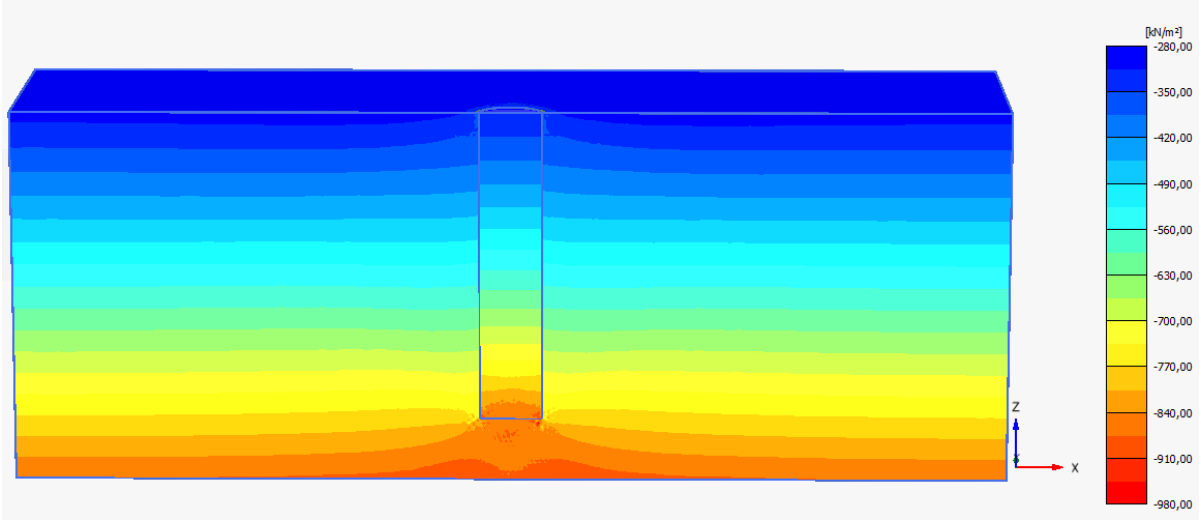

Fig. 6.5 – Total stresses in the soil at rest on the xx direction

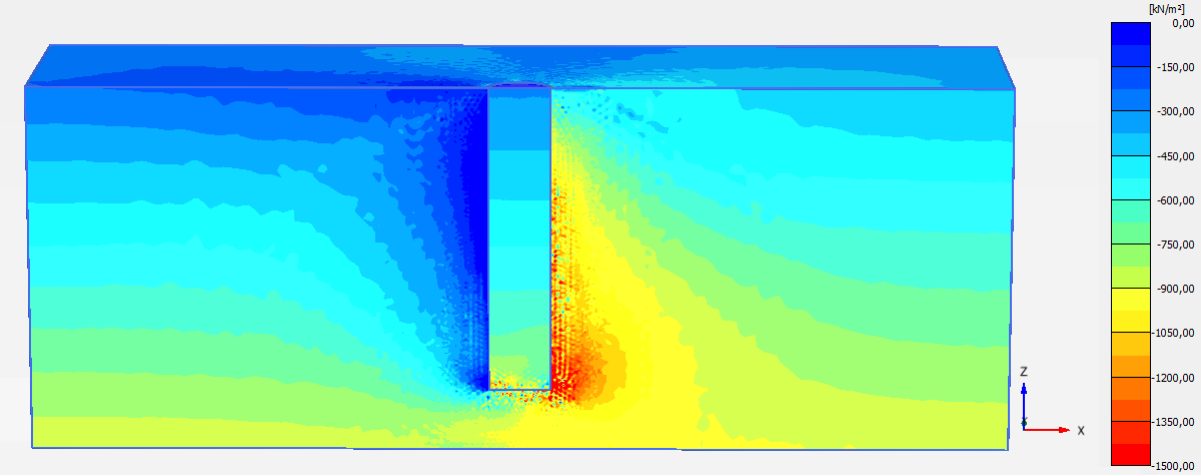

Fig. 6.6 – Total stresses in the soil with applied displacement on the xx direction

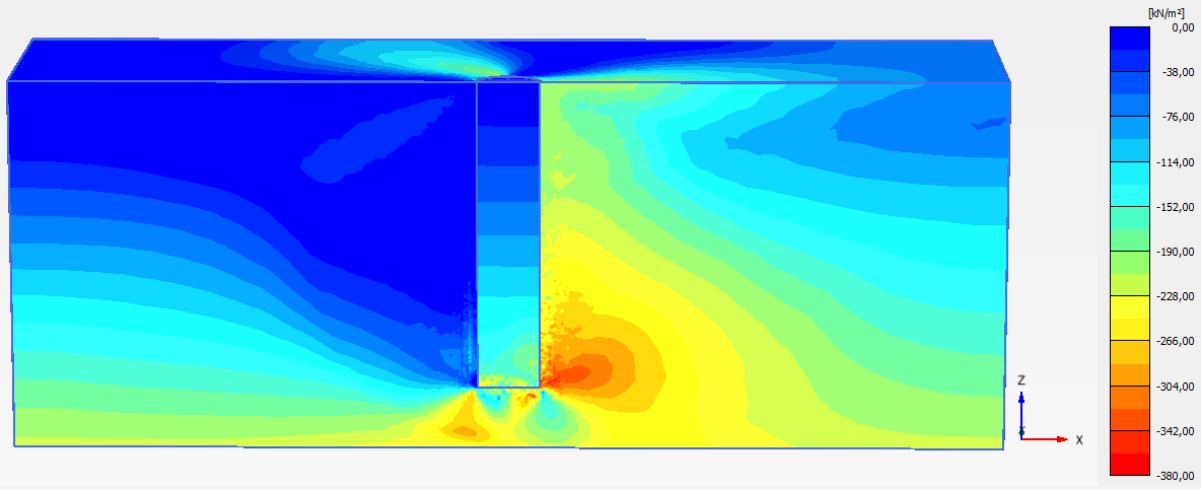

Fig. 6.7 – Effective stresses in the soil with applied displacement on the xx direction

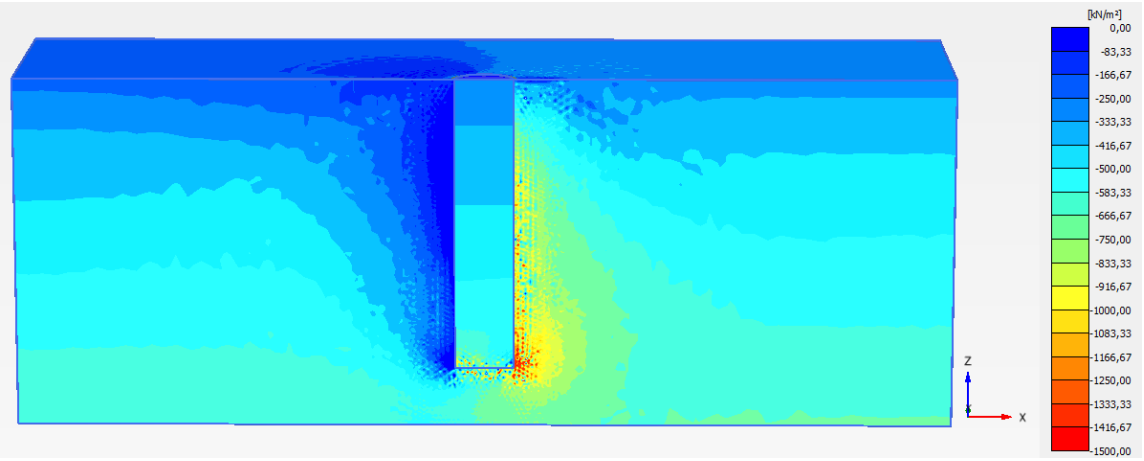

Fig. 6.8 – Pore pressures on the soil with applied displacement

The exported data from PLAXIS 3D was the information shown in Figure 6.6 with the value for the total stresses on the soil on the xx direction for every phase of the calculation. MatLab was then used to process all this information in a fast way.

The *griddata* command of MatLab interpolates a surface at some requested points using data points previously defined. Having this interpolated surface, the *surf* command creates a three-dimensional shaded surface.

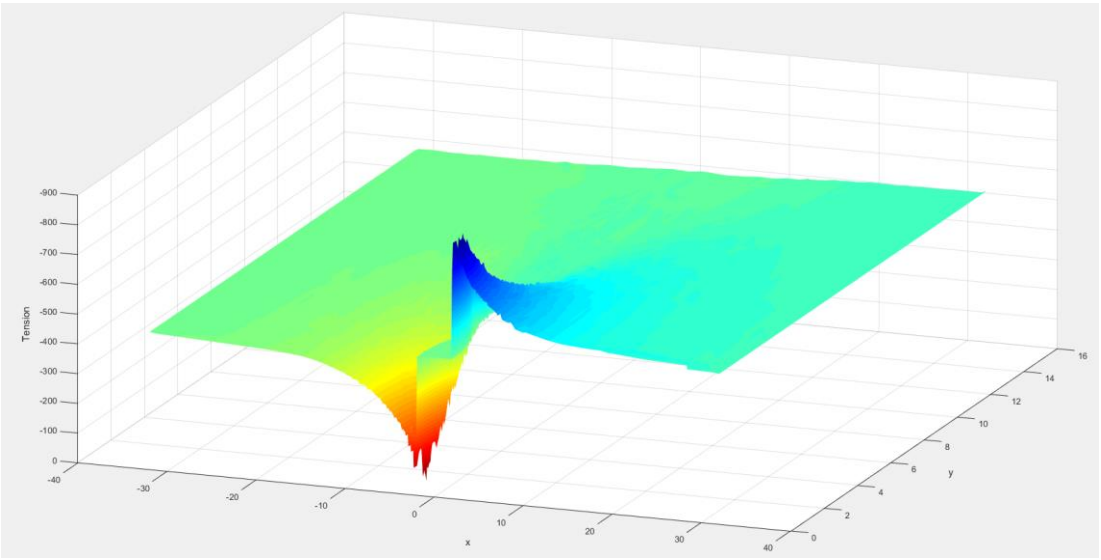

Fig. 6.9 – Three- dimensional representation of the stresses on the xx direction at a certain depth

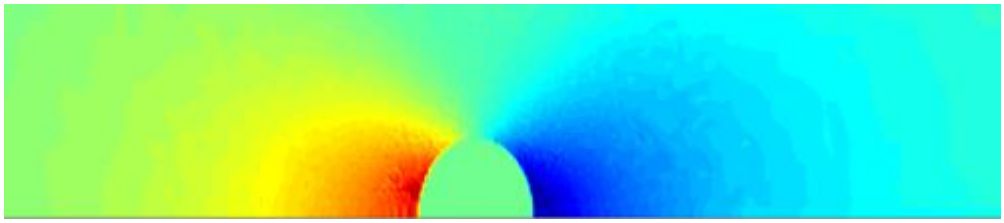

Fig. 6.10 – Upper view of the three- dimensional representation of the stresses on the xx direction at a certain depth

Figure 6.9 shows a surface that represents a horizontal plane crossing a model, at a certain depth, showing the stresses on the xx direction on the soil, like Figure 6.6, and plotting it in a 3D graph (the colors of the scale are opposite as one is taken from PLAXIS and the other from MatLab). Figure 6.10 shows the upper view of the three-dimensional surface.

By crossing a surface like the one of Figure 6.9 with a vertical plane parallel to the boundary that defines the symmetry of the model, a development of the horizontal stresses along the model is observed: on the unloading side the stresses tend to decrease when closer to the pile and tend to the at rest stress state the further it gets from the pile; on the loading side the stresses tend to increase when closer to the pile and also tend to the at rest stress state the further it gets from the pile (Figure 6.11).

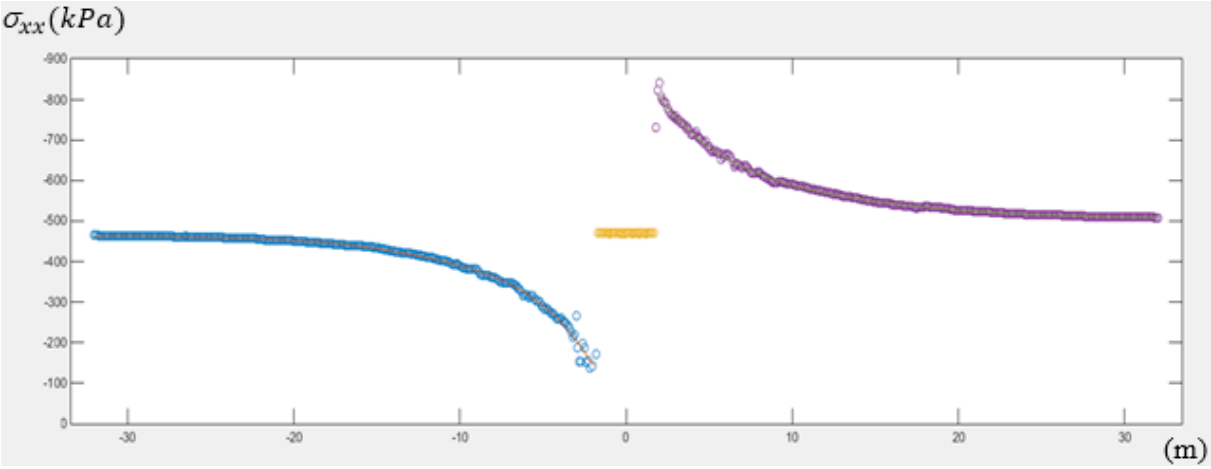

Fig. 6.11 – Two-dimensional development of the horizontal stresses on the xx direction along the model

By approximating these points of values of stresses to a curve (for this case, a 6th degree polynomial curve was concluded as the best fit), it is easier to obtain the stresses on the soil surrounding the pile by doing this for several vertical planes. This method also avoids numerical errors.

The result for this analysis is shown in Figure 6.12.

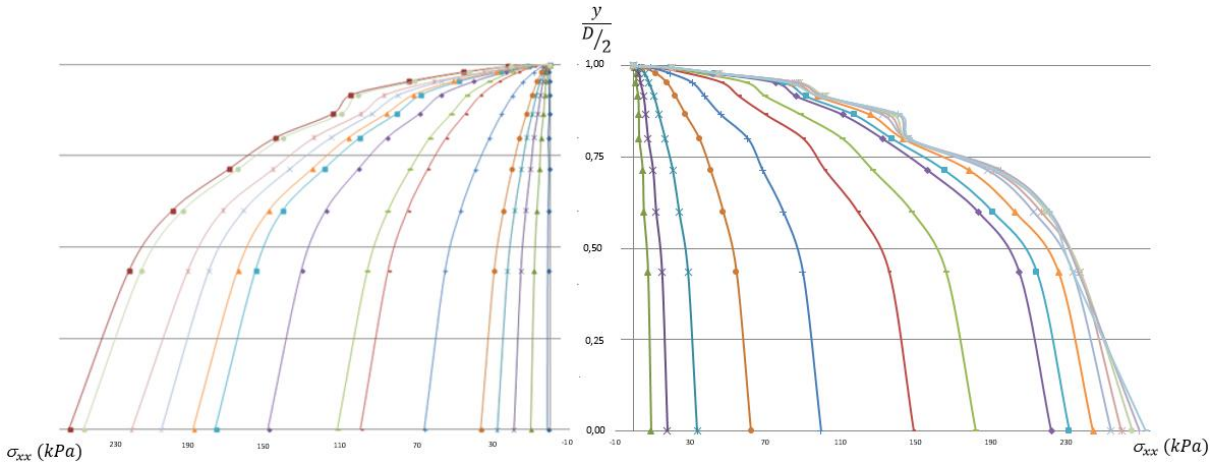

Fig. 6.12 – Obtained results for xx stresses around the pile using the Soil

6.3.3. Comparison between Methods and Final Solution

Having analyzed how the stresses around the pile develop using the interface and the soil, it is now time to define the curve that will be used.

As stated before, the interface was noticed as one of the big problems of PLAXIS 3D still unsolved: there are points with a large concentration of stresses and the factor of coarseness of this structure must be very well chosen in order to avoid failure of the interface instead of failure of the soil.

On the other hand, although there are also some numerical errors when using the stresses in the soil, these problems were easier solved using the interpolation of MatLab and the approximation of the development of the stresses along the length of the model to a polynomial curve.

That being said, the results from the interface work as a confirmation of the shape of the stresses around the pile but the results from the soil will be the ones that will be taken into account as they were considered more accurate and reliable. Figure 6.13 shows a comparison between a common shape of the stresses around the pile using the interface and the soil.

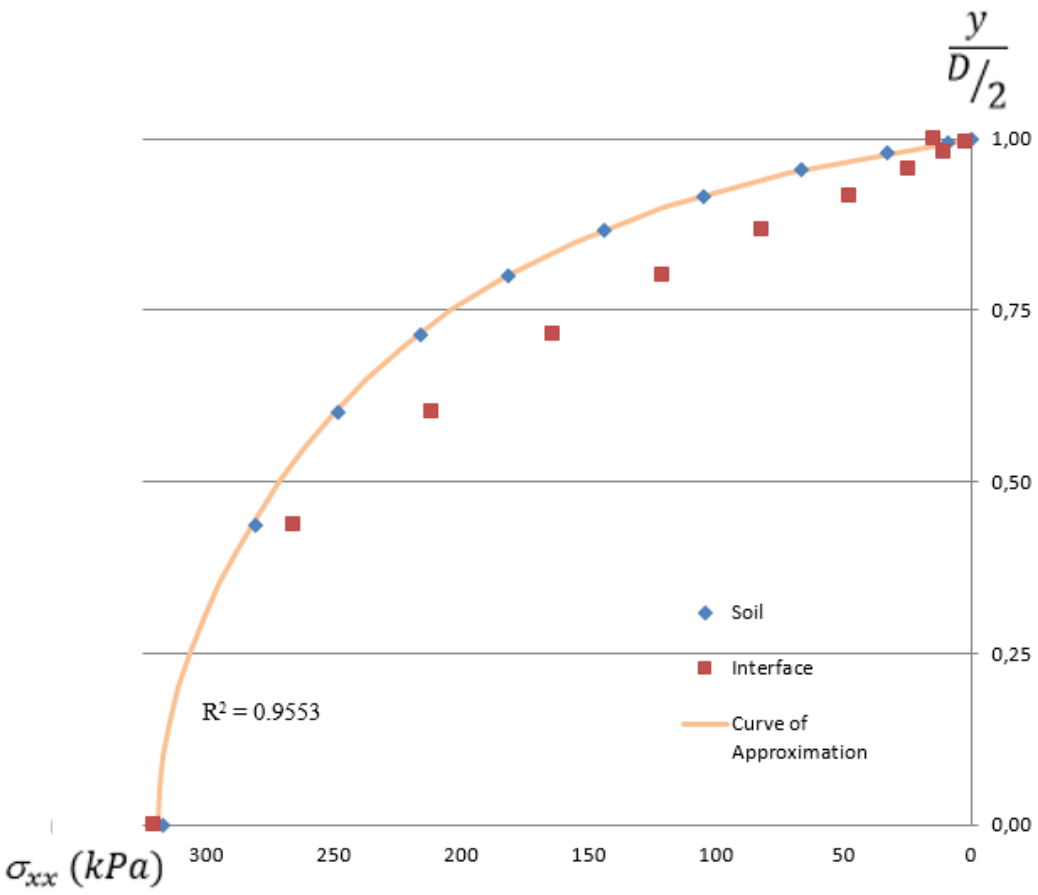

Fig. 6.13 – Comparison between the stresses around the pile using the interface and the soil

For the characterization of the curve defining the shape of the stresses around the pile several options were explored. The first try was with a hyperbola but it was soon concluded that this wasn't a good fit for this case. The second try was an exponential curve (equation (6.1)) that had a similar development to the one that was being searched for but it overestimated in a significant value the expected stresses.

The constant *K* on equation (6.1) is the value of the stress on the soil on the xx direction right on the border of the model (around 320 for the case shown in the figure) and *b* is a constant calculated in order for the value of the stress at the furthest point of the border of the model (*y/(D/2)=1.00)* being zero (*ln(K)/2*). In fact, the value at this point is not zero: although there is no stress on the xx direction, this point is the one with the highest shear stress. Yet, it was notice that, when it concerns the area inside the curve defining the shape of the stresses, it doesn't have any influence as the value of the shear stresses are very small when compared to the stresses on the xx direction.

$$\sigma_{xx} = \left(K - e^{b*y}\right) \tag{6.1}$$

In order to adapt this exponential curve to the obtained results, the cosine of the angle of the between the center of the pile and a point on the circumference (Figure 6.14) of it was used and equation (6.2) was at last reached as a final solution for the shape of the stresses around the pile.

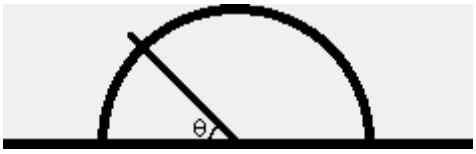

Fig. 6.14 – Angle used in the empirical curve for the shape of the stresses around the pile

$$\sigma_{xx} = \left(K - e^{b*y}\right) * (\cos\theta)^{\cos^2\theta} \tag{6.2}$$

Figure 6.15 sums up the result of the process described so far. The integration of the curve defined as the shape of the stresses around the pile (equation (6.3)) is what will lead to the subgrade reaction modulus for the p-y curve. Equation (6.3) is the same as equation (6.2) but it is expressed only in terms of *y* (*R* is the radius of the pile).

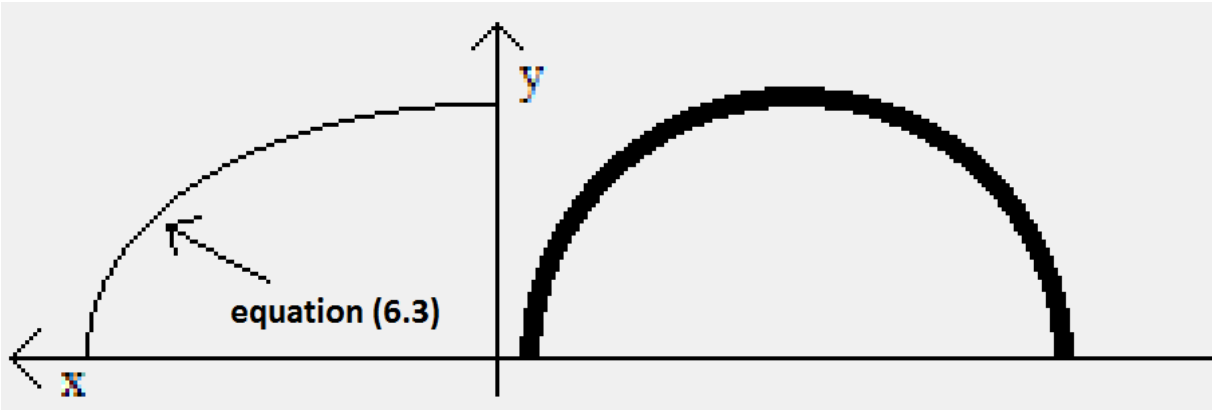

Fig. 6.15 – Curve fitting the shape of the stresses around the pile

$$\sigma_{xx} = \left(K - e^{by}\right) * \cos\left(tan^{-1}\left(\frac{y}{\sqrt{(R^2-y^2)}}\right)\right)^{\cos\left(tan^{-1}\left(\frac{y}{\sqrt{(R^2-y^2)}}\right)\right)^2} \tag{6.3}$$

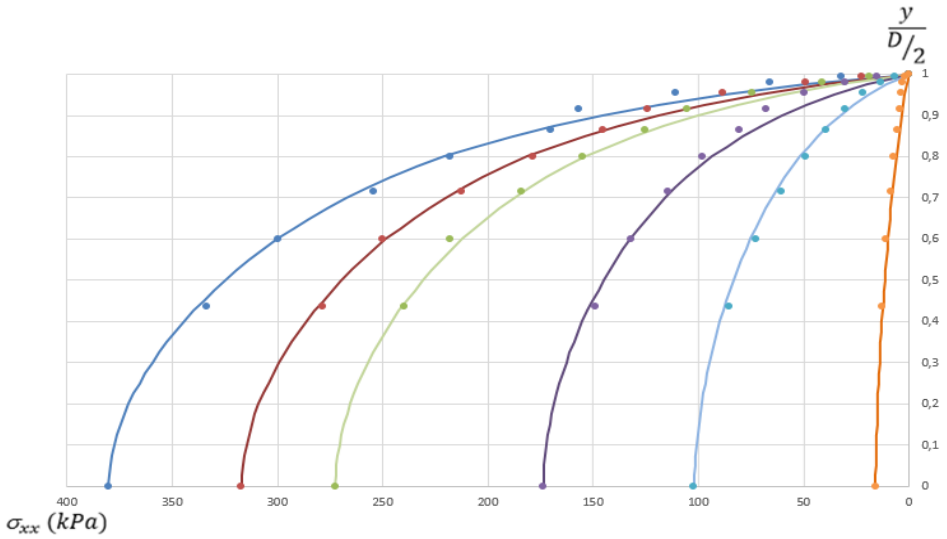

Fig. 6.16 – Curve defining the shape of the stresses around the pile fitting the data from PLAXIS 3D

6.4. NUMERICAL RESULTS FOR P-Y CURVES

Each applied displacement will lead to different values of stresses generated around the pile – although its shape is always the same and the one determined it *6.3.3.* will be the used one. After integrating the area of the curve used to define the shape of the stresses around the pile, the subgrade reaction modulus of the soil to a specific load/displacement can be obtained in two ways: subtracting the value of the unloaded side of the pile to the value of the loaded side; or by subtracting the values of both sides to the values at the resting state of the model and then sum these two values. In this work it is of interest to analyse the soil reaction, *p*, per meter of length of the pile so its value is the same as the subgrade reaction modulus.

Appling this procedure, for a specific displacement and at a certain depth, one point of a p-y curve is obtained. Figure 6.17 shows a typical result for one of the p-y curves and Figure 6.18 the different p-y curves obtained for different depths – the red dots refer to a deeper depth that the blue dots.

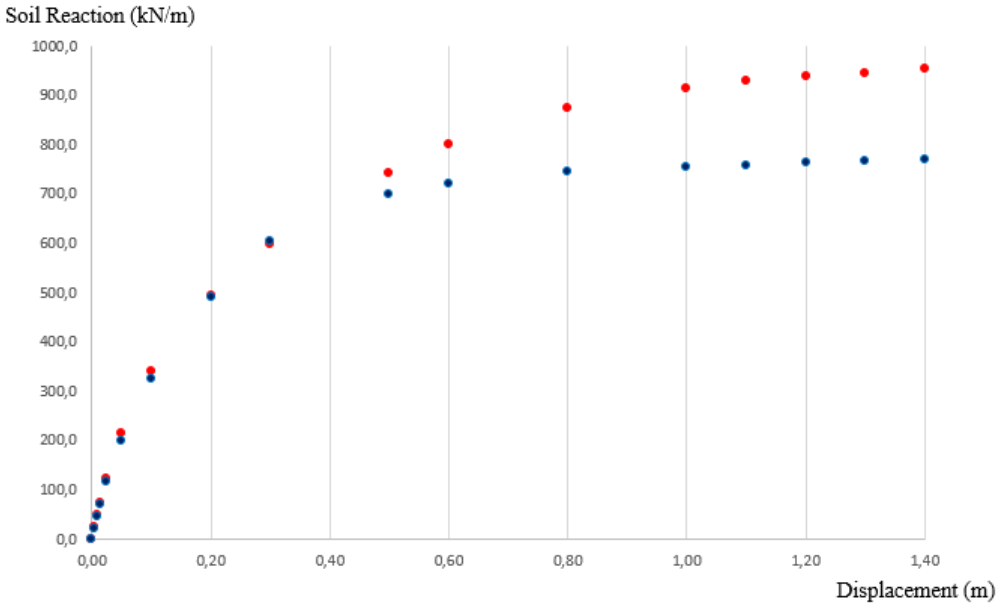

Fig. 6.17 – Typical result for a p-y curve with the different points represented

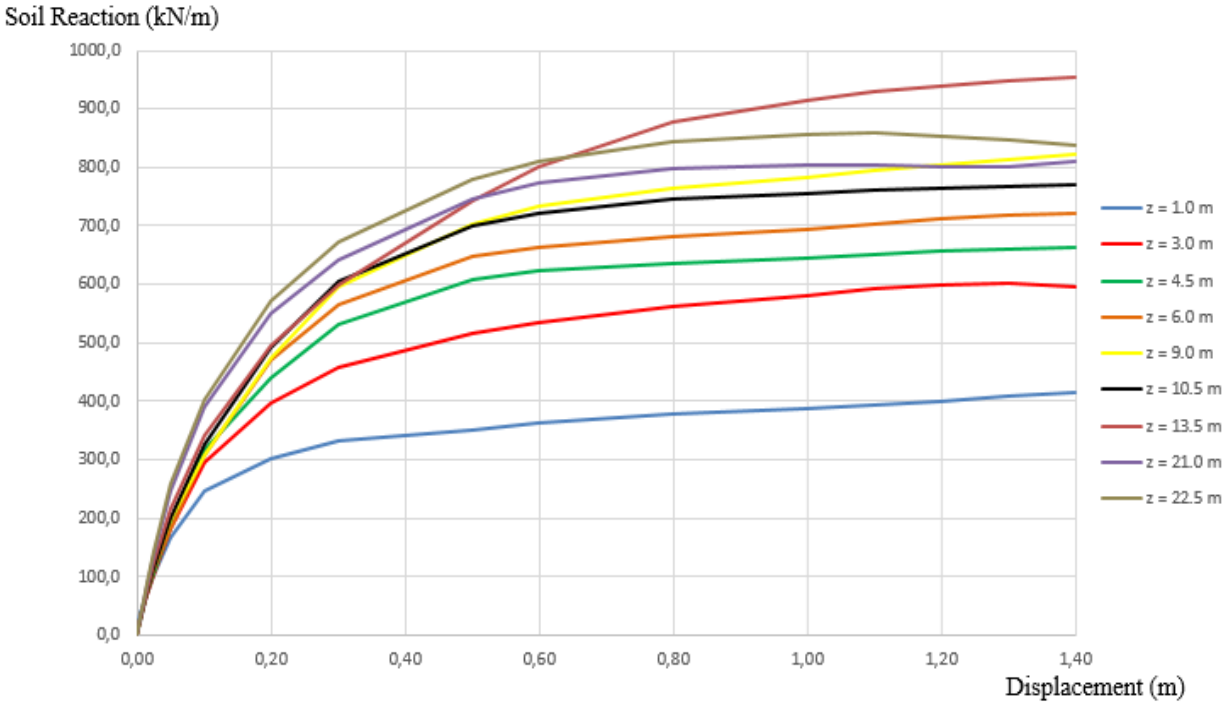

Fig. 6.18 – p-y curves for different depths

Both figures show a very satisfactory development of the p-y curves with a very well defined ultimate bearing capacity for the soil and a constant increase of initial stiffness over the length of the pile. Yet, as it is possible to observe in Figure 6.18, the p_u does not present a stable behaviour. The curves start to get unsystematic as the imposed displacements start to increase and p-y curves of lower depths present ultimate bearing capacities higher than the ones of p-y curves of deeper depths.

Because of this problem, an analytical solution for the numerical results obtained from PLAXIS 3D will be developed in order to regulate the curves and find a way to better understand the parameters that influence the most the shape of the curves.

6.5. Analytical Solution for p-y Curves

Here an analytical solution that best suits the obtained results of the p-y curves will be searched in order to normalize the results and eventually identify the critical parameters.

Two different hypotheses will be tested: the first one is Matlock's p-y curve, which is the one suggested by the API, with equation (6.4); the second one is equation (6.5) which was proposed by Georgiadis et al. (1992). The parameter k_s in equation (6.5) is the initial stiffness of the p-y curve to which Vesic (1961) expressed as in equation (6.6).

$$p = 0.5 * p_u \left(\frac{y}{y_c}\right)^{\frac{1}{3}} \tag{6.4}$$

$$p = \frac{y}{\frac{1}{k_s}+\frac{y}{p_u}} \tag{6.5}$$

$$k_s = \frac{0.65}{D} \sqrt[12]{\frac{E_s D^4}{EI}} \frac{E_s}{1-\mu^2} \tag{6.6}$$

MatLab has a command *lsqcurvefit* that solves nonlinear curve-fitting (data-fitting) problems in least squares sense. Given the input data, displacements (y), and the observed output data, soil reaction (p), this command finds the coefficients for the unknown variables in order to get an equation that best fits the data. For Matlock's p-y curve the unknown variables are the p_u and y_c and for Georgiadis' p-y curve the unknown variables are the p_u and k_s.

Figure 6.19 shows the best fit of equation (6.4) for the given data of a p-y curve and Figure 6.20 the best fit of equation (6.5). By looking at both figures it is obvious that the hyperbolic equation proposed by Georgiadis has a perfect fitting for the results obtained from PLAXIS 3D and that Matlock's method for the definition of the p-y curves underestimates a lot the capacity of the soil.

To finalize, the hyperbola of equation (6.4) is the one that will be used from hereafter in order to evaluate how the p-y are influenced by the diameter of the pile and its critical parameters that influence its shape over the length of the pile.

The blue dots represent the numerical results obtained from PLAXIS 3D and the red lines represent the p-y curve of the referred methods that best fit the numerical results.

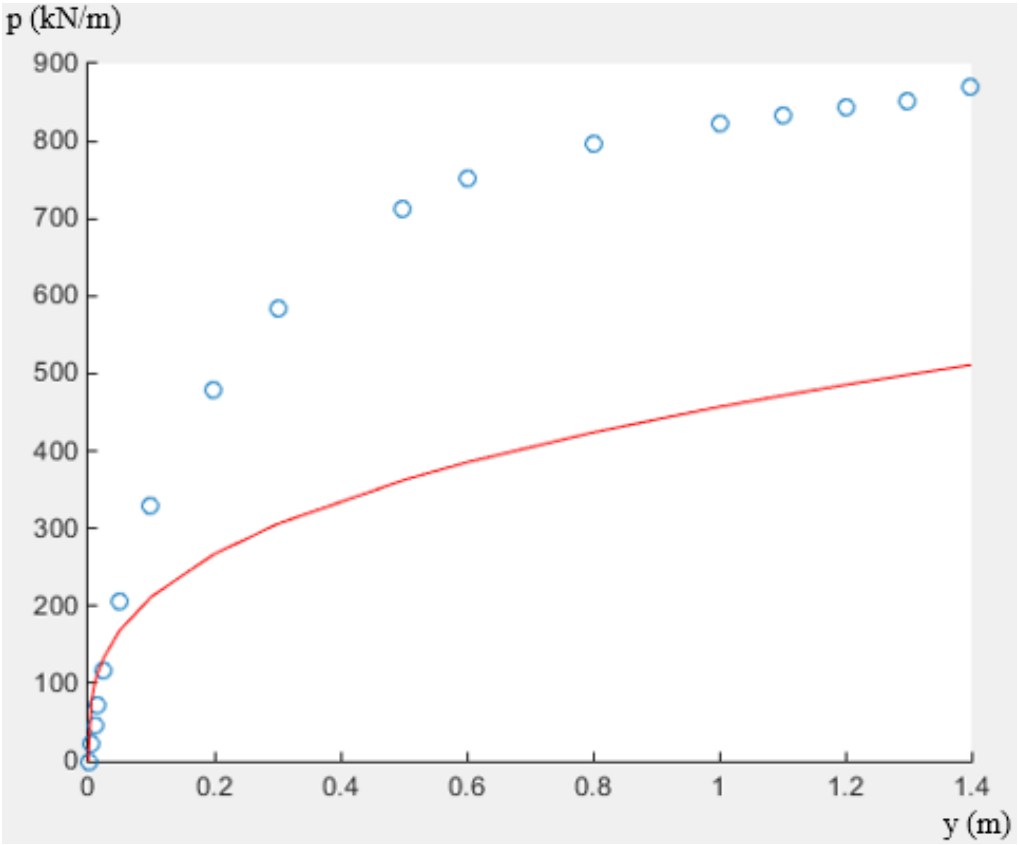

Fig. 6.19 – Fitting of the p-y curve proposed by Matlock for the given data

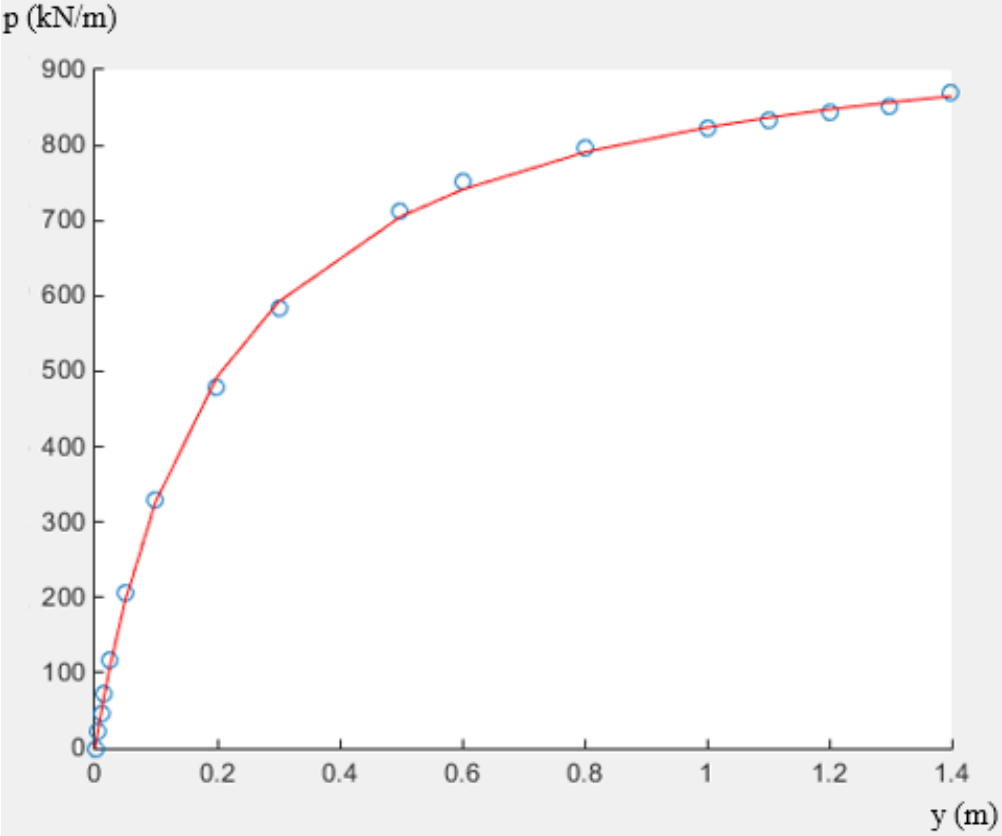

Fig. 6.20 – Fitting of the p-y curve proposed by Georgiadis for the given data

6.6. FINAL COMMENTS

At this point, all the data exported from PLAXIS 3D has been processed using MatLab and the equation of the hyperbola that is going to be used to describe the obtained p-y curves is defined. The integration of the stresses on the soil surrounding the pile was performed and the procedure to obtain the numerical results was optimized and programmed in MatLab.

The next step is to study the different p-y curves obtained from the different sensitivity studies performed and define a law that characterizes the parameters used in the equation of Georgiadis. These sensitivity studies consisted on the variation over the depth of the undrained shear strength of the soil and the Young's modulus of the soil and on the variation of the diameter of the pile.

The proposal for the characterization of the p-y curves is then compared to the method suggested by the API, which is the one used nowadays by most engineers for the design of the foundations of monopiles.

7

PROPOSED METHOD FOR THE CHARACTERIZATION OF p-y CURVES FOR THE DESIGN OF MONOPILES FOUNDATIONS

7.1. OVERVIEW

The aim of this chapter is to develop and present a proposal for the definition of the p-y curves that characterize the interaction between the soil and the pile subjected to lateral loading in clay.

On the previous chapter, an analytical solution for the p-y curves was defined. For this solution, the ultimate bearing capacity of the soil, p_u, and the initial stiffness of the p-y curve, k_s, are the critical parameters, in others words, the parameters that define the p-y curves. By calculating both these parameters for the different p-y curves over the length of the pile it is possible to obtain their evolution over the depth. Creating graphs representing the evolution of these parameters allows the characterization and regularization of these critical parameters through equations, as it is already used in the method suggested by the API.

For this, it is necessary to perform sensitivity studies on the model in order to find out which aspects have an impact on the critical parameters of equation (6.5). E.g., in subchapter 3.4.4., equations (3.37) and (3.38) define the ultimate bearing capacity – a critical parameter for the p-y curves suggested by API – as a function of the depth, the submerged unit weight, the diameter of the pile and the undrained shear strength.

The sensitivity studies performed in this work were the following ones:

- Undrained shear strength;
- Diameter of the pile;
- Young's Modulus (Secant Modulus, E_{50}^{ref}, in the Hardening Soil model of PLAXIS 3D).

Firstly, an analysis for the results of the behaviour of the ultimate bearing capacity of the soil will be performed and then the same will be done for the initial stiffness.

A law for the definition of the ultimate bearing capacity and the initial stiffness of the p-y curves will be suggested at the end of the chapter and it will be put side by side with the one of API. Also, a comparison between the p-y curves suggested by API – currently used for engineering purposes – and the ones obtained in this work will be carried out and some conclusions and suggestions will be presented.

7.2. ULTIMATE BEARING CAPACITY, P_U

7.2.1. API

As in the case of the hyperbola used to define the p-y curves obtained from PLAXIS 3D, the API method also uses two parameters to define its curves: the ultimate bearing capacity, p_u; and a parameter y_c (or y_{50} as used in 3.4.4.). Figure 7.1 shows the influence of the p_u on the p-y curves of the API.

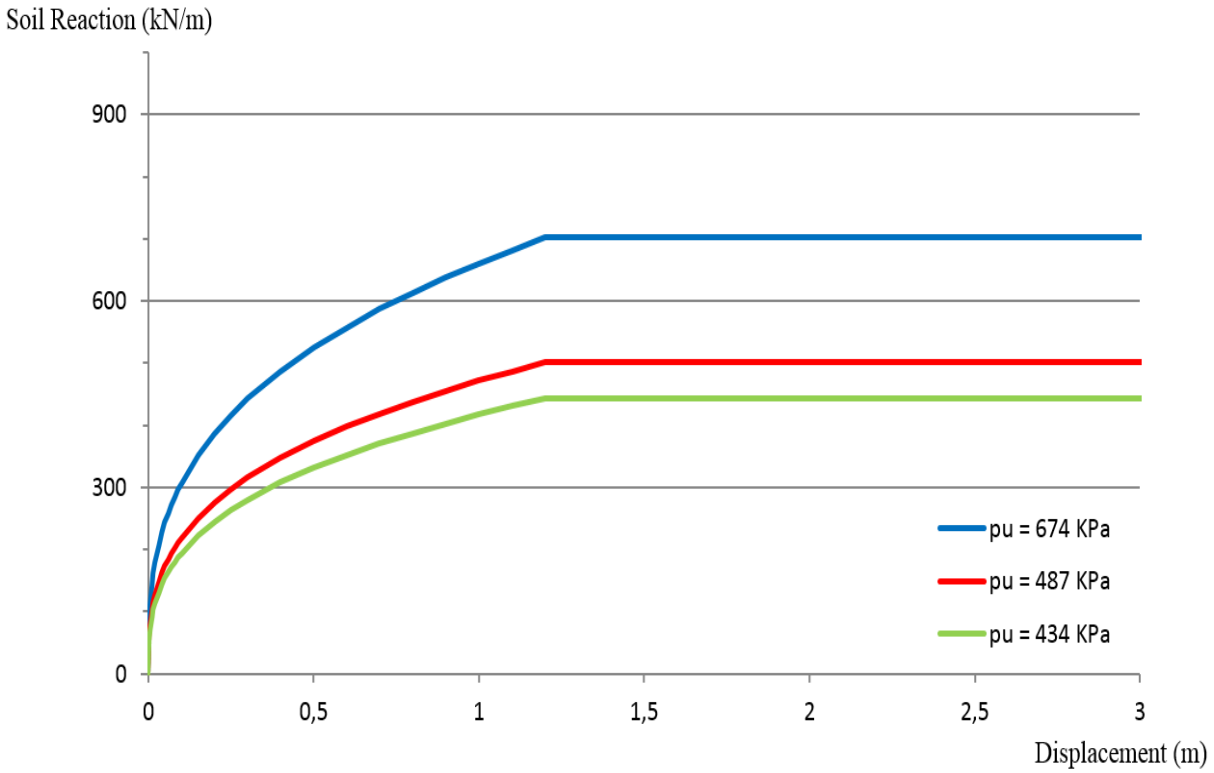

Fig. 7.1 – API p-y curves for different values of ultimate bearing capacity

As it is possible to observe in Figure 7.1, the API p-y curves are characterized for having a hyperbolic development in its initial phase until it reaches a constant value for the ultimate bearing capacity of the soil. This value for the ultimate bearing capacity increases with the depth and the objective of this section is to investigate the way this capacity evolves over the depth and weather the method suggested by API is correct or not.

API takes into account two types of failure of the soil: a wedge failure mechanism at shallow depths – with the ultimate bearing capacity increasing with depth and defined by equation (3.37) – and a flow failure mechanism of the soil around the pile in the horizontal plane for deep depths – constant over depth and defined by equation (3.38). The *J* parameter on equation (3.37) assumes a value of 0.5 for soft clays and 0.25 for medium clays.

A typical evolution of the ultimate bearing capacity of the soil suggested by the API is shown in Figure 7.2.

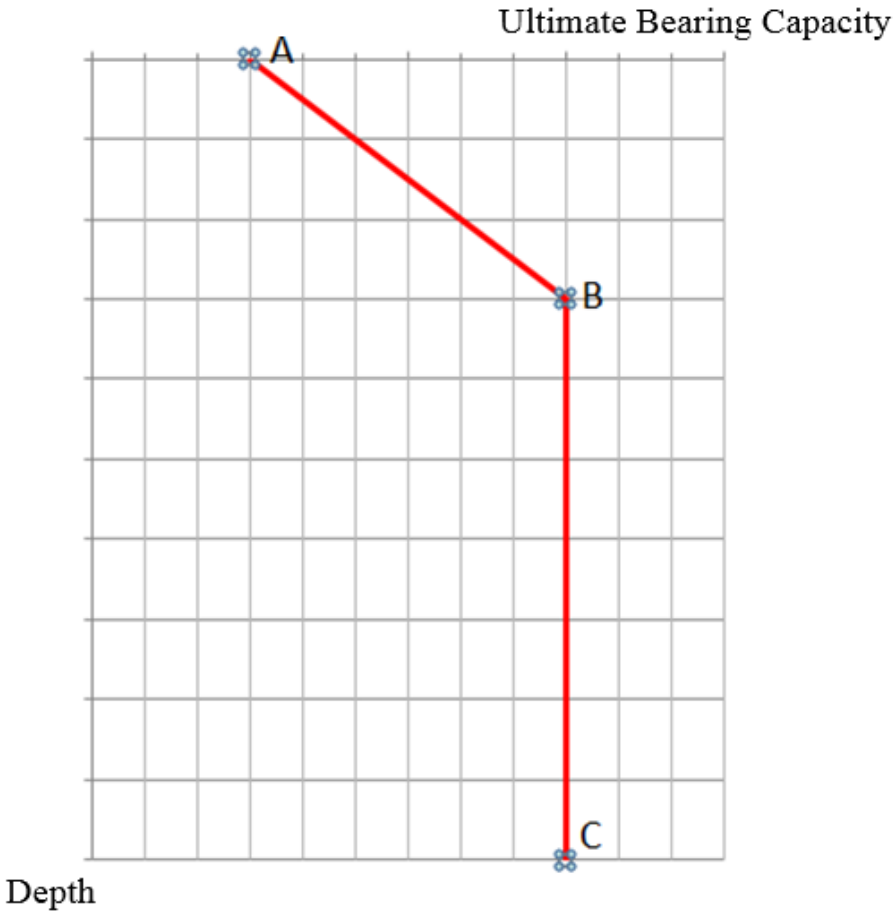

Fig. 7.2 – Typical evolution of the ultimate bearing capacity of the soil suggested by the API

Point A represents the ultimate bearing capacity at surface of the soil and its value is of three times the value of the undrained shear strength ($3S_u$). From point A to point B the failure mechanism is a wedge with an increasing bearing capacity of the soil over the depth and from B to C the failure mechanism is a flow of the soil with an ultimate bearing capacity of the soil constant over the depth.

Therefore, three aspects will be analyzed:

- The value for the ultimate bearing capacity of the soil at the surface (Point A);
- The value at which there is a change of failure mechanisms (Point B);
- The equation defining the ultimate bearing capacity of the soil for shallow depths (from point A to B).

The results obtained from PLAXIS 3D show an evolution of the ultimate bearing capacity of the soil over the depth just like the one presented by the API. Yet, by comparing the results obtained using the method suggested by API with the ones from the models run in PLAXIS 3D, it is possible to see that the influence of the different parameters are taken into account in different ways. This is what is going to be analyzed next.

7.2.2. Constant Undrained Shear Strength over Depth

Knowing that the undrained shear strength would be the most influent parameter of the soil on its ultimate lateral bearing capacity for an undrained loading case, several tests were run using different values for this parameter.

The value for the undrained shear strength assumed initially in the model was a constant value over the depth of 100 KPa. In order to have significant and reliable results (enough results to formulate a law) the following models were run: the initial value of 100 KPa; one model with half of the initially assumed value - 50 KPa; another model with the double of the initially assumed value - 200 KPa.

The results for the ultimate bearing capacity of the soil obtained from the different values of a constant undrained shear strength over the depth are shown in Figure 7.3 for the case of a pile with a diameter of 6 meters. On the xx axis is the p_u in KN/m^2 and on the yy axis is the normalized length of the pile (z/D). This was chosen in this way, and that's how it is going to be from here on, so that it would be easier to compare all the results and to analyze them in terms of diameter of the pile.

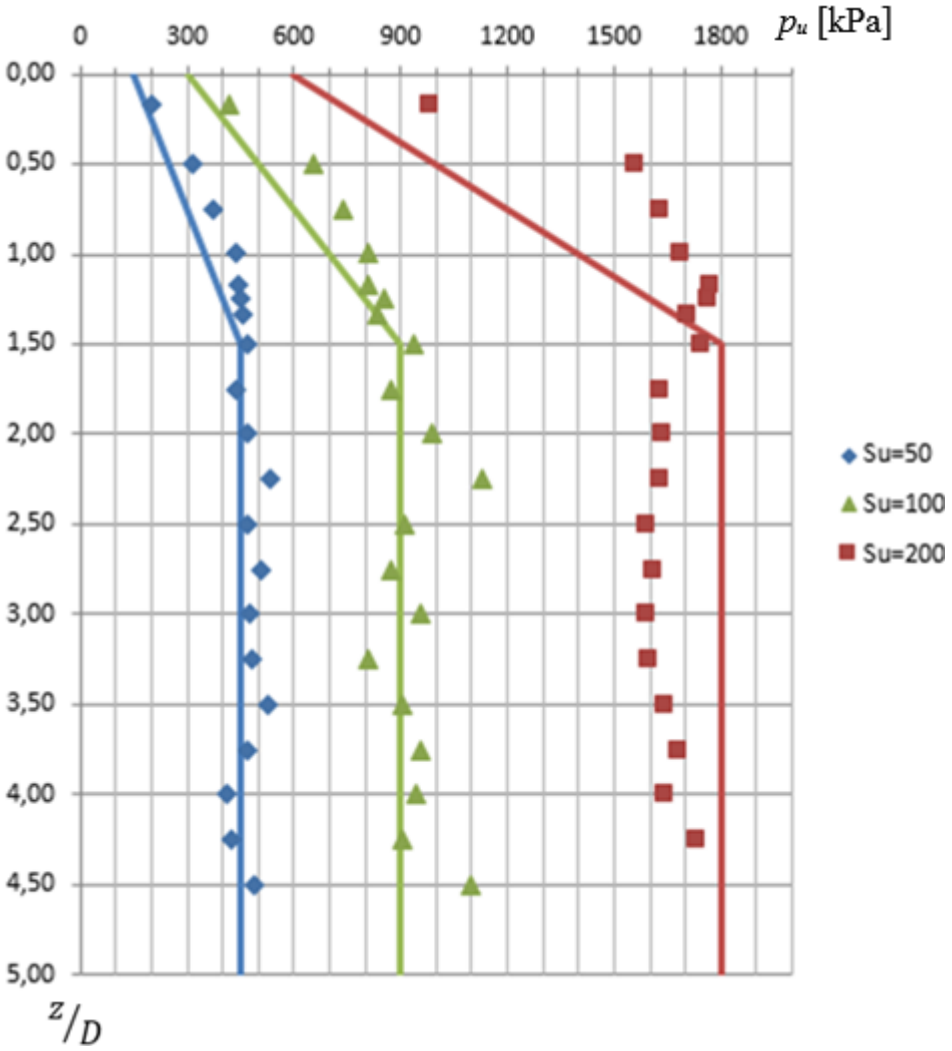

Fig. 7.3 – Ultimate bearing capacity of the soil over the depth for different values of undrained shear strength using PLAXIS 3D (D=6m)

It is important to notice that by imposing a constant value of undrained shear strength over the depth of the model some unrealistic and inaccurate results will appear at the shallow depths of the soil. This happens because on one hand the OCR is imposed as 1 (normally consolidated) but on the other hand, in order to have high values of undrained shear strength, this over consolidation ratio needs to be higher than 1 (maybe higher than 5 for the case of 200 KPa).

Also, at the both tips of the pile, the behaviour of the soil is not very representative of a laterally loaded pile which lead to some unreliable results at these depths of the soil.

By observing the results depicted on Figure 7.3, it is possible to approximate them to the lines shown in the same figure (these lines and the following conclusions were based on many other results, not only these ones). There are three important things to conclude from these results: 1) the value of $3S_u$ for the ultimate bearing capacity of the soil at the surface (point A) seems to be accurate, although better cases will be presented further that support better this statement; 2) the depth at which the ultimate bearing capacity of the soil remains constant over the depth (point B) seems to be independent from the undrained shear strength of the soil and to always assume a value of 1.50 times the diameter of the pile, on the contrary of what happens with the API method shown in Figure 7.4; 3) the value for the constant ultimate bearing capacity of the soil (from point B on) appears to be $9S_u$, as suggested by the API.

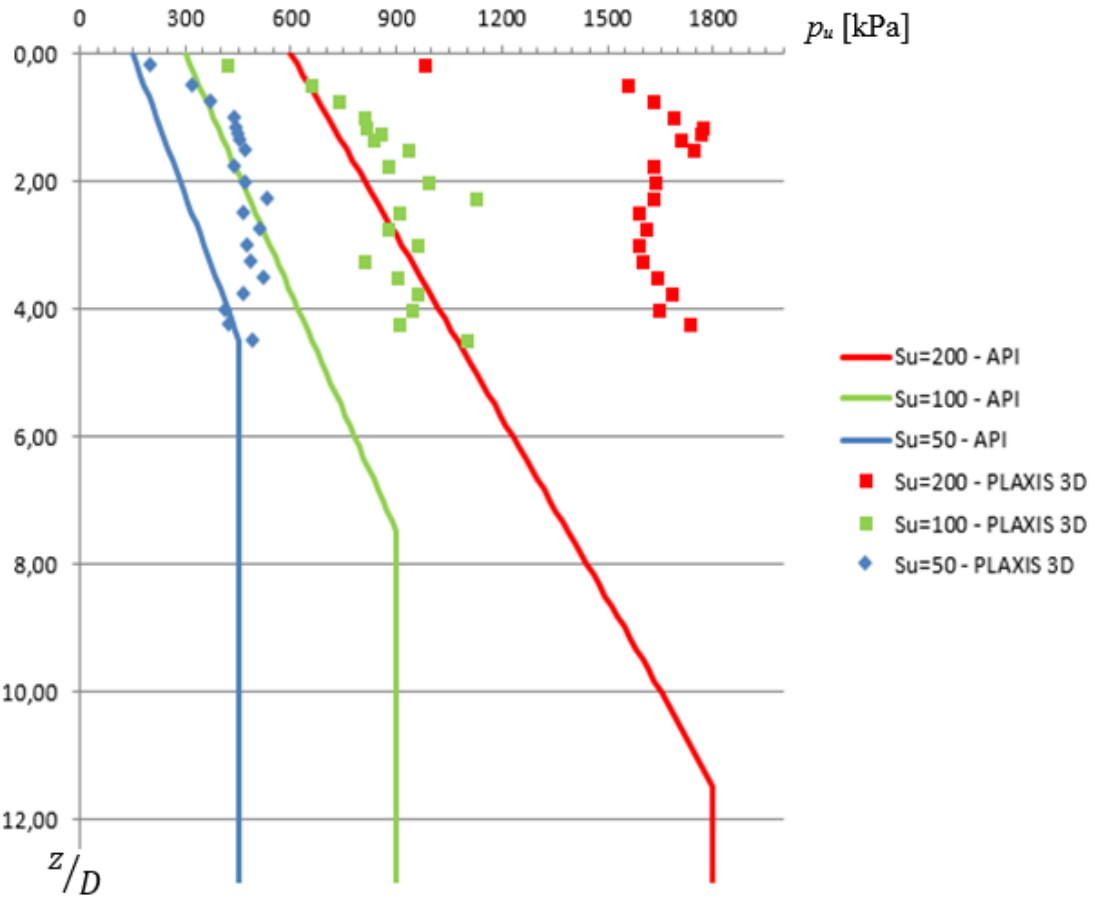

Fig. 7.4 – Comparison between the ultimate bearing capacity of the soil over the depth using the API method and PLAXIS 3D for three different values of constant undrained shear strength over the depth of the soil

7.2.3. Increasing Undrained Shear Strength over Depth

For the case of an increasing undrained shear strength over the depth two different cases were tested: one with an increase of 3 KPa of the undrained shear strength over the depth and one with an increase of 4 KPa. These values of 3 and 4 KPa for the evolution of the S_u over the depth is based on a constant ratio of S_u and σ'_{v0} of around 0.3 and 0.4.

The results for the ultimate bearing capacity of the soil over the depth obtained for the two cases of an increasing undrained strength over the depth are presented in Figure 7.5.

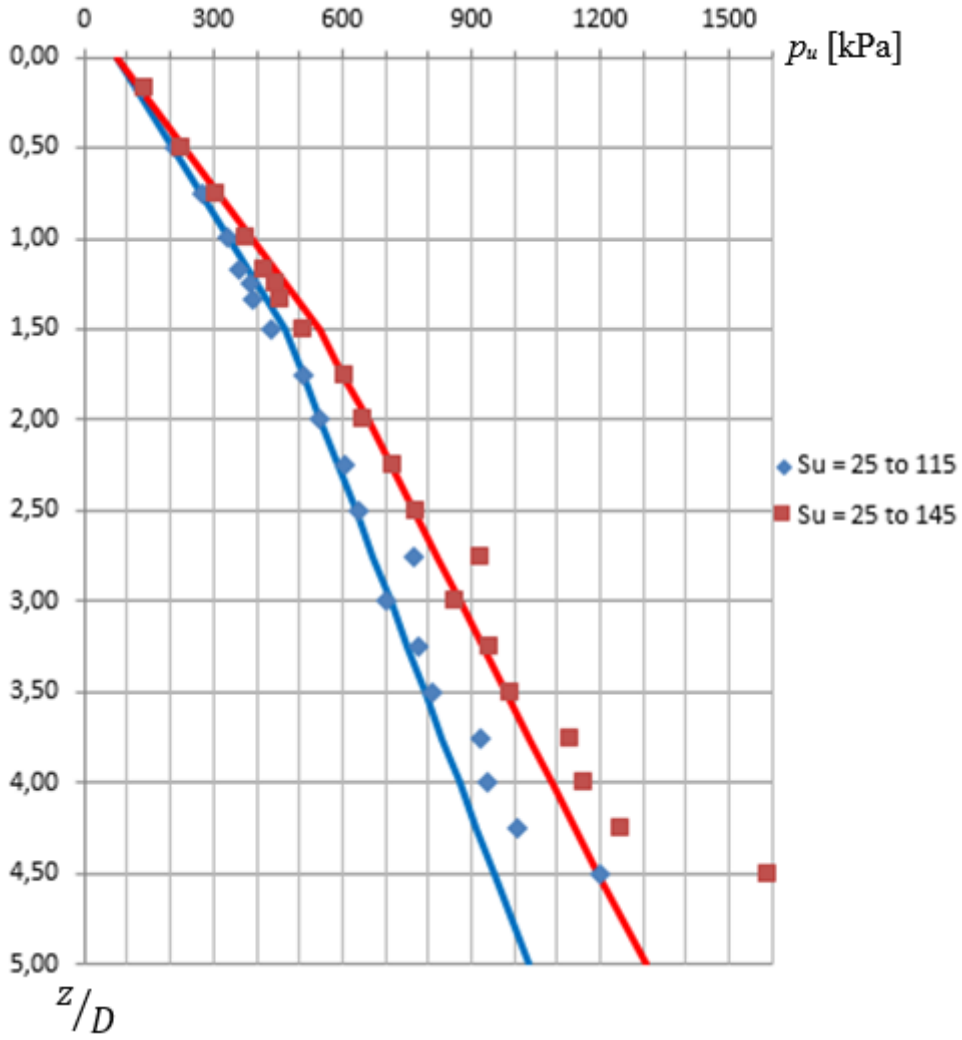

Fig. 7.5 – Ultimate bearing capacity of the soil over the depth for a variation of the undrained shear strength over the depth of 3 kPa and 4 kPa

The blue and the red lines presented in Figure 7.5 show that, imposing a change of failure mechanisms at a relative depth of 1.50 but still using the value of 3 times the S_u for the p_u at the surface and 9 times the S_u for the p_u at deep depths, the approximation of the API method to results obtained from PLAXIS 3D is very accurate.

7.2.4. DIAMETER

To test whether the diameter of the pile has any influence on the p-y curves three different models, each one with a different size of diameter, were run and analysed. The diameters used on the three models were of 6, 4 and 2 meters. The results for the ultimate bearing capacity of the soil obtained for the different diameters are shown in Figure 7.6.

Figure 7.7 shows a comparison between the results for the p_u of the soil of PLAXIS 3D (dots) and the results of the suggest method of API (lines). Notice that the values obtained from PLAXIS can only go until a relative depth of 5.0 as this is the depth at the toe of the foundation of the monopile.

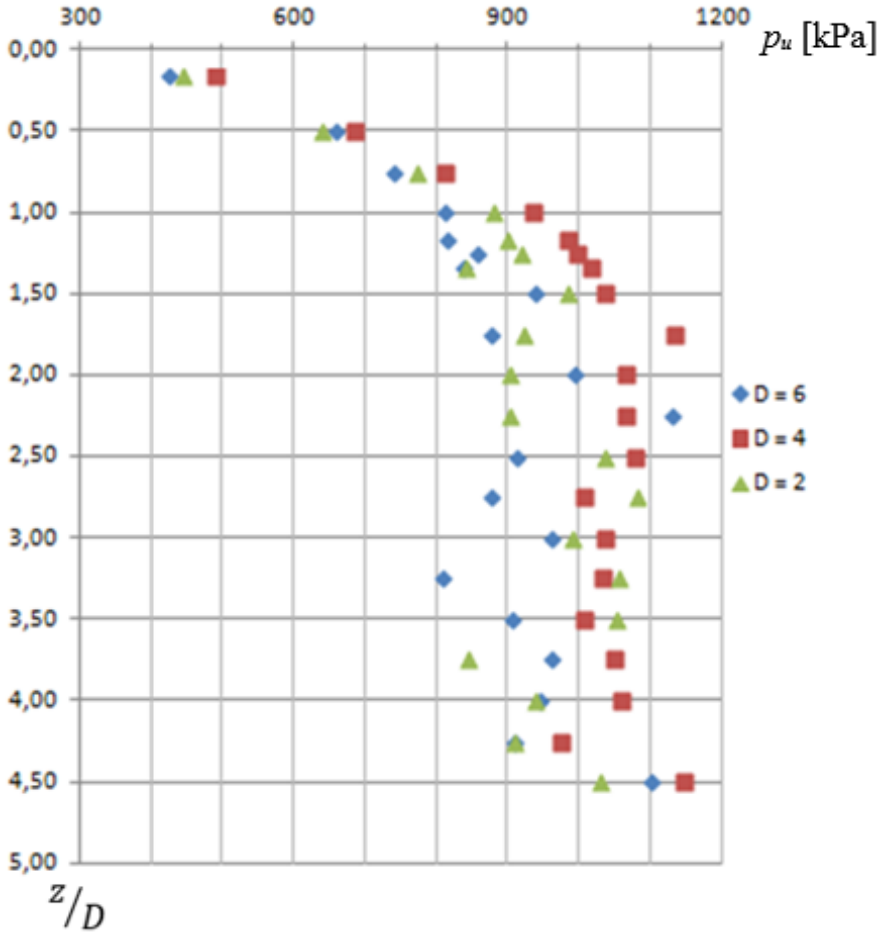

Fig. 7.6 – Ultimate bearing capacity of the soil for different diameters of the pile

The results presented in Figure 7.7 seem to be very similar between each other and it looks like they have a well-defined law comparable to the one of API. However, the relative depth, *z/D*, at which a wedge failure mechanism changes into a flow mechanism is very different. From the obtained results of PLAXIS 3D this change of failure mechanism always occurs at a normalized depth of about 1.50 diameters. According to the API, this point of change of failure mechanism, not only occurs at a much deeper depth, but it varies when the diameter of the pile is different.

Figure 7.8 shows the results of the ultimate bearing capacity of the soil for the different diameters using the variation of undrained shear strength over the depth of 3 kPa.

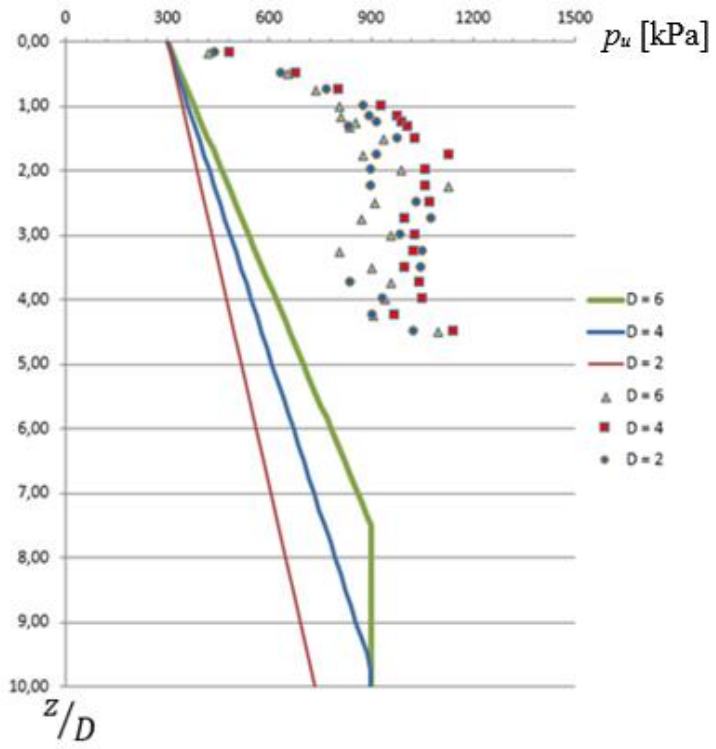

Fig. 7.7 – Comparison between the results obtained from PLAXIS 3D and the results of the suggested method of API

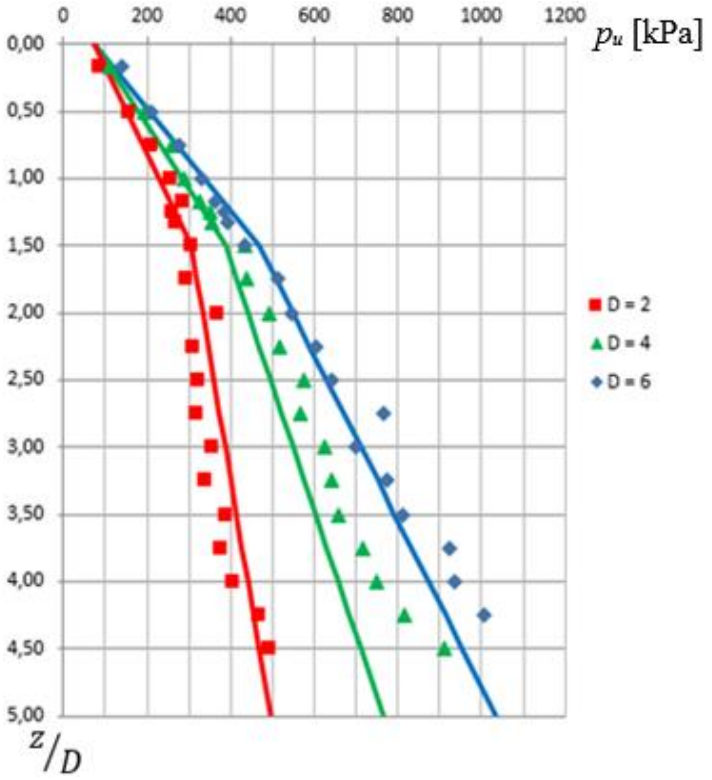

Fig. 7.8 – Ultimate bearing capacity of the soil for different diameters of the pile for an increase of 3 kPa of undrained shear strength over the depth

There are two aspects to take into account in Figure 7.8. The first one is the confirmation that the point of change of failure mechanisms is of 1.50 time the diameter of the pile and the value of 3 times the S_u for the p_u at the surface and 9 times the S_u for the p_u at deep depths (the lines represent these conditions).

The second one is that what was previously verified in Figure 7.6 – the diameter of the pile does not have any influence on the ultimate bearing capacity of the soil (in terms of stresses) – does not seem to be valid for this case as the p_u for the different diameters increase with the increase to the diameter. This is not true because, as the undrained shear strength of the soil increases with the depth and pile have different lengths, the p_u of the soil for the relative depths will be different. This is verified by Figure 7.9 where, instead of representing the relative depths, the yy axis represents the real depth in meters.

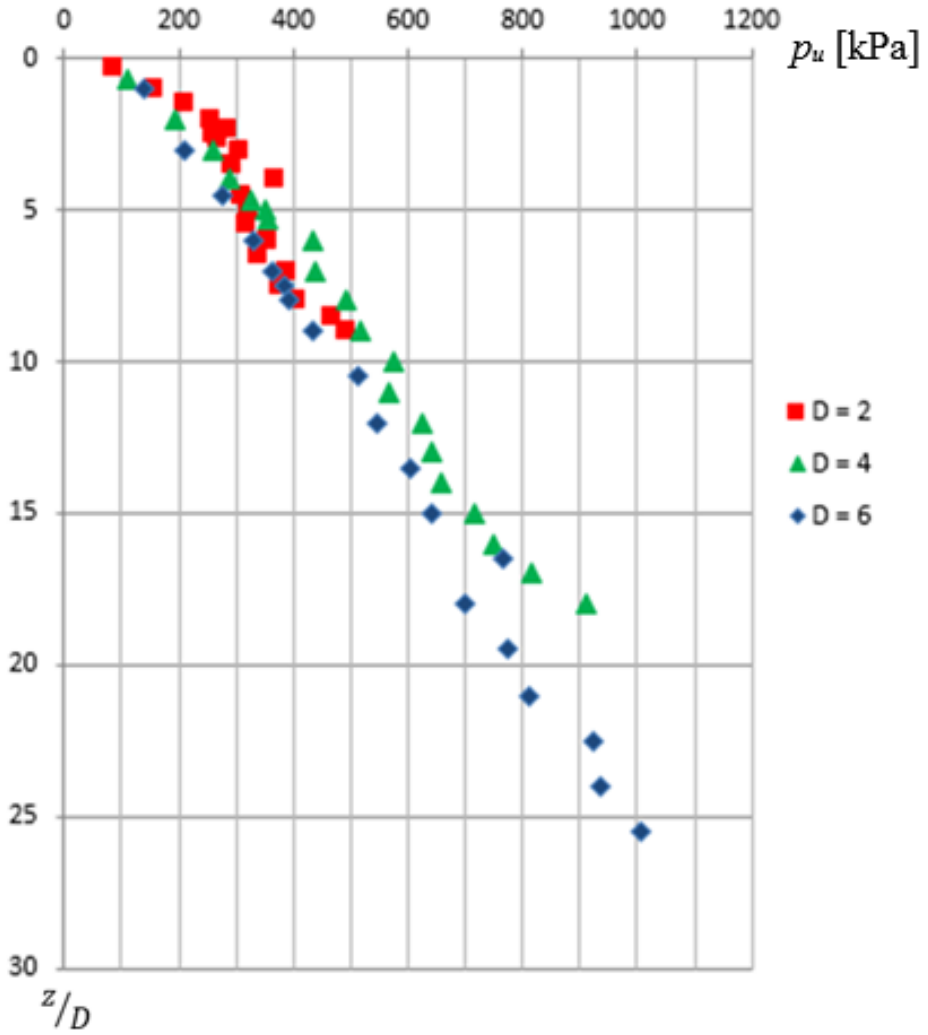

Fig. 7.9 – Results obtained from PLAXIS 3D for different diameters with an increase of undrained shear strength over the depth

7.2.5. YOUNG'S MODULUS

API does not take into account the soil deformation modulus (or soil elastic Young's modulus) on its method for the calculation of the p-y curves (it uses the y_c parameter to define the deformation of the soil). Yet, as it is a parameter that effects a lot the behaviour of the soil, a sensitivity study on this property of the soil was carried out and its results are presented in Figure 7.10. The Hardening Soil model of PLAXIS 3D characterizes the deformation of the soil through a Secant Modulus (E_{50}^{ref}) and the cases studied were of values of 10 MPa, 20 MPa and 50 MPa for this parameter (always with a S_u of 100 kPa).

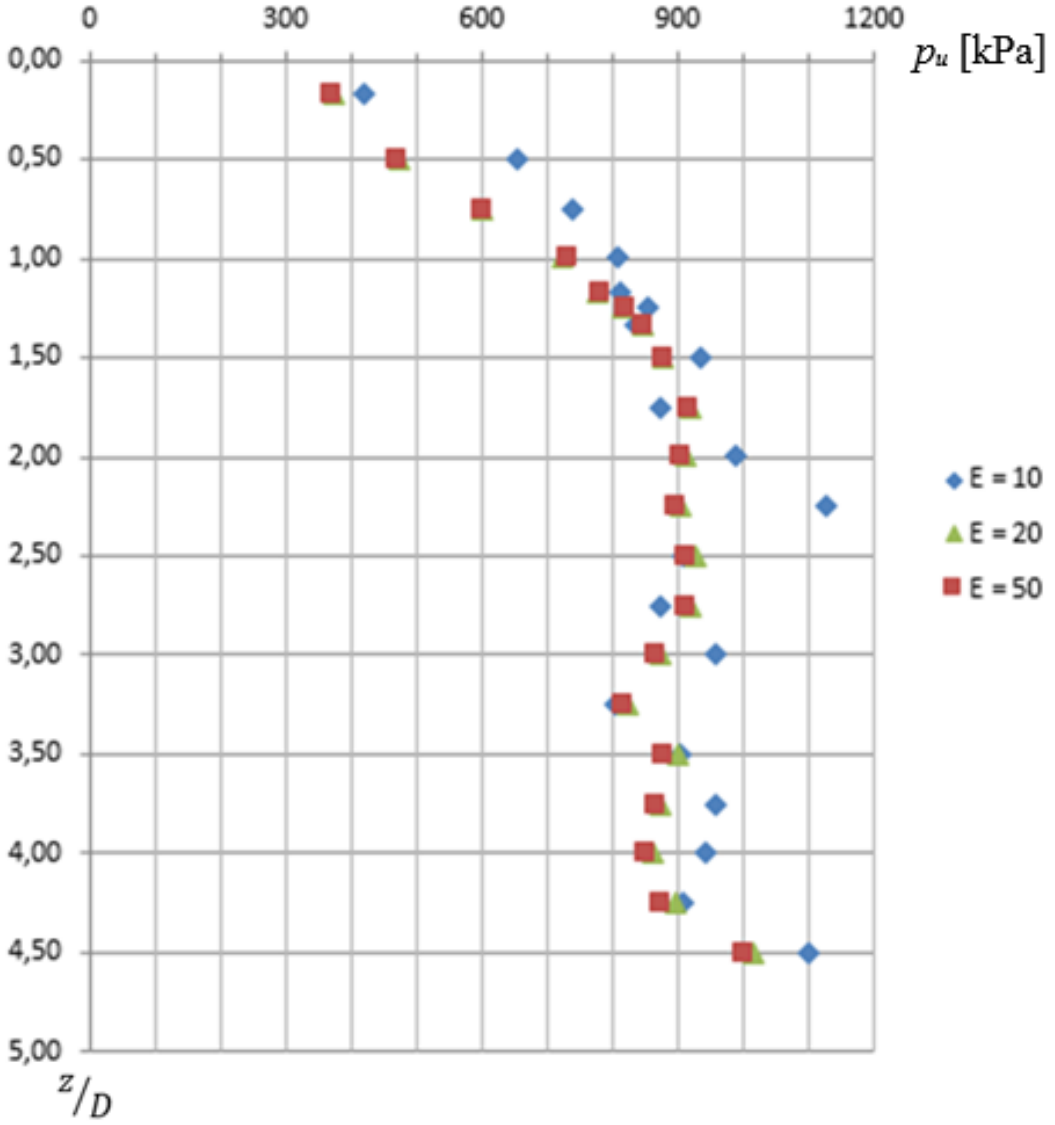

Fig. 7.10– Results obtained from PLAXIS 3D for different values of Young's Modulus

By observing Figure 7.10 is it possible to conclude that the soil Young's modulus has no impact on the ultimate bearing capacity of the soil.

7.2.6. Conclusions and Definition of a Law

Three main statements can be concluded from the previous results concerning the ultimate bearing capacity of the soil:

- The value for the ultimate bearing capacity of the soil at the surface is of $3S_u$;
- The constant value for the ultimate bearing capacity of the soil at deep depths is $9S_u$;
- The depth at which there is a change of failure mechanisms is always 1.5 diameters.

That being said, the method proposed for the definition of the ultimate bearing capacity of the soil consists on using equations (7.1) and (7.2).

$$p_u^{shallow} = 3S_u + \frac{4S_u}{D}z \tag{7.1}$$

$$p_u^{deep} = 9S_u \tag{7.2}$$

The application of the equations is the same as in the method suggested by API: the ultimate soil resistance at a certain depth, z, is the smaller of the values given by the two equations. Again, equation (7.1) corresponds to a wedge failure mechanism at shallow depths – with the ultimate bearing capacity increasing with depth – and equation (7.2) to a flow failure mechanism of the soil around the pile in the horizontal plane for deep depths – constant over depth.

In terms of p_u, there is one big difference between the method proposed in this work and the one suggested by the API: The flow failure mechanism of the soil of the API occurs at very deep depths compared to the depth of 1.5 diameters here suggested which leads to a big underestimation of the ultimate bearing capacity of the soil by the API. The reason of this might be because of the API method being based on tests on slender piles where the failure of soil is difficult to identify as the cross section of the pile is what fails first. Figure 7.11 shows a typical development of the ultimate bearing capacity of the soil over the depth using this new proposed method.

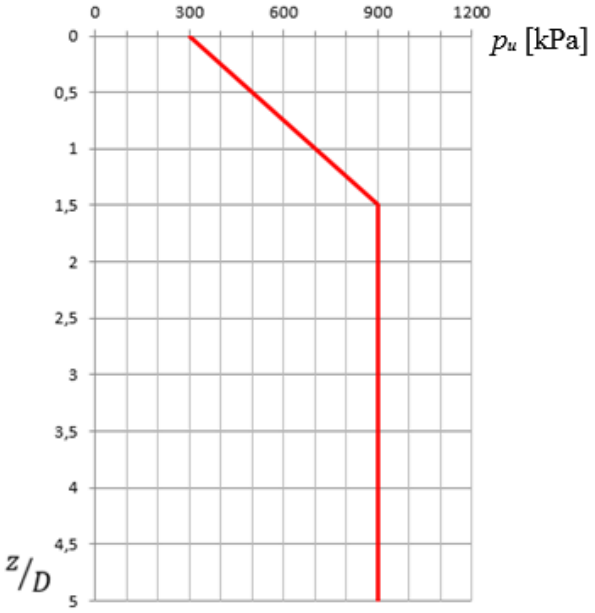

Fig. 7.11– Ultimate bearing capacity of the soil over the depth using this new proposed method

7.3. INITIAL STIFFNESS OF THE P-Y CURVE, K_s

7.3.1. API

The parameter y_c used in the API method defines the stiffness of the p-y and the shape of the hyperbola. Figure 7.12 shows how a different value of this parameter interferes on the p-y curves.

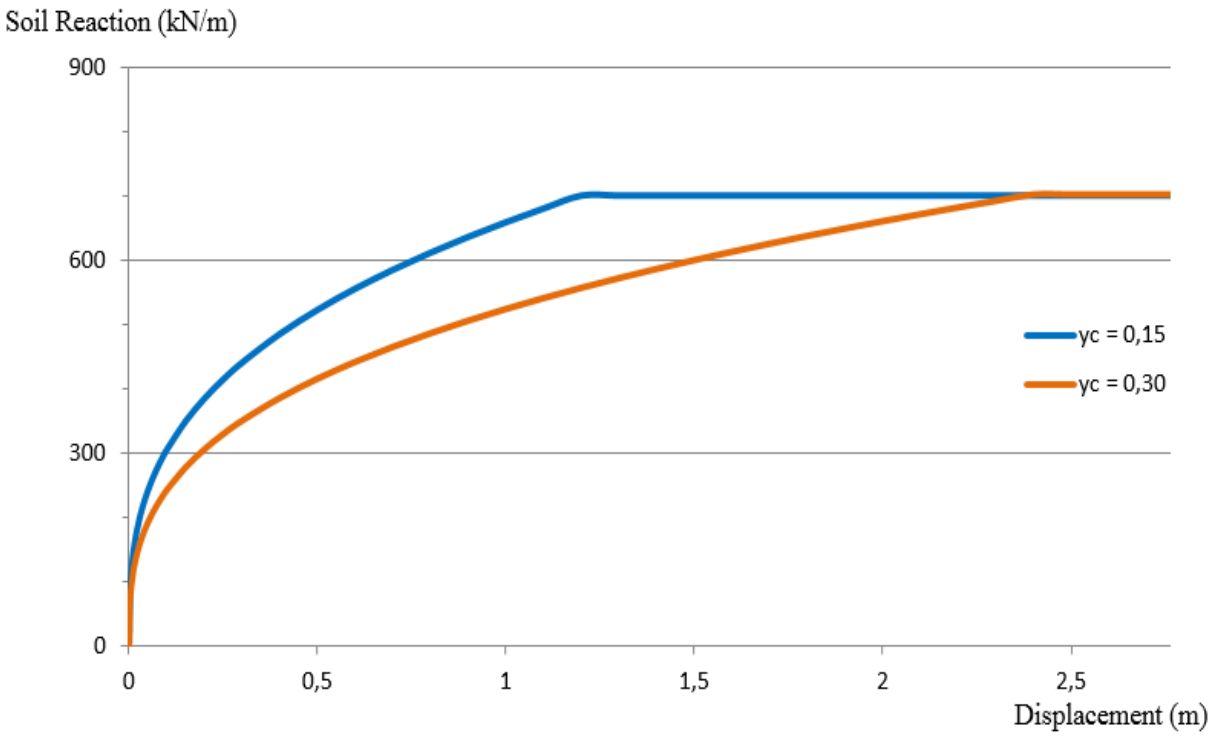

Fig. 7.12 – API p-y curves for different values of y_c

By observing Figure 7.12 it is possible to conclude that it is this parameter that defines the point at which the hyperbola intersects the constant line of ultimate bearing capacity of the soil: a lower value of y_c defines a much stiffer curve as it reaches its ultimate bearing capacity at lower displacements. Yet, the biggest concern of nowadays researchers is with the initial stiffness of the p-y curve, which is the reaction of the soil for small displacements.

Unlike what happens with the ultimate bearing capacity of the soil, the API method does not take into consideration the initial stiffness of the curve and its p-y curves do not look as if it varies with the depth or any other property of the soil. Whereas the ultimate bearing capacity of the soil might have different values for different depths, the y_c parameter is the same for every depth.

The lack of a law by the API for the definition of the initial stiffness of the p-y curve – like the one for the ultimate bearing capacity (Figure 7.2) – makes it more difficult to identify its real behaviour and development over the depth as there is no reference or starting point.

7.3.2. Undrained Shear Strength

Obtained from the same models as the results for the ultimate bearing capacity of the soil, Figure 7.13 shows the results for the initial stiffness, k_s, for different values of undrained shear strength over the depth. Based on the results obtained, no distinction was made between a constant and an increasing undrained shear strength over the depth.

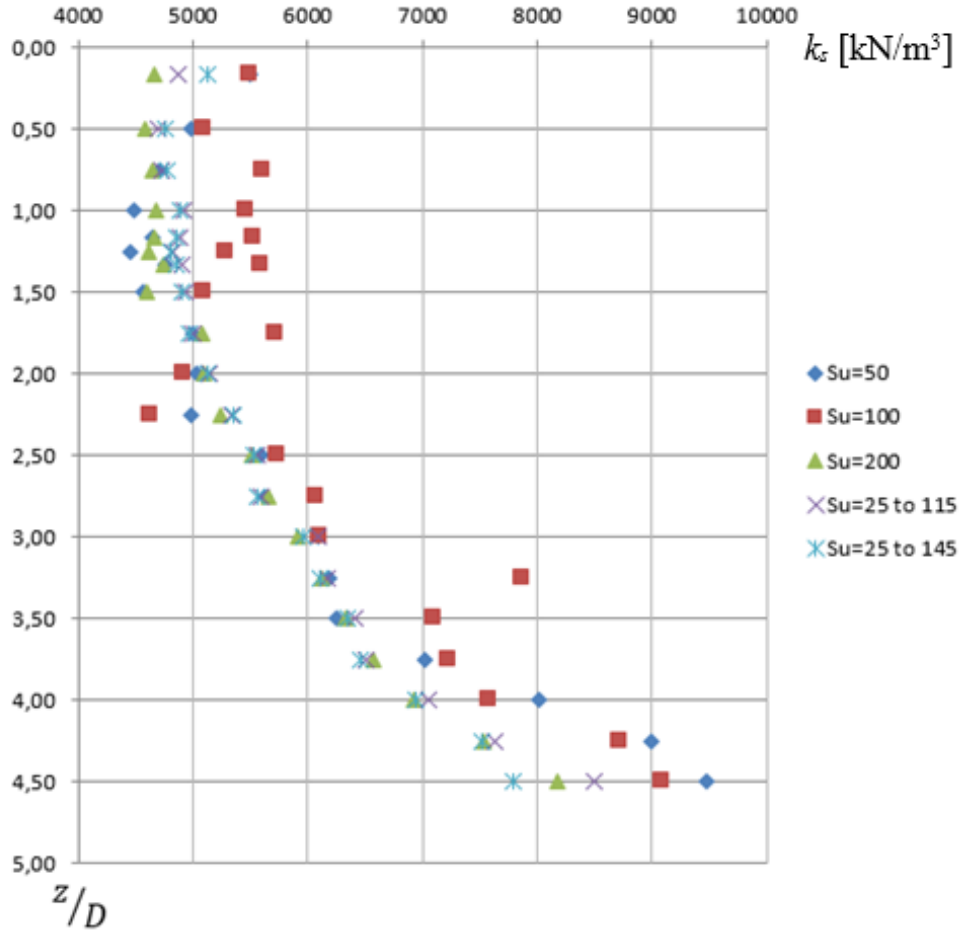

Fig. 7.13 – Initial stiffness of the p-y curves obtained from PLAXIS 3D for different values of undrained shear strength

A few conclusions are possible to point out by observing Figure 7.13 and the first one is that the undrained shear strength of the soil does not have any impact on the initial stiffness as the results for every case present, more or less, the same outcome.

It is possible to identify two important resemblances between the development over the depth of the results here presented and the ones of the ultimate bearing capacity of the soil: first, there are to different lines which might be for the same reason as in the ultimate bearing capacity: two different failure mechanisms of the soil that change at a certain depth; and secondly, the point at which one line changes into the other seems to be the same as the one observed in the cases of the ultimate bearing capacity – 1.50 times the diameter of the pile.

7.3.3. DIAMETER

The influence of the diameter of the pile on the evolution of the initial stiffness of the curves over the depth is shown in Figure 7.14.

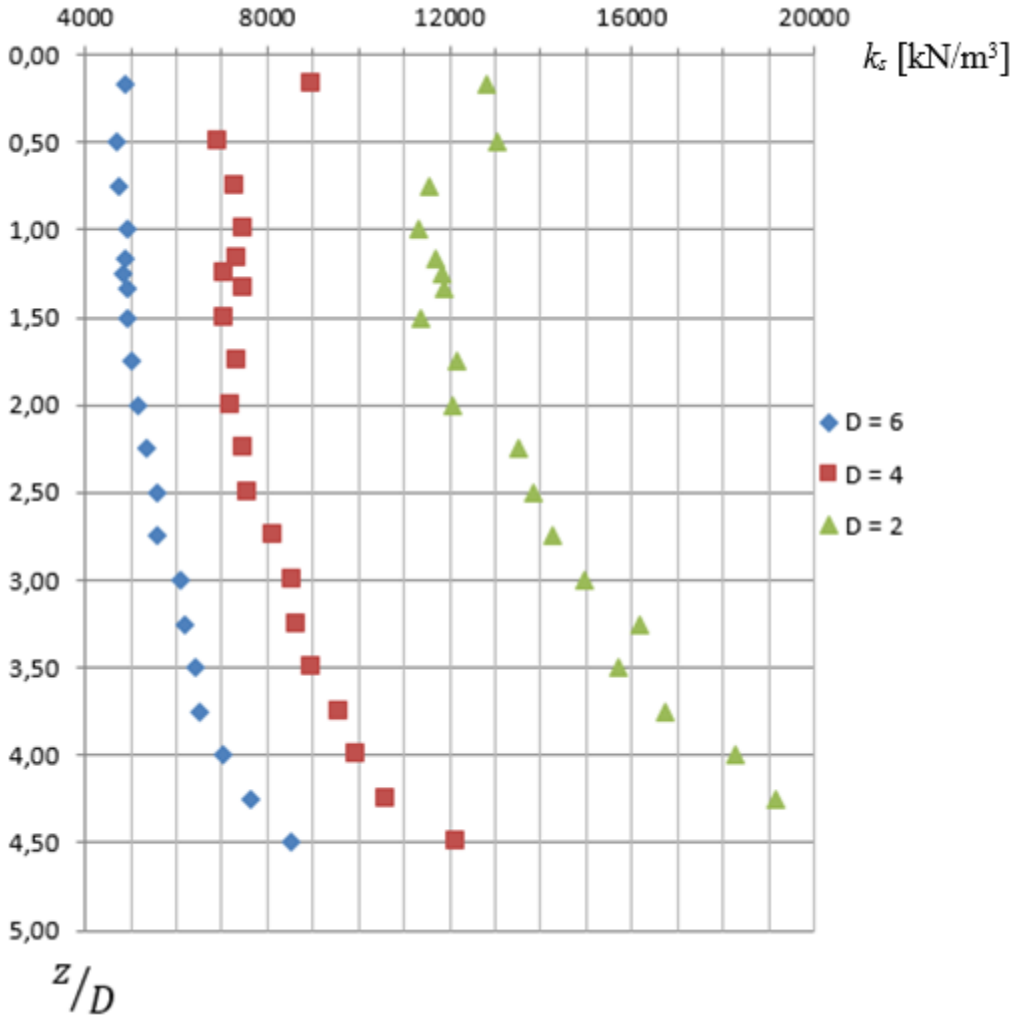

Fig. 7.14 – Initial stiffness of the p-y curves obtained from PLAXIS 3D for different diameters of the pile

The effect of the diameter of the pile on the initial stiffness of the p-y curves is clear in Figure 7.14: the smaller the diameter of the pile is, the stiffer the curve is for very small deformations. Yet, the relation between the diameter of the pile and the initial stiffness is not easy to identify: the difference between the initial stiffness for the diameter of 6 meters and the one for 4 meters is much smaller than the difference between the initial stiffness for the diameter of 4 meters and the one for 2 meters although the difference between diameters is always 2 meters.

Besides that, the same trends for the development of the initial stiffness of the p-y curves over the depth seem to appear as in the case of the undrained shear strength.

As it is possible to conclude by looking at equation (3.20), the API takes into account diameter of the pile when it comes to the stiffness of the p-y curves.

7.3.4. YOUNG'S MODULUS

Finally, the results for the initial stiffness the p-y curves obtained from the different values of the Young's modulus are presented in Figure 7.15.

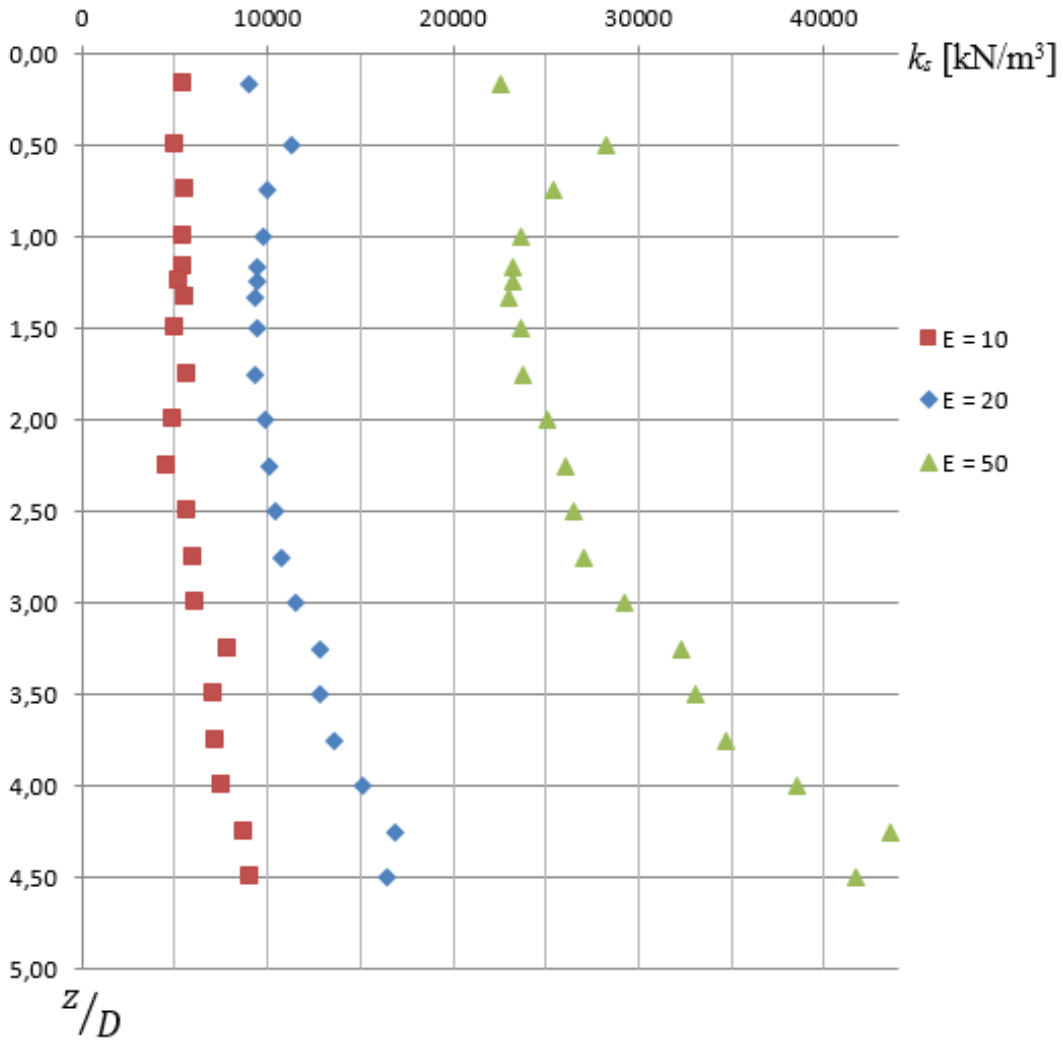

Fig. 7.15 – Initial stiffness of the p-y curves obtained from PLAXIS 3D for different values of Young's modulus

Again, notice that the values presented here for the Young's modulus is the value used for the Secant Modulus (E_{50}^{ref}) requested by the Hardening soil model in PLAXIS 3D.

By looking at Figure 7.15 it is possible to see that the influence of the soil deformation modulus on the initial stiffness of the p-y curves is large and, the higher this value is, the stiffer the curve is. Once more, the relation between the increase of the Young's modulus and the increase of the initial stiffness of the curves is not linear.

7.3.5. Conclusions and Definition of a Law

As observed on the preceding sections, the initial stiffness of the of the p-y curves depends on both the diameter of the pile and the soil deformation modulus. Therefore, to define a law for the evolution of k_s over the depth it is necessary to find out how these parameters affect the initial stiffness of the curves. In order to do so, it was chosen to dimensionless the previous results, starting with the Young's modulus (Figure 7.16).

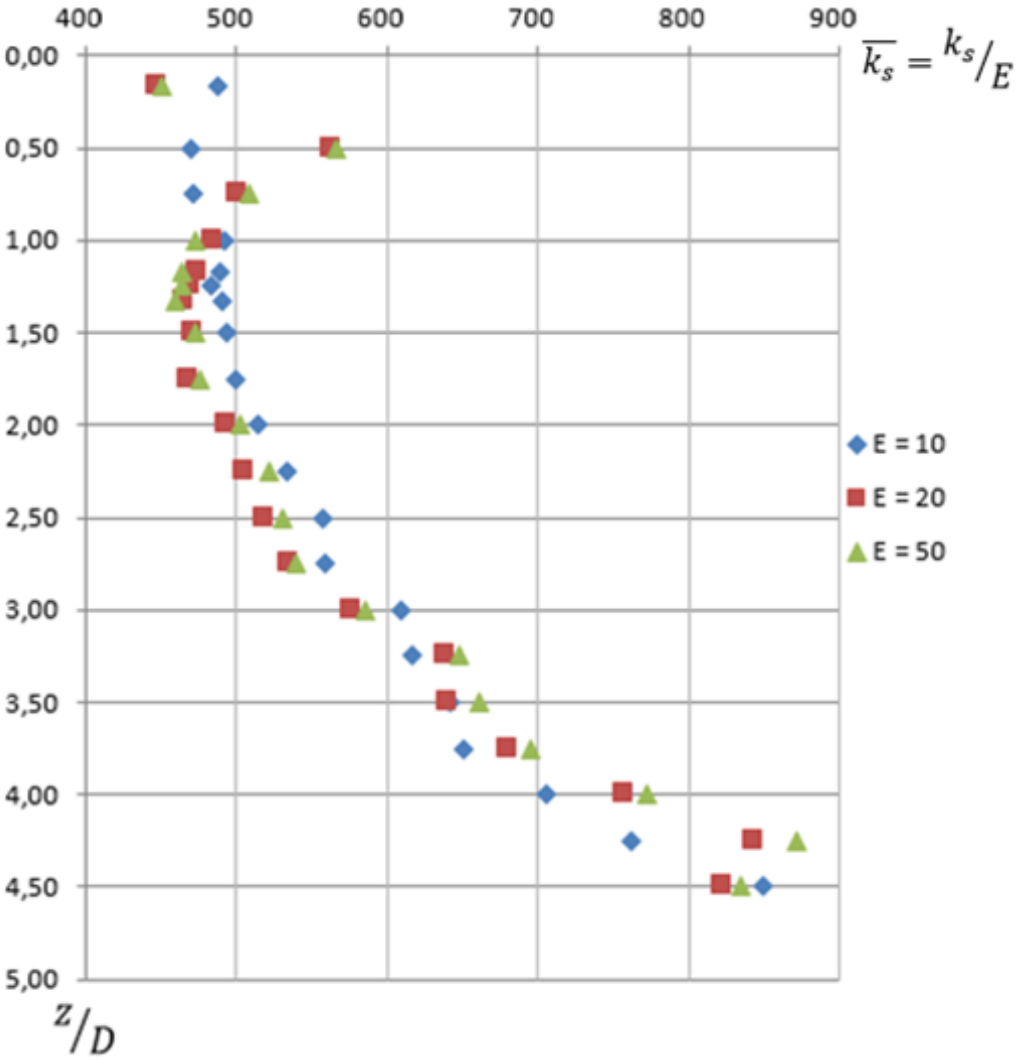

Fig. 7.16 – Initial stiffness of the p-y curves normalized by the Young's modulus

In order to obtain the results of Figure 7.16, it was chosen to normalize the initial stiffness by the Young's modulus. Figure 7.16 shows a perfect correlation when this procedure is applied which allows the statement that the relation between the initial stiffness of the p-y curves and the deformation modulus of the soil is linear and in the same direction – higher values of deformation modulus leads to higher initial stiffness.

For the results obtained for the different diameters of the pile – shown in Figure (7.17) – a different procedure was used.

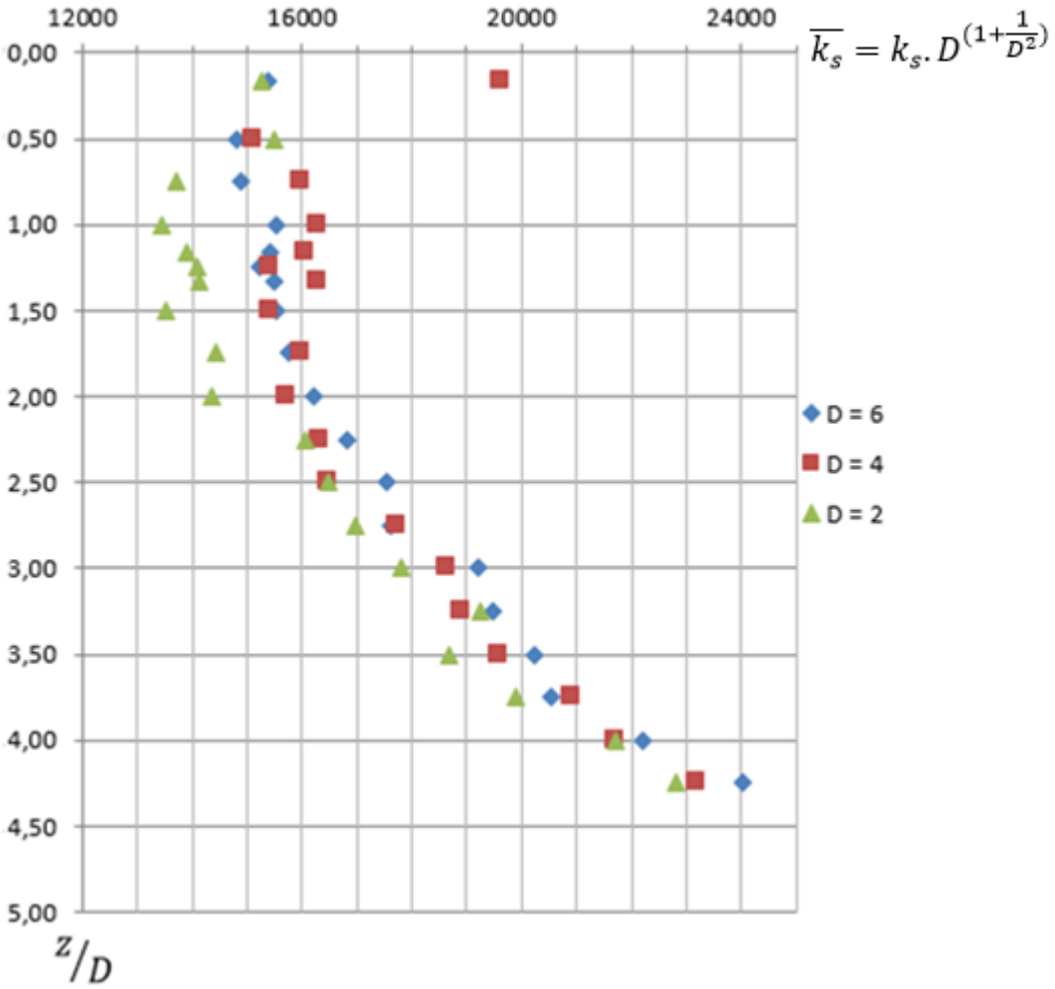

Fig. 7.17 – Initial stiffness of the p-y curves normalized by the diameter of the pile

On the contrary of what happened with the Young's modulus, the relation between the diameters of the pile is not linear and the Young's modulus grows with the decrease of the diameter. The fact that is not the same direction is obvious from Figure (7.14) where the initial stiffness increases as the diameter of the pile is lower. As for the linear relation, the different results were not matching when this was applied so a new relation was searched and the final outcome was the one shown in equation (7.3).

$$D^{(1+\frac{1}{D^2})} \tag{7.3}$$

Table 7.1 – Relation between diameters

D (m)	1	2	4	6	8
Equation (7.3)	1	2.378	4.362	6.306	8.264

By observing the results and Figures 7.16 and 7.17 equations (7.4) and (7.5) were deducted and presented as the solution for the evolution over the depth of initial stiffness of the p-y curves (E_{50} in MPa and D in meters).

$$k^{shallow} = 3000 \frac{E_{50}}{D^{(1+\frac{1}{D^2})}} \tag{7.4}$$

$$k^{deep} = 600(\frac{z}{D} + 3.5) \frac{E_{50}}{D^{(1+\frac{1}{D^2})}} \tag{7.5}$$

In the same way as the ultimate bearing capacity, the initial stiffness of the p-y curves has one equation for shallow depths concerning a wedge failure mechanism and one other equation for deep depths due to a flow failure mechanism of the soil and, at the certain depth, the higher k from the two equations should be the one assumed.

The typical evolution over the depth of the initial stiffness is very similar to the one of the ultimate bearing capacity of the soil, as shown in Figure 7.18.

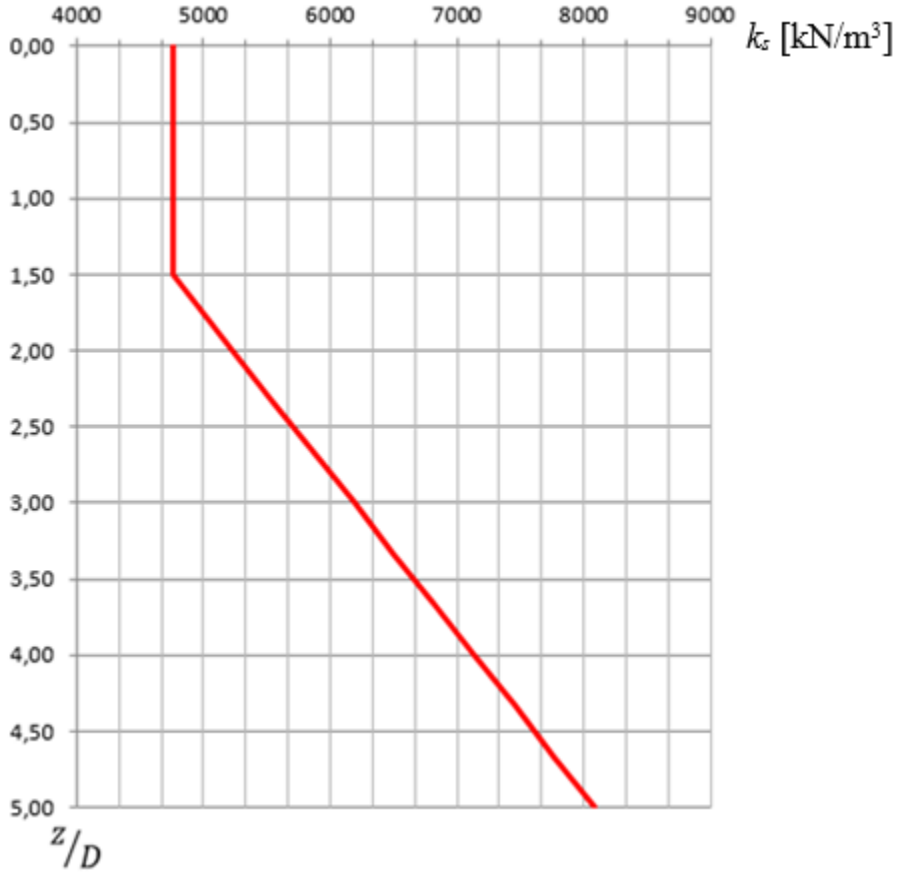

Fig. 7.18 – Initial stiffness of the p-y curves over the depth using this new proposed method

7.4. P-Y CURVES

Having defined the new proposed method for the characterization of the p-y curves, a comparison between this method and the one suggested by the API will be now performed. The comparison will be made for the case of the Zomergen clay mentioned in chapter 4 of which the parameters used in both methods are known (4.4.1. – Table 4.1).

The biggest difference between the two methods is in the definition of the failure mechanisms of the soil which controls the evolution of the ultimate bearing capacity of the soil over the depth. Figure 7.19 compares the p_u over the depth of the two methods.

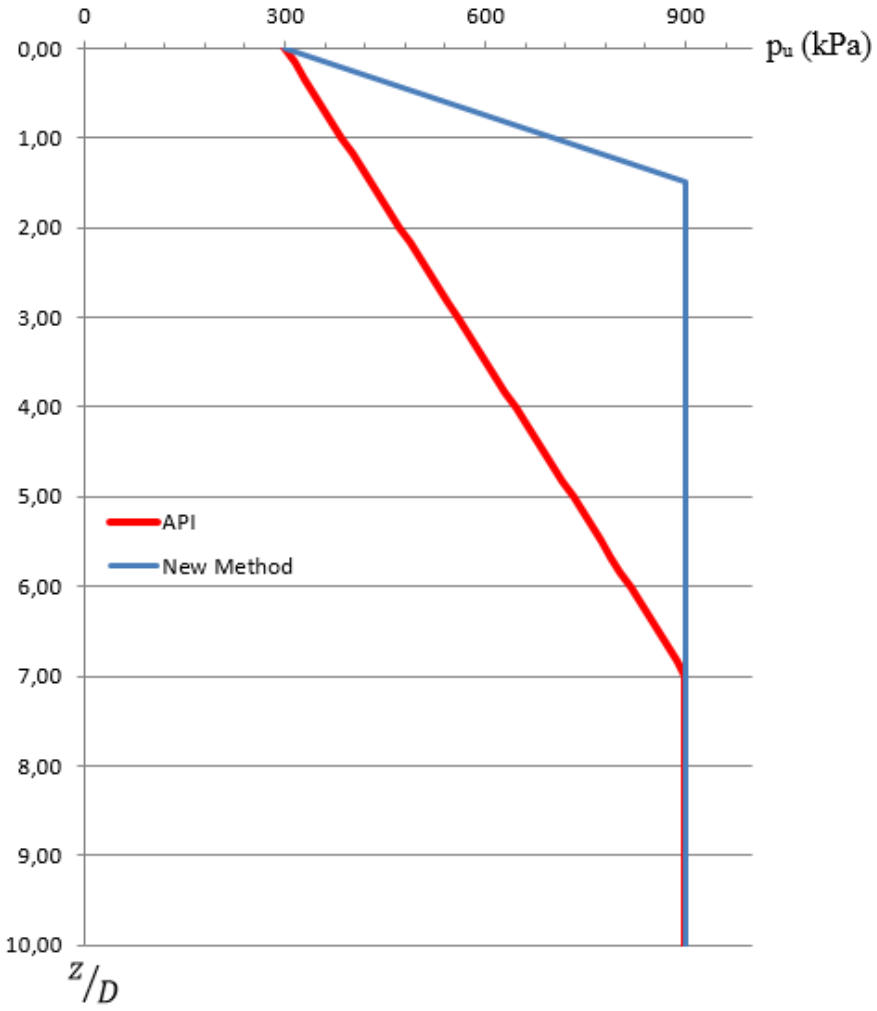

Fig. 7.19 – Evolution of the ultimate bearing capacity of the soil over the depth

By observing Figure 7.19 it is clear that, as stated before, the API method underestimates a lot the ultimate bearing capacity of the soil for the shallow depths. This underestimation leads to an oversizing of the piles on the design of these monopiles foundations which, consequently, implicates much more expenses on these structures.

Figures 7.20 and 7.21 show, for a case of a pile with 6 meter of diameter and 30 of length, the p-y curves using the two different methods (curves presented from 0 to 30 meters, each 3 meters) increasing the depth from the bottom to the top of the graphs.

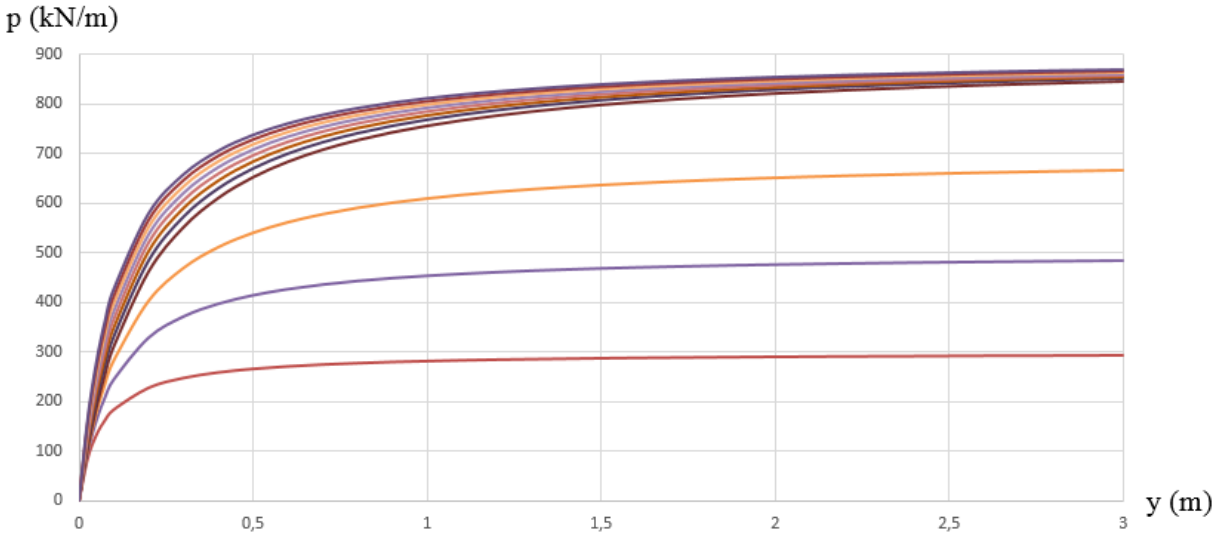

Fig. 7.20 – p-y curves of the new proposed method

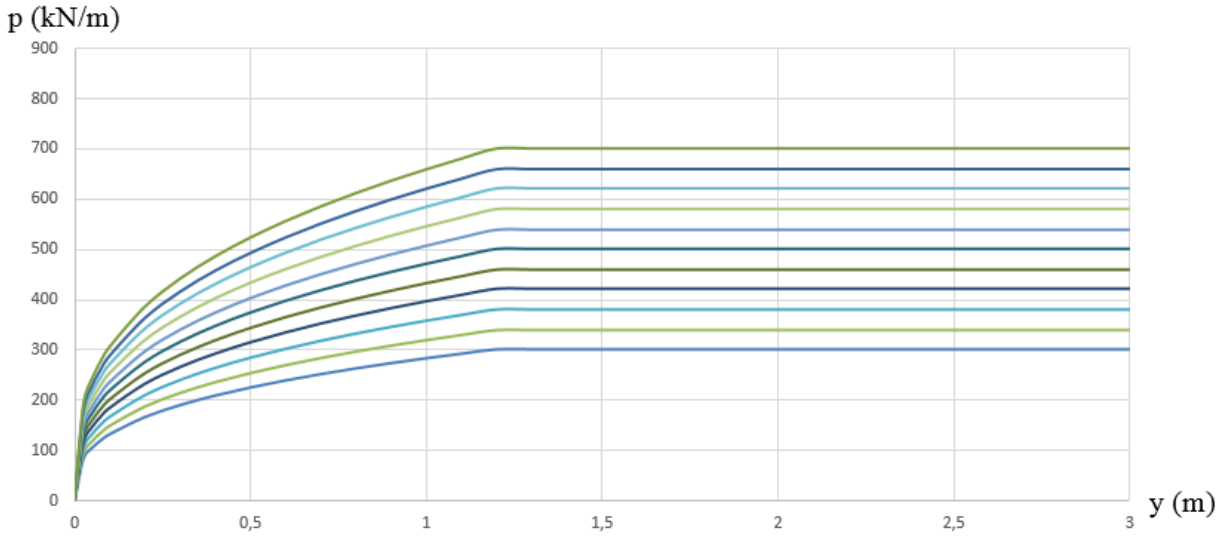

Fig. 7.21 – p-y curves suggested by the API

The first aspect to notice when looking at these figures is that, while the new proposed method reaches the ultimate soil reaction of $9S_u$ (900 kPa in this case) very early, the API never actually reaches this value which means that it considers that along the all length of the pile there is a wedge failure mechanism, which is very unrealistic.

The same thing happens for small displacements, which are the ones of real interest for engineering design, with the soil reaction being much lower in the API method.

One other thing to notice is that, in the API once the depth of the soil flow failure mechanism is reached, the p-y curves are always the some below that depth as the ultimate bearing capacity is always the same and the y_c never changes. On the contrary, in the new proposed method once the ultimate bearing capacity of $9S_u$ is reached the p_u will the same for the depths below this one but the k_s is still different and increasing over the depth. This is in better accordance with the reality as, although the capcity of

the soil might not increase more, its confinement should always increase with the depth as both the vertical and the horizontal stresses are increasing.

The effect of the undrained shear strength on both methods is shown in Figure 7.22 and is as expected: a stretch of the curves on the soil reaction's axis (yy axis).

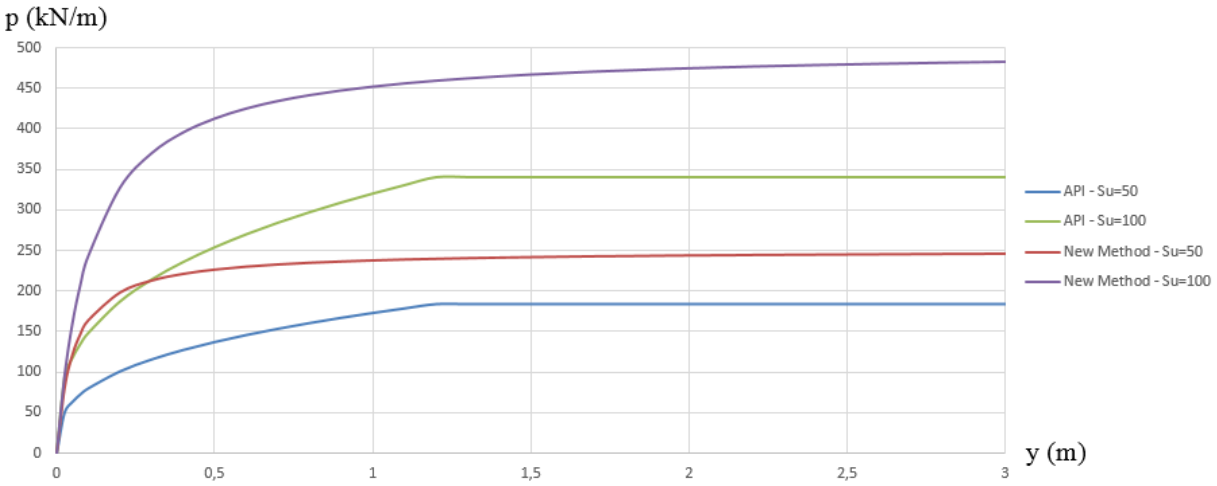

Fig. 7.22 – Effect of the undrained shear strength of the soil on the p-y curves of the two methods

The effect of the parameter y_c and the soil deformation modulus on, respectively, the API and the new proposed method p-y curves is shown in Figure 7.23. The effect on the curves is the same, which is higher stiffness for the curve. Yet, the y_c parameter is a parameter of the soil difficult to evaluate and much less used to characterize a soil when compared to the Young's modulus which leads to the conclusion that a method using a parameter as the E instead of the y_c is greatly more appreciated by the general engineer.

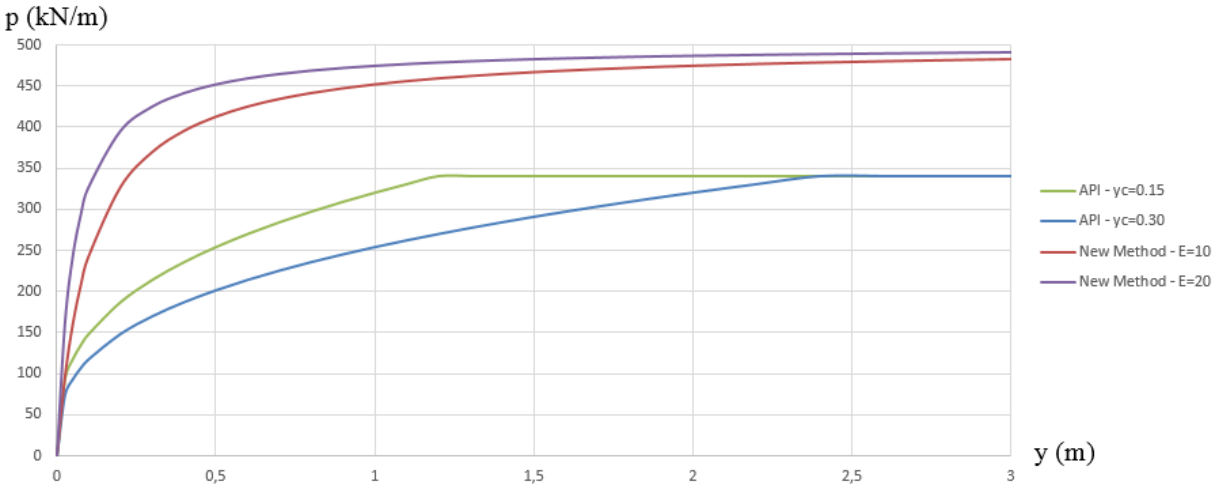

Fig. 7.23 – Effect of the parameters of deformation of the soil on the p-y curves of the two methods

7.5. DIAMETER EFFECTS ON THE P-Y CURVES

Figure 7.24 shows a case of the p-y curves of the method suggested by API and the method proposed in this work for the diameters of 2, 4 and 6 meters. Figure 7.25 shows the same case but with the displacements normalized by the relation from equation (7.3).

As stated before, the p-y curves shown throughout this work are expressed in term of soil reaction, kN/m, and displacement, m, but, as what it is being here analysed is the soil reaction per unit of length of the pile, the subgrade reaction modulus, kN/m^2, assumes the same value as the soil reaction.

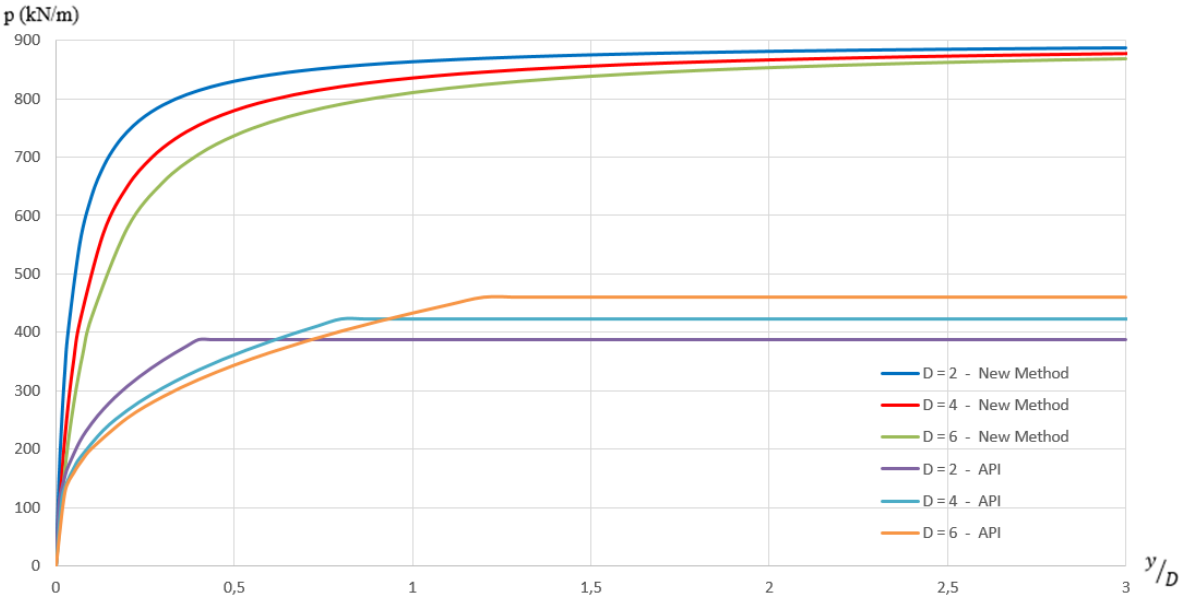

Fig. 7.24 –p-y curves of the two methods for different diameters

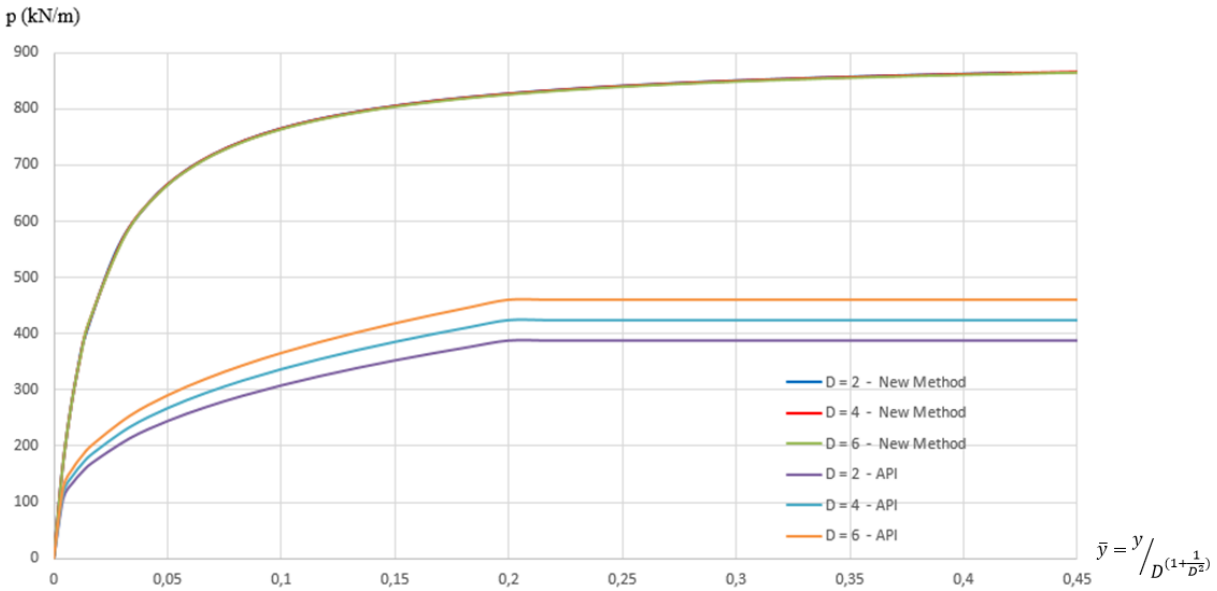

Fig. 7.25 –p-y curves of the two methods for different diameters with the displacement, y, normalized

By observing the two figures one main aspect is possible to stress: the API method assumes that the resistance of the curves depends on the diameter but its stiffness does not. On the other hand, the new proposed method assumes that the diameter of the pile as no influence on the resistance of the p-y curves whereas its stiffness does depend on it.

8

CONCLUSIONS AND FUTURE DEVELOPMENTS

8.1. CONCLUSIONS

In this work a finite element numerical model was developed in PLAXIS 3D to simulate a rigid (short) pile subject to a static lateral load. The purpose was to study the interaction between the soil and the pile and to investigate whether the diameter of the piles influence this relationship. The soil-pile interaction in usually characterized by the so called p-y curves – curves relating, at a certain depth, the reaction of the soil, p, and the displacement, y.

Some differences were observed between the design method suggested by the American Petroleum Institute (API) to calculate the p-y curves and the results obtain from the FEM model.

The soil here used was a Zomergen Clay, a clay characteristic of the seas around the United Kingdom and Scandinavia – North Sea and Baltic Sea. A Hardening Soil model with an undrained behaviour was used to emulate the soil behaviour in all the performed analyses. The description of the properties of the soil, the constitutive model and the geometry of the model is made in Chapter 4.

From the two different analyses performed, the first one, described in Chapter 5, is a simulation of a typical real case scenario of a monopile laterally loaded. The numerical simulations showed a deformation of the pile and the soil similar to the reality and, using the differential equation developed by Hetenyi (1946), the obtaining of the soil reaction was tried to be done through the deflection of the pile. However, no results were obtained concerning the p-y curves as the differential equation does not take into account the properties of the soil and its nonlinear behaviour.

The second analysis consisted on applying a translation of the pile. The advantage of this scenario, described in Chapter 6, is that the same displacement is applied along the whole depth of the pile, unlike the previous case where there were some parts of the pile with almost no displacement (mainly, in the rotation area). The method used to obtain the soil reaction was the integration of the stresses around the pile, which was only possible using MatLab to process the whole amount of exported data from the FEM model.

After having defined and optimized a procedure to calculate the soil reaction using the integration of the stresses around the pile, the equation suggested by Georgiadis in 1992 was concluded to be the best fitting curve for the obtained p-y curves. The input parameters of this equation are the ultimate bearing capacity of the soil, p_u, also an input parameter on the API suggested method, and the initial stiffness of the p-y curves, k_s, as in opposite to the parameter y_c used in the API method that, indirectly, defines the initial stiffness of the curves.

Using MatLab, again, it was possible to evaluate how the parameters of the equation of Georgiadis develop over the depth and formulate a law based on these results. But first, in order to have a reliable and credible law, some sensitivity studies were perform on parameters that were believed to have an influence on the p_u and the k_s. These parameters were the undrained shear strength of the soil, S_u, the Young's modulus of the soil (Secant modulus in the Hardening Soil model of PLAXIS 3D), E_{50}, and the diameter of the pile, D.

The evolution of the ultimate bearing capacity of the soil over the depth using the API suggested method is not very different from the one observe in the results of PLAXIS 3D. There is an equation defining p_u for shallow depths that increases over the depth – characteristic of a wedge failure mechanism – and one other equation for deep depths that remains constant over the depth – soil flow failure mechanism. However, while the API supports the idea that the evolution of this parameter over the depth is a function of the diameter of the pile, the undrained shear strength and the vertical effective stress, on the results of PLAXIS 3D the ultimate bearing capacity of the soil only depends on the undrained shear strength. Also, the point at which there is a change of one failure mechanism into another was observed to be always the same (1.5 diameters in depth) in PLAXIS 3D while in the API method it varies with the different parameters that affect the p_u. Although no sensitivity studies were performed on the unit weight of the soil, γ, this parameter is believed to have a small or even a null influence on the results of the FEM model.

For the initial stiffness of the p-y curves, k_s, a similar law to the one of the ultimate bearing capacity was deduced. However, the constant value of k_s was observed to happen at shallow depths (where the p_u was increasing) and increasing from that point on (where the p_u was constant). There is no possible comparison with the API method as it defines the stiffness of the p-y curve using the y_c parameter with the same value over the whole depth.

Having defined the equation for the p-y curves and the equation to define the evolution of the parameters p_u and k_s over the depth, a comparison with the p-y curves of the API suggested method was performed. As concluded for the evolution of the ultimate bearing capacity of the soil over the depth, the p-y curves of the API method underestimates the bearing capacity of the soil for shallow depths. The reason of this is because it overestimates the depth at which the wedge failure mechanism changes into a soil flow failure mechanism which affects the capacity of the soil.

As for the stiffness of the p-y curves, while the API method uses a constant value for the y_c over the depth, the proposed method takes into account the increase of the confinement state of the soil over the depth through the increase of the initial stiffness of the curves, k_s, over the depth.

The diameter of the pile was concluded to have an important influence on the initial stiffness of the p-y curves but no influence on the resistance while on the API suggested method it is the opposite that occurs.

Finally, the method proposed in this thesis is considered by the author considerably more coherent with the reality as in both the resistance and the stiffness of the p-y curves. Also, as it uses the Young's modulus to define the stiffness, as in opposite to the y_c parameter of the API method, it is possible to say that it is a much more friendly method to use by an engineer for the current design of the monopoles foundations

8.2. FUTURE DEVELOPMENTS

The results that were obtained suggest that the new proposed method is reliable in its assumptions and conclusions. However, some improvements should be incorporated in order to support even more the results here obtained such as improvements in the FEM model, validations of results and sensitivity studies. Future studies are now suggested:

- Evaluate the effect the mesh on the results provided by PLAXIS 3D. The coarseness of the mesh of both the soil and the plate representing the pile was found to be very influent not only on the calculation time (as expected) but also on the results obtained. To accomplish this goal it is important to increase the knowledge on the behaviour of the interfaces of PLAXIS 3D, as these usually are the source of many problems.
- Sensitivity studies on the unit weight of the soil, γ, in order to evaluate whether this property of the soil is irrelevant for the definition of the p-y curves or if it actually influences them in any aspect;
- Sensitivity studies on the relationship between the length and the diameter of the pile. In fact, throughout this work, all the calculations were performed with the same L/D of 5 and it is important to know if a different relationship between the length and the diameter of the pile, always keeping the pile rigid, leads to different results;
- Sensitivity studies on more diameters of the pile. The relation assumed for the initial stiffness of the p-y curves and the diameter (equation (7.3)) has a perfect fitting for the cases here studied but there is not certain that it works for bigger and smaller diameters.

Performing these suggested developments should fully complete the work develop in this thesis. Having more sensitivity studies to confirm the verified results and add new results to this investigation should strengthen the proposed method and make it very reliable.

At the end, the author of this thesis thanks COWI A/S for having proposed this research work and hopes that the work here developed and the obtained conclusions can be helpful of the activities of this company.

REFERENCES

API (2002). *Recommended Practice for Planning, Design and Constructing Fixed Offshore Platforms – Working Stress Design*. American Petroleum Institute, December 2002

Brinkgreve (2014). *Bearing capacity of offshore foundations.* Workshops on Plaxis 3D and Offshore Applications, Setember 29th-30th 2014, Technische Universität Hamburg-Harburg, Hamburg, Germany.

Brinkgreve (2014). *Introduction to Plaxis 3D.* Workshops on Plaxis 3D and Offshore Applications, Setember 29th-30th 2014, Technische Universität Hamburg-Harburg, Hamburg, Germany.

Hetényi, M. (1946). *Beams on Elastic Foundation*. The University of Michigan Press, USA.

McClelland, B. and Focht, J., J.A. (1956). *Soil modulus for laterally loaded piles.* American Society of Civil Engineers (ASCE), Journal of the Soil Mechanics and Foundations Division, vol. 82, 1-22.

Reese, L.C. and Matlock, H. (1956). *Non-dimensional solutions for laterally-loaded piles with soil modulus assumed proportional to depth*. Association of Drilled Shaft Contractors, Dallas, Texas.

Matlock, H. (1970). *Correlations for Design of Laterally Loaded Piles in Soft Clay*. Second Annual Offshore Technology Conference, Houston, Texas, Vol 1, 577-588.

Reese, L. C., Cox, W.R., and Koop, F.D., (1974). *Analysis of laterally loaded piles in sand*. Sixth Offshore Technology conference, Houston, Texas.

Reese, L.C. and Welch, R.C. (1975). *Lateral Loadings of Deep Foundations in Stiff Clay*. American Society of Civil Engineers (ASCE), Journal of Geotechnical Engineering, vol. 101, No 7, 633-649.

Mayne, P. W. (2001). *Stress-strain-strength-flow parameters from enhanced in-situ tests.* International Conference on In-Situ Measurement of Soil Properties & Case Histories, Bali, Indonesia, 27-48.

Duncan, J.M. and Chang, C.M. (1970). *Nonlinear analysis of stress and strain in soils.* American Society of Civil Engineers (ASCE), Journal of Soil Mechanics and Foundations, 96 (SM5), 1629-1653.

Sousa, C. T. (2006). *Ensaios e Análise de Resposta de Estacas em Solo Residual do Granito sob Acções Horizontais.* M. Sc. Thesis, Department of Civil Engineering, Faculdade de Engenharia da Universidade do Porto.

Zhang, L., Silva, F. and Grismala, R. (2005). *Ultimate Lateral Resistance to Piles in Cohesionless Soils*. American Society of Civil Engineers (ASCE), Journal of Geotechnical and Geoenvironmental Engineering 131, January 1st 2005, 78-83.

Georgiadis, M., Anagnostopoulos, C. and Saflekou, S. (1992). *Cyclic lateral loading of piles in soft clay*. American Society of Civil Engineers (ASCE), Journal of Geotechnical Engineering, Vol. 23, GT1, 47-59.

Vesic, A. S. (1961). *Beams on elastic subgrade and the Winkler's hypothesis*. Fifth International Conference of Soil Mechanics, vol. 1, 845-850.

Broms, B. (1964). *Lateral resistance of piles in cohesive soils.* American Society of Civil Engineers (ASCE), Journal of the soil mechanic and foundation, vol. 90 (2), 27-63.